

# Appendix A

## List of Abbreviations

<b>APC/C</b>	Anaphase promoting complex/Cyclosome
<b>APOBEC</b>	apolipoprotein B mRNA editing enzyme, catalytic polypeptide-like
<b>BAM</b>	Binary sequence alignment and mapping
<b>BER</b>	Base excision repair
<b>BIR</b>	Break-induced replication
<b>bp</b>	Base pairs
<b>CDK</b>	Cyclin-dependent kinase
<b>ChIP</b>	chromatin immunoprecipitation
<b>CNV</b>	Copy number variation
<b>CPD</b>	Cyclobutane pyrimidine dimer
<b>CPT</b>	Camptothecin D-loop Displacement loop
<b>DDC</b>	Duplication–degeneration–complementation model
<b>DDT</b>	DNA damage tolerance
<b>DNA</b>	Deoxyribonucleic acid
<b>dNTP</b>	Deoxynucleoside triphosphate
<b>DSB</b>	Double strand break

<b>DSBR</b>	Classical double-strand break repair
<b>dsDNA</b>	Double-stranded DNA
<b>EtBR</b>	Ethidium bromide
<b>EtOH</b>	Ethanol
<b>f.c.</b>	Final concentration
<b>FISH</b>	Fluorescence in situ hybridization
<b>gDNA</b>	Genomic DNA
<b>GG-NER</b>	Global genome-wide nucleotide excision repair
<b>GRCh37</b>	Genome Reference Consortium human genome (build 37)
<b>HR</b>	Homologous recombination
<b>HU</b>	Hydroxurea
<b>IARC</b>	International Agency for Research on Cancer
<b>INDEL</b>	Small insertion/deletion
<b>IR</b>	Ionising radiation
<b>kb</b>	Kilobase pairs
<b>LOF</b>	loss-of-function
<b>LP-BER</b>	Long patch base excision repair
<b>LTR</b>	Long terminal repeats
<b>MMEJ</b>	Microhomology-mediated end joining
<b>MMR</b>	DNA mismatch repair
<b>MMS</b>	Methyl methanesulfonate
<b>NER</b>	Nucleotide excision repair
<b>NGS</b>	Next-generation sequencing

<b>NHEJ</b>	Non-homologous end joining
<b>NIR</b>	Non-ionising radiation
<b>NMD</b>	Nonsense-mediated decay
<b>NMF</b>	Nonnegative matrix factorization
<b>PCR</b>	Polymerase chain reaction
<b>PEG</b>	Polyethylene Glycol Pol Polymerase
<b>Phleo</b>	Phleomycin
<b>ORF</b>	Open Reading Frame
<b>RFC</b>	Replication factor C
<b>RNA</b>	Ribonucleic acid
<b>RNS</b>	Reactive nitrogen species
<b>ROS</b>	Reactive oxygen species
<b>rpm</b>	Revolutions per minute
<b>RT</b>	Room Temperature
<b>SAC</b>	Spindle assembly checkpoint
<b>SDSA</b>	Synthesis-dependent strand annealing
<b>SGA</b>	Synthetic Gene Array
<b>SGD</b>	Saccharomyces Genome Database
<b>SNP</b>	Single nucleotide polymorphism
<b>SNV</b>	Single nucleotide variant
<b>SSA</b>	single-strand annealing
<b>ssDNA</b>	Single-stranded DNA
<b>SV</b>	Structural Variant

<b>TC-NER</b>	Transcription-coupled nucleotide excision repair
<b>TCGA</b>	The Cancer Genome Atlas
<b>TE</b>	Transposable Element
<b>TLS</b>	Translesion synthesis
<b>T<sub>m</sub></b>	Melting temperature (e.g. for oligonucleotides)
<b>Tris</b>	Tris(hydroxymethyl)aminomethane
<b>UPD</b>	Uniparental disomy
<b>UV</b>	Ultraviolet
<b>UV-A</b>	Ultraviolet A
<b>UV-B</b>	Ultraviolet B
<b>UV-C</b>	Ultraviolet C
<b>VEP</b>	Variant Effect Predictor
<b>WES</b>	Whole-exome sequencing
<b>WGS</b>	Whole-genome sequencing
<b>YNB</b>	Yeast Nitrogen Base
<b>YPD</b>	Yeast Extract - Peptone - Dextrose

# Appendix B

## Supplementary Tables, Electronic Files and Articles Published

### B.1 Supplementary figures, tables and notes

#### B.1.1 Software tools and parameters used

##### B.1.1.1 Software tools and parameters used for simulated genomes and capillary sequencing analysis

Step	Software/Tool	Command	Command
ABI sequence alignment	BWA[908]	bwasw	-
Variant Calling of ABI files	SAMTools [903]	mpileup	-u
Variant Calling of ABI files	BCFtools[903]	view	-c -v
Filtering of ABI vcf files	VCFtools [905]	vcf-annotate	-f +/d=2/D=5
Generate INDEL Set	pIRS[840]	pirs diploid	-a 3 -v 0 -d 0.000075
Generate Control Set	pIRS[840]	pirs diploid	-s 0.0001
Generate Mutated Set	pIRS[840]	pirs diploid	-s 0.000025
Simulate sequencing	pIRS[840]	pirs simulate	-x 40(20,30,50) -m 450
Alignment	BWA[908]	v0.6.2	-q 15
Variant Calling	SAMTools [903]	mpileup	-g-tDP,DV-C50-pm3-F0.2-d10000
Variant Calling	BCFtools[903]	call	-vm -f GQ
Intersecting Variants	BEDtools[906]	intersect	-a -b -v
Visualising variants	IGV[909, 910]	-	-

B.1.1.2 Software tools and parameters used for sequencing analysis of *S. cerevisiae*

Step	Software/Tool	Parameters
Read alignment	BWA[901]	bwa aln -l 32 -t 6 -f
Read alignment	BWA[901]	bwa sampe -P -a 742
Mark PCR Duplicates	Picard MarkDuplicates[902]	-
Variant Calling	SAMTools mpileup[903]	-g-t DP,DV-C50-pm3-F0.2-d10000
Variant Calling	BCFtools call[903]	-vm -f GQ
Variant Annotation	Variant Effect Predictor[904]	--species saccharomyces_cerevisiae
Normalising INDELS	BCFtools norm[903]	-
Variant Filtering	VCFtools vcf-annotate[905]	-H -f +/q=30/Q=50/SnpGap=7
Variant Filtering	VCFtools vcf-annotate[905]	customn written filters (see B.1.4)
Subsetting samples	VCFtools vcf-subset[905]	-e
Sorting vcf files	VCFtools vcf-sort[905]	-
Intersecting vcf files	VCFtools vcf-iseq[905]	-f -a -c
Merging vcf files	VCFtools vcf-merge[905]	-

## B.1.2 Strains used in mutation accumulation (MA) experiments experiments

### B.1.2.1 Manual propagation of strains heterozygous diploid for candidate polymerase mutations

Yeast strain	polymerase mutation	ploidy & genotype	parallel lines
YMH9/YMH68	wild-type	diploid	72
YMH29	<i>pol2-4</i>	heterozygous diploid	54
YMH27	<i>pol2-A480V</i>	heterozygous diploid	18
YMH21	<i>pol2-D290V</i>	heterozygous diploid	18
YMH13	<i>pol2-L439V</i>	heterozygous diploid	18
YMH23	<i>pol2-M459K</i>	heterozygous diploid	18
YMH19	<i>pol2-P301R</i>	heterozygous diploid	18
YMH25	<i>pol2-Q468R</i>	heterozygous diploid	18
YMH17	<i>pol2-S312F</i>	heterozygous diploid	18
YMH15	<i>pol2-V426L</i>	heterozygous diploid	18
YMH71	<i>pol3-01</i>	heterozygous diploid	18
YMH69	<i>pol3-P332L</i>	heterozygous diploid	18
YMH72	<i>pol3-R316C</i>	heterozygous diploid	18
YMH70	<i>pol3-S375R</i>	heterozygous diploid	18

### B.1.2.2 Automated propagation of strains haploid and heterozygous diploid for candidate polymerase mutations

Table of strains included in the population bottleneck mutation accumulation experiment. Both heterozygous diploid (Het.) mutant strains and haploid mutant strains were propagated.

Het.	Haploid	polymerase mutation	parallel lines
YMH9	YMH8	wild-type	28
YMH29	YMH28	<i>pol2-4</i>	28
YMH27	YMH26	<i>pol2-A480V</i>	18
YMH21	YMH20	<i>pol2-D290V</i>	18
YMH13	YMH12	<i>pol2-L439V</i>	18
YMH23	YMH22	<i>pol2-M459K</i>	18
YMH19	YMH18	<i>pol2-P301R</i>	18
YMH25	YMH24	<i>pol2-Q468R</i>	18
YMH17	YMH16	<i>pol2-S312F</i>	18
YMH15	YMH14	<i>pol2-V426L</i>	18
YMH11	YMH10	<i>pol3-S384N</i>	18

### B.1.3 6-Thioguanine suppressor screen of haploid mouse cells

Bait locations for the exon-capture experiment (6Thioguanine haploid mouse cell suppressor screen)

Gene	Chr	Location	No of exons	Mean coverage (fold)
Dnmt1	9	20907206-20959888	39	604.7
Hprt	X	52988137-53021659	9	317.2
Mlh1	9	111228228-111271791	19	527.5
Mlh3	12	85234529-85270591	12	528.6
Msh2	17	87672330-87723713	16	566.9
Msh3	13	92211872-92355003	24	497.3
Msh4	3	153857149-153906138	20	511.5
Msh5	17	35028605-35046745	24	560.8
Msh6	17	87975050-87990883	10	572
Pms1	1	53189187-53297018	13	488.4
Pms2	5	143909964-143933968	15	541.4
Setd2	9	110532597-110618633	21	577.7

### B.1.4 Custom filters for DNA sequencing Filters

The custom quality filters on any variant with a sequencing depth of less than 10 reads and a genotype quality if less than 25.

## B.2 Electronic files of supplementary information

The remaining supplementary information has been placed in the Cambridge research repository Apollo as these are large files that do not need to be printed. Here included is the name under which they can be found and a short description of the data they contain. The DOI links under which they can be viewed are <https://doi.org/10.17863/CAM.7296> (the mouse synthetic lethality screen) and <https://doi.org/10.17863/CAM.7299> (the polymerase mutation project). Supplementary files for the Puddu, et al. (2015) publication [801] can be found with the journal article online.

### B.2.1 Supplementary files for the mouse synthetic lethality screens

The sequencing data generated in the course of this project is available for download in the European Nucleotide Archive (PRJEB4302, PRJEB5755, PRJEB12638).fsdjakl

#### B.2.1.1 6TG\_mouse\_Sup1.xlsx

This file includes two tables. Table 1 includes all homozygous mutations identified through whole-exome sequencing of the first 7 suppressor clones we submitted for sequencing. Table 2 includes all mutations of the clones in which no mutation in Hprt could be identified.

#### B.2.1.2 6TG\_mouse\_Sup2.xlsx

This file includes four tables. Table 1 includes all homozygous mutations affecting Dnmt1, Hprt, Mlh1, Msh2, Msh6 and Pms2 genes identified on the targeted exon-capture experiment performed on 189 clones. Table 2 includes all heterozygous mutations. Table 3 includes PROVEAN and SIFT predictions for identified mutations. Table 4 summarizes the potential causative mutation for all suppressor screens with references when identified mutations were previously described.

#### B.2.1.3 6TG\_mouse\_Sup3.xlsx

This file includes three tables. Table 1 includes all homozygous mutations identified in 66 suppressor clones (23 orphan clones plus 43 clones with identified mutations). Table 2 includes all heterozygous mutations identified in the same clones. Table 3 contains all mutations identified in the 23 orphan clones.

#### **B.2.1.4 6TG\_mouse\_Sup4.xlsx**

This file includes three tables. Table 1 describes the bait regions used in the exon capture experiment. Table 2 includes the average coverage of targeted sequences in the exon-capture sequencing experiment. Table 3 includes DNA sequencing coverage for the whole-exome sequencing experiments.

### **B.2.2 Supplementary files for the mouse synthetic lethality screens**

#### **B.2.2.1 MA\_SampleNames.pdf**

This file lists all the samples used in manual propagation experiments and their corresponding sample name in the sequencing data files.

#### **B.2.2.2 S1-3.experiment\_merge.vcf**

This file contains all acquired mutations across Set 1-3 (all *pol2* mutants and *pol3-S483N* plus control samples) of the manual mutation accumulation experiments.

#### **B.2.2.3 S4.experiment\_merge.vcf**

This file contains all acquired mutations across Set 4 (all remaining *pol3* strains plus control samples) of the manual mutation accumulation experiments.

#### **B.2.2.4 S5.experiment\_merge.vcf**

This file contains all acquired mutations across Set 5 (used for the figures in Chapter 4.3 and 4.4) of the manual mutation accumulation experiments.

## **B.3 Articles published during my PhD**

During the course of this work, I was part of several publications, two of which are published or accepted for publication, one of which is in review and three of which are in preparation. In this appendix, published or accepted publications are listed and a short summary of the work as well as a description of my contribution is included. The articles can be found at the end of the dissertation.

**Synthetic viability genomic screening defines Sae2 function in DNA repair.** Fabio Puddu, Tobias Oelschlaegel, Ilaria Guerini, Nicola J Geisler, Hengyao Niu, Mareike Herzog, Israel Salguero, Bernardo Ochoa-Montaña, Emmanuelle Viré, Patrick Sung, David J Adams, Thomas M Keane, Stephen P Jackson. *EMBO J.* 2015 **34**(11):1509-22. doi: 10.15252/embj.201590973. PMID: 25899817

In this work synthetic viability screening was used in budding yeast to identify mutations that can suppress the DNA sensitivity phenotype that results from the loss of Sae2, a protein involved in DNA repair. These suppressor mutations all affected specific residues in the Mre11 protein which is also involved in DNA repair. Further analysis revealed that the mutated Mre11 protein has a decreased affinity to ssDNA suggesting that in wild type cells Sae2 is required to remove Mre11 from the damaged DNA site in the course of the repair. My main contribution to this work is the analysis of whole genome sequencing data of 48 suppressor colonies under the supervision of Thomas Keane, leading to the identification of the *mre11-H37R* and *mre11-H37Y* mutations.

**Genome-wide genetic screening with chemically-mutagenized haploid embryonic stem cells** Josep Forment, Mareike Herzog, Julia Coates, Tomasz Konopka, Bianca Gapp, Sebastian Nijman, David Adams, Thomas Keane and Stephen Jackson. *Nature Chemical Biology* [Accepted 24th Aug 16]

This is a proof-of-principle work showing that synthetic viability screening in haploid, mouse embryonic stem cells is feasible. All known genes whose inactivation leads to suppression were identified in this work. This work demonstrates that causative mutations can be identified, that synthetic viability screens can map essential domains of a protein and that causative mutations can be identified even if mutagenesis generated more “passenger” mutations to sift through. This work is a demonstration of the feasibility of classical genetic screenings in mammalian cells and provides a new, powerful tool to explore mammalian genetic interactions. My contribution to this work is the analysis of all sequencing data of DNA from resistant clones and the identification of all critical mutations identified in this work.

**Chromatin determinants impart camptothecin hypersensitivity in the absence of the Tof1/Csm3 replication pausing complex** Fabio Puddu, Mareike Herzog, Nicola Geisler, Vincenzo Costanzo, Steve Jackson. *Nucleic Acids Research* [Submitted]

In budding yeast the absence of the Tof1/Csm3 complex causes hypersensitivity to camptothecin. Using a synthetic viability approach, we have identified that disruption of Sir-dependent heterochromatin by inactivation of histone H4-K16 deacetylation can suppress this

sensitivity in *tof1Δ* and wild-type cells. My main contribution to this work is the analysis of all suppressor colonies whole genome sequencing and identification of inactivating mutations in the genes *SIR3* and *SIR4*, as well as analysis of ChIP-Seq data together with Fabio Puddu.



# Synthetic viability genomic screening defines Sae2 function in DNA repair

Fabio Puddu<sup>1,†</sup>, Tobias Oelschlaegel<sup>1,†</sup>, Ilaria Guerini<sup>1</sup>, Nicola J Geisler<sup>1</sup>, Hengyao Niu<sup>3</sup>, Mareike Herzog<sup>1,2</sup>, Israel Salguero<sup>1</sup>, Bernardo Ochoa-Montaña<sup>1</sup>, Emmanuelle Viré<sup>1</sup>, Patrick Sung<sup>3</sup>, David J Adams<sup>2</sup>, Thomas M Keane<sup>2</sup> & Stephen P Jackson<sup>1,2,\*</sup>

## Abstract

DNA double-strand break (DSB) repair by homologous recombination (HR) requires 3' single-stranded DNA (ssDNA) generation by 5' DNA-end resection. During meiosis, yeast Sae2 cooperates with the nuclease Mre11 to remove covalently bound Spo11 from DSB termini, allowing resection and HR to ensue. Mitotic roles of Sae2 and Mre11 nuclease have remained enigmatic, however, since cells lacking these display modest resection defects but marked DNA damage hypersensitivities. By combining classic genetic suppressor screening with high-throughput DNA sequencing, we identify Mre11 mutations that strongly suppress DNA damage sensitivities of *sae2Δ* cells. By assessing the impacts of these mutations at the cellular, biochemical and structural levels, we propose that, in addition to promoting resection, a crucial role for Sae2 and Mre11 nuclease activity in mitotic DSB repair is to facilitate the removal of Mre11 from ssDNA associated with DSB ends. Thus, without Sae2 or Mre11 nuclease activity, Mre11 bound to partly processed DSBs impairs strand invasion and HR.

**Keywords** Mre11; Sae2; suppressor screening; synthetic viability; whole-genome sequencing

**Subject Categories** DNA Replication, Repair & Recombination

**DOI** 10.15252/emboj.201590973 | Received 8 January 2015 | Revised 16 March 2015 | Accepted 2 April 2015 | Published online 21 April 2015

**The EMBO Journal (2015) 34: 1509–1522**

## Introduction

The DSB is the most cytotoxic form of DNA damage, with ineffective DSB repair leading to mutations, chromosomal rearrangements and genome instability that can yield cancer, neurodegenerative disease, immunodeficiency and/or infertility (Jackson & Bartek, 2009). DSBs arise from ionising radiation and radiomimetic drugs and are generated when replication forks encounter single-stranded DNA breaks or other DNA lesions, including DNA alkylation adducts and sites of

abortive topoisomerase activity. DSBs are also physiological intermediates in meiotic recombination, being introduced during meiotic prophase I by the topoisomerase II-type enzyme Spo11 that becomes covalently linked to the 5' end of each side of the DSB (Keeney *et al*, 1997). The two main DSB repair pathways are non-homologous end-joining (NHEJ) and homologous recombination (Lisby *et al*, 2004; Symington & Gautier, 2011). In NHEJ, DNA ends need little or no processing before being ligated (Daley *et al*, 2005). By contrast, HR requires DNA-end resection, a process involving degradation of the 5' ends of the break, yielding 3' single-stranded DNA (ssDNA) tails that mediate HR via pairing with and invading the sister chromatid, which provides the repair template.

Reflecting the above requirements, cells defective in resection components display HR defects and hypersensitivity to various DNA-damaging agents. This is well illustrated by *Saccharomyces cerevisiae* cells harbouring defects in the Mre11–Rad50–Xrs2 (MRX) complex, which binds and juxtaposes the two ends of a DSB (Williams *et al*, 2008) and, through Mre11 catalytic functions, provides nuclease activities involved in DSB processing (Furuse *et al*, 1998; Williams *et al*, 2008; Stracker & Petrini, 2011). Once a clean, partially resected 5' end has been generated, the enzymes Exo1 and Sgs1/Dna2 are then thought to act, generating extensive ssDNA regions needed for effective HR (Mimitou & Symington, 2008; Zhu *et al*, 2008). Notably, while Mre11 nuclease activity is essential in meiosis to remove Spo11 and promote 5' end resection, in mitotic cells, resection is only somewhat delayed in the absence of Mre11 and almost unaffected by *mre11-nd* (nuclease-dead) mutations (Ivanov *et al*, 1994; Moreau *et al*, 1999), indicating the existence of MRX-nuclease-independent routes for ssDNA generation.

Another protein linked to resection is *S. cerevisiae* Sae2, the functional homolog of human CtIP (Sartori *et al*, 2007; You *et al*, 2009). Despite lacking obvious catalytic domains, Sae2 and CtIP have been reported to display endonuclease activity *in vitro* (Lengsfeld *et al*, 2007; Makharashvili *et al*, 2014; Wang *et al*, 2014), and their functions are tightly regulated by cell cycle- and DNA damage-dependent phosphorylations (Baroni *et al*, 2004; Huertas *et al*, 2008; Huertas & Jackson, 2009; Barton *et al*, 2014). In many ways, Sae2 appears to

1 The Gurdon Institute and Department of Biochemistry, University of Cambridge, Cambridge, UK

2 The Wellcome Trust Sanger Institute, Hinxton, Cambridge, UK

3 Molecular Biophysics and Biochemistry, Yale University School of Medicine, New Haven, CT, USA

\*Corresponding author. Tel: +44 1223 334088; E-mail: sjackson@gurdon.cam.ac.uk

†These authors contributed equally to this work

function together with MRX in DSB repair. For instance, *mre11-nd* as well as *mre11S* and *rad50S* hypomorphic alleles phenocopy *SAE2* deletion (*sae2Δ*) in meiosis, yielding unprocessed Spo11–DNA complexes (Keeney & Kleckner, 1995; Nairz & Klein, 1997; Prinz et al., 1997). Furthermore, recent findings have indicated that Sae2 stimulates Mre11 endonuclease activity to promote resection, particularly at protein-bound DSB ends (Cannavo & Cejka, 2014). Also, both *sae2Δ* and *mre11-nd* mutations cause hypersensitivity towards the anti-cancer drug camptothecin (Deng et al., 2005), which yields DSBs that are repaired by HR. Nevertheless, key differences between MRX and Sae2 exist, since *sae2Δ* leads to persistence of MRX at DNA damage sites (Lisby et al., 2004) and hyperactivation of the MRX-associated Tel1 protein kinase (Usui et al., 2001), the homolog of human ATM, while MRX inactivation abrogates Tel1 function (Fukunaga et al., 2011). These findings, together with *sae2Δ* and *mre11-nd* cells displaying only mild resection defects (Clerici et al., 2005), highlight how Sae2 functions in HR cannot be readily explained by it simply cooperating with MRX to enhance resection.

As reported below, by combining classic genetic screening for suppressor mutants with whole-genome sequencing to determine their genotype, we are led to a model that resolves apparent paradoxes regarding Sae2 and MRX functions, namely the fact that while deletion of either *SAE2* or *MRE11* causes hypersensitivity to DNA-damaging agents, the resection defect of *sae2Δ* strains is negligible compared to that of *mre11Δ* cells, and lack of Sae2 causes an increase in Mre11 persistence at DSB ends rather than a loss. Our model invokes Mre11/MRX removal from DNA as a critical step in allowing HR to proceed effectively on a resected DNA template.

## Results

### SVGS identifies Mre11 mutations as *sae2Δ* suppressors

To gain insights into why yeast cells lacking Sae2 are hypersensitive to DNA-damaging agents, we performed synthetic viability genomic screening (SVGS; Fig 1A). To do this, we took cultures of a *sae2Δ* yeast strain (bearing a full deletion of the *SAE2* locus) and plated them on YPD plates supplemented with camptothecin, which stabilises DNA topoisomerase I cleavage complexes and yields replication-dependent DSBs that are repaired by Sae2-dependent HR (Deng et al., 2005) (Fig 1A). Thus, we isolated 48 mutants surviving camptothecin treatment that spontaneously arose in the population analysed. In addition to verifying that all indeed contained the *SAE2* gene deletion yet were camptothecin resistant, subsequent analyses revealed that 10 clones were also largely or fully suppressed for *sae2Δ* hypersensitivity to the DNA-alkylating agent methyl methanesulphonate (MMS), the replication inhibitor hydroxyurea (HU), the DSB-generating agent phleomycin and ultraviolet light (Supplementary Fig S1).

To identify mutations causing these suppression phenotypes, genomic DNA from the 48 clones was isolated and analysed by next-generation Illumina sequencing. We then used bioinformatics tools (see Materials and Methods) to identify mutations altering open reading frames within the reference *S. cerevisiae* genome (Fig 1A). This revealed that 24 clones displaying camptothecin resistance but retaining *sae2Δ* hypersensitivity towards other DNA-damaging agents possessed *TOP1* mutations (Fig 1B and C), thereby providing proof-of-principle for the SVGS methodology (*TOP1* is

a non-essential gene that encodes DNA topoisomerase I, the camptothecin target). Strikingly, of the remaining clones, 10 contained one or other of two different mutations in a single *MRE11* codon, resulting in amino acid residue His37 being replaced by either Arg or Tyr (*mre11-H37R* and *mre11-H37Y*, respectively; Fig 1B and C and Supplementary Fig S1; note that *TOP1* and *MRE11* mutations are mutually exclusive). While some remaining clones contained additional potential suppressor mutations worthy of further examination, these were only resistant to camptothecin. Because of their broader phenotypes and undefined mechanism of action, we focused on characterising the *MRE11 sae2Δ* suppressor (*mre11<sup>SUPsae2Δ</sup>*) alleles.

### *mre11<sup>SUPsae2Δ</sup>* alleles suppress many *sae2Δ* phenotypes

Mre11 His37 lies within a functionally undefined but structurally evolutionarily conserved  $\alpha$ -helical region, and the residue is well conserved among quite divergent fungal species (Fig 2A). As anticipated from previous studies, deleting *MRE11* did not suppress the DNA damage hypersensitivities of *sae2Δ* cells, revealing that *mre11-H37R* and *mre11-H37Y* were not behaving as null mutations (unpublished observation). In line with this, the *mre11-H37R* and *mre11-H37Y* alleles did not destabilise Mre11, producing proteins that were expressed at equivalent levels to the wild-type protein (Fig 2B). Nevertheless, expression of wild-type Mre11 resensitised the *mre11<sup>SUPsae2Δ</sup> sae2Δ* strains to camptothecin, and to a lesser extent to MMS (Fig 2C), indicating that *mre11-H37R* and *mre11-H37Y* were fully or partially recessive for the camptothecin and MMS resistance phenotypes, respectively. Furthermore, this established that expression of wild-type Mre11 is toxic to *sae2Δmre11<sup>SUPsae2Δ</sup>* cells upon camptothecin treatment. Importantly, independent introduction of *mre11-H37R* and *mre11-H37Y* alleles in a *sae2Δ* strain confirmed that each conferred suppression of *sae2Δ* hypersensitivity to various DNA-damaging agents (Fig 2D). The *mre11-H37R* and *mre11-H37Y* alleles also suppressed camptothecin hypersensitivity caused by mutations in Sae2 that prevent its Mec1/Tel1-dependent (*sae2-MT*) or CDK-dependent (*sae2-S267A*) phosphorylation (Baroni et al., 2004; Huertas et al., 2008) (Fig 2E and F). By contrast, no suppression of *sae2Δ* camptothecin hypersensitivity was observed by mutating His37 to Ala (*mre11-H37A*; Fig 2G), suggesting that the effects of the *mre11<sup>SUPsae2Δ</sup>* alleles were not mediated by the abrogation of a specific function of His37 but more likely reflected functional alteration through introducing bulky amino acid side chains.

### *mre11<sup>SUPsae2Δ</sup>* alleles do not suppress all *sae2Δ* phenotypes

In the absence of Sae2, cells display heightened DNA damage signalling as measured by Rad53 hyperphosphorylation (Clerici et al., 2006). As we had found for the DNA damage hypersensitivities of *sae2Δ* cells, this read-out of Sae2 inactivity was also rescued by *mre11-H37R* (Fig 3A). By contrast, *mre11-H37R* did not suppress the sporulation defect of *sae2Δ* cells (unpublished observation). In line with this, *mre11-H37R* did not suppress impaired meiotic DSB processing caused by Sae2 deficiency, as reflected by aberrant accumulation of 5'-bound Spo11 repair intermediates within the *THR4* recombination hot spot (Goldway et al., 1993; Fig 3B; as shown in Supplementary Fig S2A, *mre11-H37R* did not itself cause meiotic defects when Sae2 was

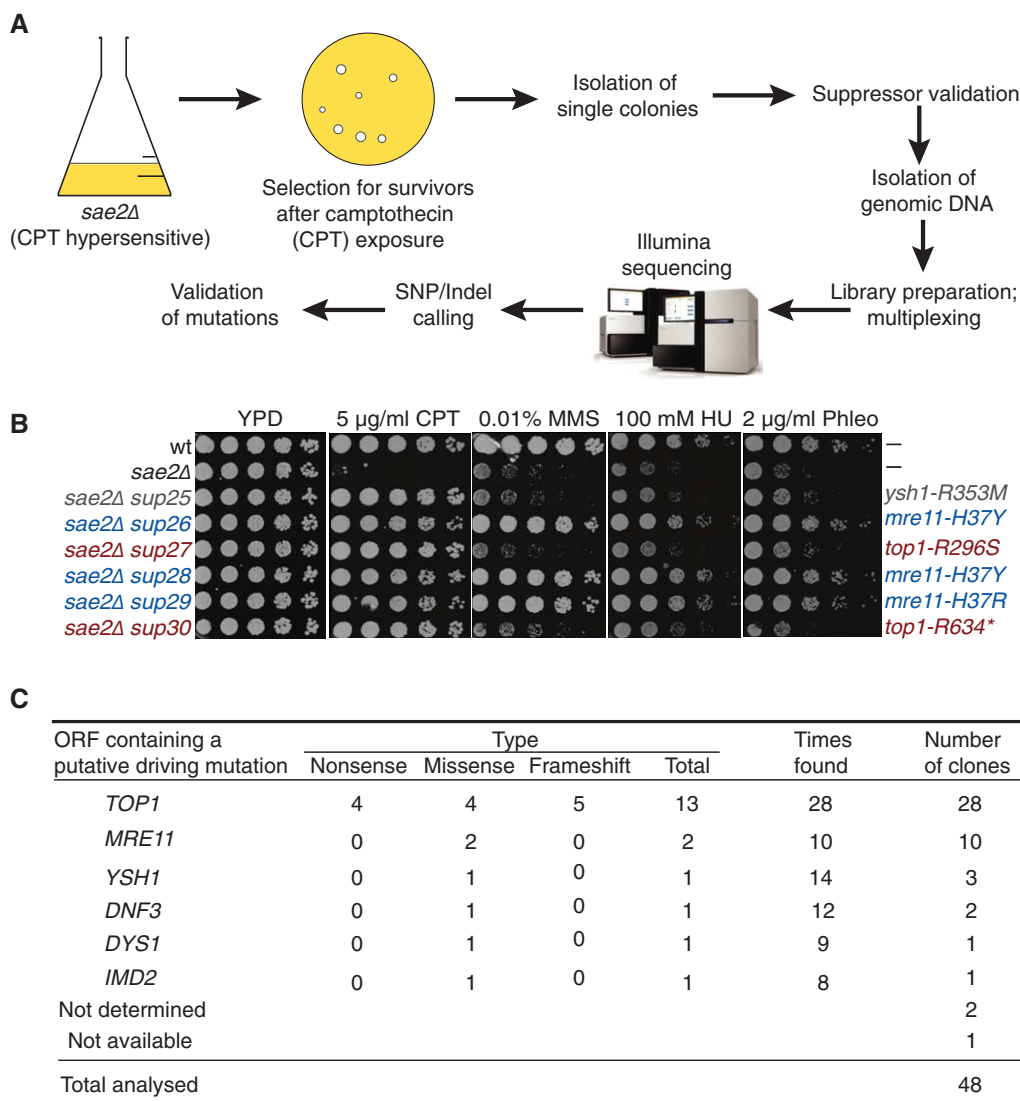


**Figure 1. SVGS identifies mutations suppressing *sae2Δ* DNA damage hypersensitivity.**

A Outline of the screening approach that was used to identify suppressors of *sae2Δ* camptothecin (CPT) hypersensitivity.

B Validation of the suppression phenotypes; a subset (sup25–sup30) of the suppressors recovered from the screening is shown along with mutations identified in each clone.

C Summary of the results of the synthetic viability genomic screening (SVGS) for *sae2Δ* camptothecin (CPT) hypersensitivity. The ORF and the type of mutation are reported together with the number of times each ORF was found mutated and the number of clones in which each ORF was putatively driving the resistance.

present). Notably, however, *mre11-H37R* rescued the hypersensitivity of *sae2Δ* cells to etoposide, which produces DSBs bearing 5' DNA ends bound to Top2 (Supplementary Fig S2B; deletion of *ERG6* was used to increase permeability of the plasma membrane to etoposide), suggesting that significant differences must exist between the repair of meiotic and etoposide-induced DSBs.

Next, we examined the effects of *mre11<sup>SUPsae2Δ</sup>* alleles on Sae2-dependent DSB repair by single-strand annealing (SSA), using a system wherein a chromosomal locus contains an HO endonuclease cleavage site flanked by two direct sequence repeats. In this system, HO induction produces a DSB that is then resected until two complementary sequences become exposed and anneal, resulting in repair by a process that deletes the region between the repeats (Fishman-Lobell et al, 1992; Vaze et al, 2002; Fig 3C). Despite displaying only mild

resection defects (Clerici et al, 2006), we observed that *sae2Δ* cells were defective in SSA-mediated DSB repair and did not resume cell cycle progression after HO induction as fast as wild-type cells, in agreement with published work (Clerici et al, 2005). Notably, *mre11-H37R* did not alleviate these *sae2Δ* phenotypes (Fig 3D and E).

Finally, we examined the effect of the *mre11-H37R* mutation on telomere-associated functions of the MRX complex and Sae2. It has been established that simultaneous deletion of *SGS1* and *SAE2* results in synthetic lethality/sickness, possibly due to excessive telomere shortening (Mimitou & Symington, 2008; Hardy et al, 2014). To test whether *mre11-H37R* can alleviate this phenotype, we crossed a *sae2Δmre11-H37R* strain with a *sgs1Δ* strain. As shown in Supplementary Fig S2C, we were unable to recover neither *sgs1Δsae2Δ* nor *sgs1Δsae2Δmre11-H37R* cells, implying that *mre11-H37R* cannot

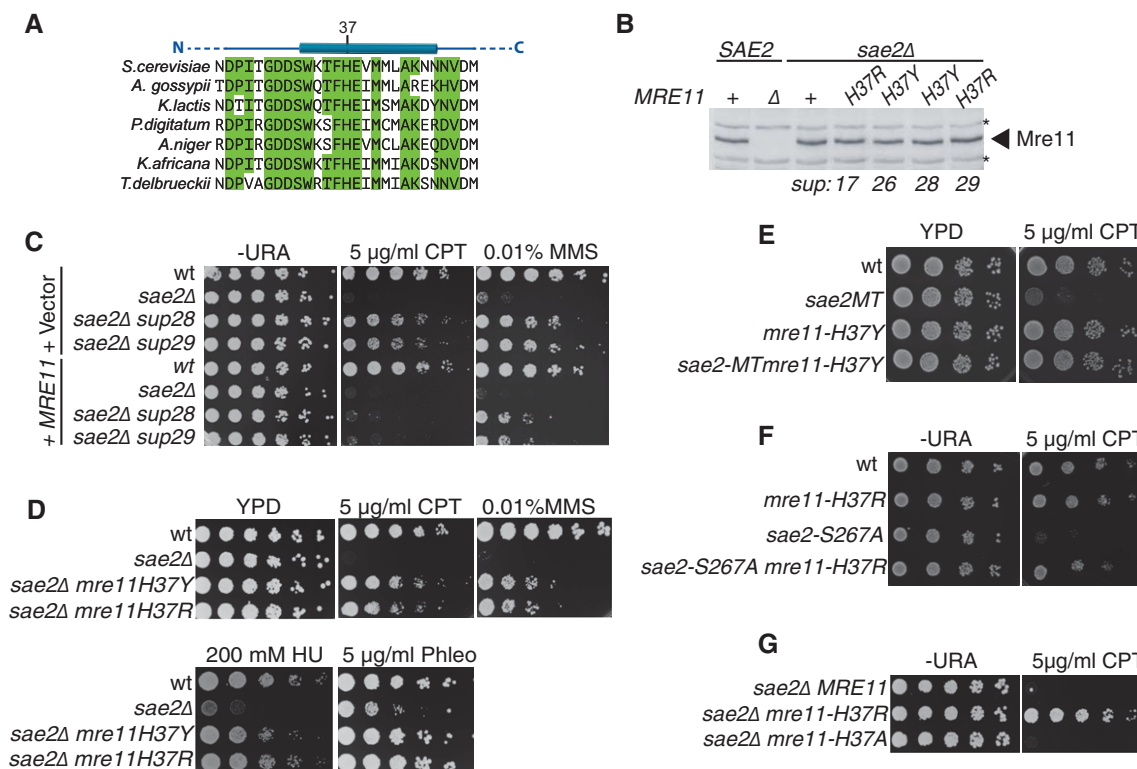


**Figure 2. *mre11-H37R* suppresses the CPT hypersensitivity of *sae2Δ* cells.**

- A Alignment of Mre11 region containing H37 in fungal species; secondary structure prediction is shown above.  
 B Western blot with anti-Mre11 antibody on protein extracts prepared from the indicated strains shows that *mre11-H37R* and *mre11-H37Y* mutations do not alter Mre11 protein levels (\* indicate cross-reacting proteins).  
 C *sup28* and *sup29* suppression is rescued by expressing wild-type (wt) Mre11.  
 D *mre11-H37R* and *mre11-H37Y* suppress *sae2Δ* DNA damage hypersensitivity.  
 E, F *mre11-H37Y* suppresses DNA damage hypersensitivities of *sae2MT* (*sae2-2,5,6,8,9*) and *sae2-S267A* cells. CPT, camptothecin; Phleo, phleomycin.  
 G *mre11-H37A* does not suppress *sae2Δ*.

suppress this phenotype. In agreement with this conclusion, the *mre11-H37R* mutation did not negatively affect Mre11-dependent telomere maintenance as demonstrated by Southern blot analysis (Supplementary Fig S2D).

Together, the above data revealed that *mre11<sup>SUPsae2Δ</sup>* alleles suppressed *sae2Δ* DNA damage hypersensitivities but not *sae2Δ* meiotic phenotypes requiring Mre11-mediated Spo11 removal from recombination intermediates, nor mitotic SSA functions that have been attributed to Sae2-mediated DNA-end bridging (Clerici *et al*, 2005). Subsequent analyses revealed that suppression did not arise largely through channelling of DSBs towards NHEJ because the key NHEJ factor Yku70 was not required for *mre11-H37R* or *mre11-H37Y* to suppress the camptothecin sensitivity of a *sae2Δ* strain (Fig 3F). In addition, this analysis revealed that the previously reported suppression of *sae2Δ*-mediated DNA damage hypersensitivity by Ku loss (Mimitou & Symington, 2010; Foster *et al*, 2011) was considerably less effective than that caused by *mre11-H37R* or *mre11-H37Y*. Also, suppression of *sae2Δ* camptothecin hypersensitivity by *mre11<sup>SUPsae2Δ</sup>* alleles did not require Exo1, indicating that in contrast to suppression of *sae2Δ* phenotypes by Ku loss (Mimitou & Symington, 2010), *mre11-H37R* and *mre11-H37Y* did not cause cells to become particularly reliant on Exo1 for DSB processing (Fig 3G). Further characterisations, focused on *mre11-H37R*, revealed that while not suppressing

camptothecin hypersensitivity of an *xrs2Δ* strain (Fig 3H), it almost fully rescued the camptothecin hypersensitivity of a strain expressing the *rad50S* allele, which phenocopies *sae2Δ* by somehow preventing functional Sae2–MRX interactions that are required for Sae2 stimulation of Mre11 endonuclease activity (Keeney & Kleckner, 1995; Hopfner *et al*, 2000; Cannavo & Cejka, 2014; Fig 3I).

### H37R does not enhance Mre11 nuclease activity but impairs DNA binding

To explore how *mre11<sup>SUPsae2Δ</sup>* mutations might operate, we over-expressed and purified wild-type Mre11, Mre11<sup>H37R</sup> and Mre11<sup>H37A</sup> (Fig 4A and Supplementary Fig S2F) and then subjected these to biochemical analyses. All the proteins were expressed at similar levels and fractionated with equivalent profiles, suggesting that the Mre11 mutations did not grossly affect protein structure or stability. Since Sae2 promotes Mre11 nuclease functions, we initially speculated that *sae2Δ* suppression would be mediated by *mre11<sup>SUPsae2Δ</sup>* alleles having intrinsically high, Sae2-independent nuclease activity. Surprisingly, this was not the case, with Mre11<sup>H37R</sup> actually exhibiting lower nuclease activity than the wild-type protein (Fig 4B). Furthermore, by electrophoretic mobility shift assays, we found that the H37R mutation reduced Mre11 binding to double-stranded DNA

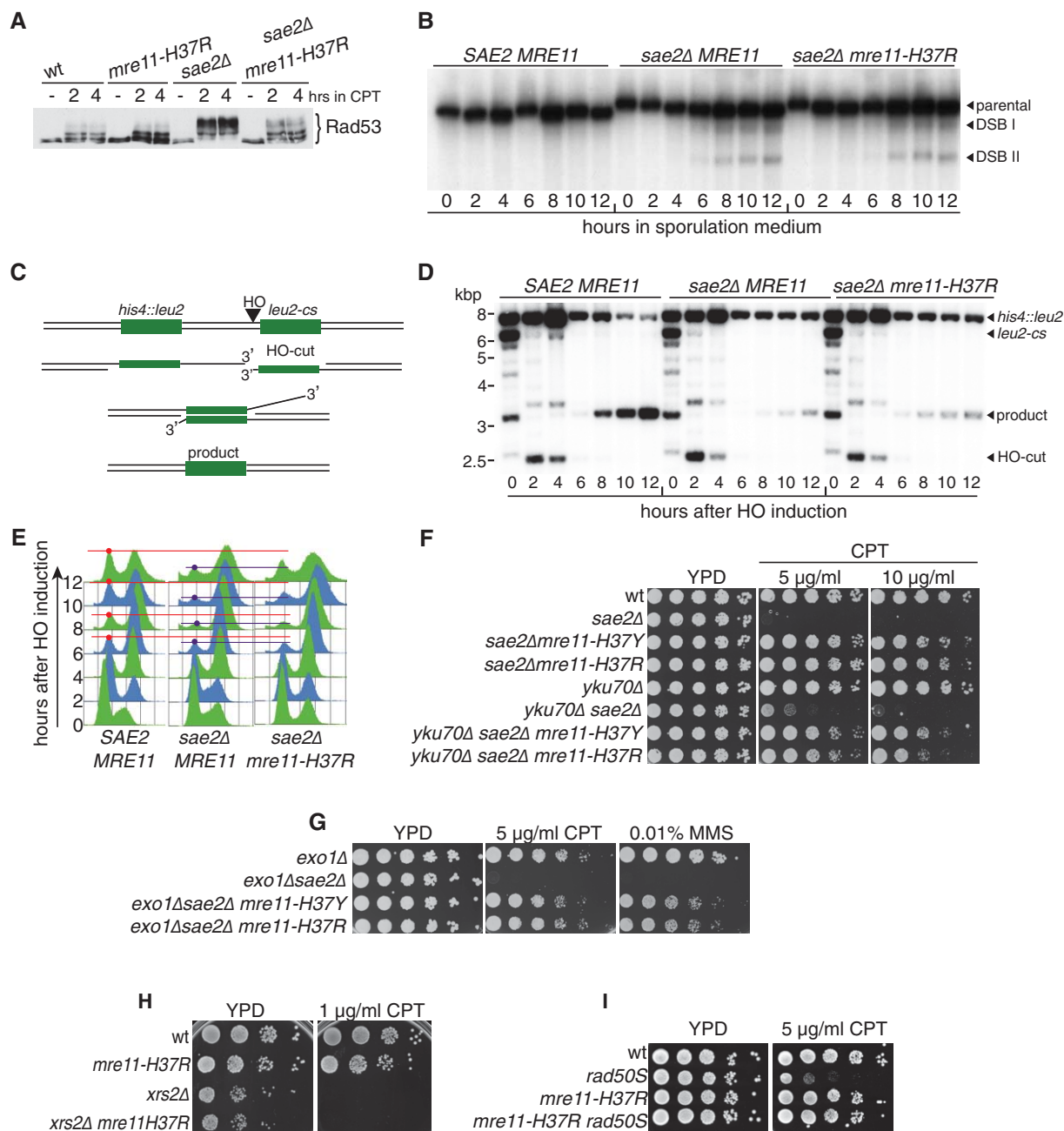


**Figure 3. mre11-H37R suppresses some but not all sae2Δ phenotypes.**

- A** *mre11-H37R* suppresses *sae2Δ* checkpoint hyperactivation.  
**B** *mre11-H37R* does not rescue *sae2Δ* meiotic DSB processing defect.  
**C** Outline of DSB repair by single-strand annealing (SSA).  
**D** *mre11-H37R* does not rescue the SSA repair defect of *sae2Δ* strains.  
**E** *mre11-H37R* does not rescue *sae2Δ*-dependent cell cycle arrest caused by DSB induction.  
**F, G** Exo1 and Ku are not required for *mre11-H37R*-mediated suppression of *sae2Δ* hypersensitivity.  
**H** *mre11-H37R* does not suppress *xrs2Δ* camptothecin (CPT) hypersensitivity.  
**I** *mre11-H37R* suppresses *rad50S* CPT hypersensitivity.

(dsDNA; Fig 4C) and abrogated Mre11 binding to ssDNA (Fig 4D). Conversely, mutation of H37 to alanine, which does not result in a *sup<sup>sae2Δ</sup>* phenotype, did not negatively affect dsDNA-binding activity (Fig 4C) and only partially impaired ssDNA binding (Fig 4D).

Taken together with the fact that the lack of Sae2 only has minor effects on mitotic DSB resection (Clerici *et al*, 2005), the above results suggested that the *sae2Δ* suppressive effects of *mre11<sup>SUPsae2Δ</sup>* mutations were associated with weakened Mre11 DNA binding and

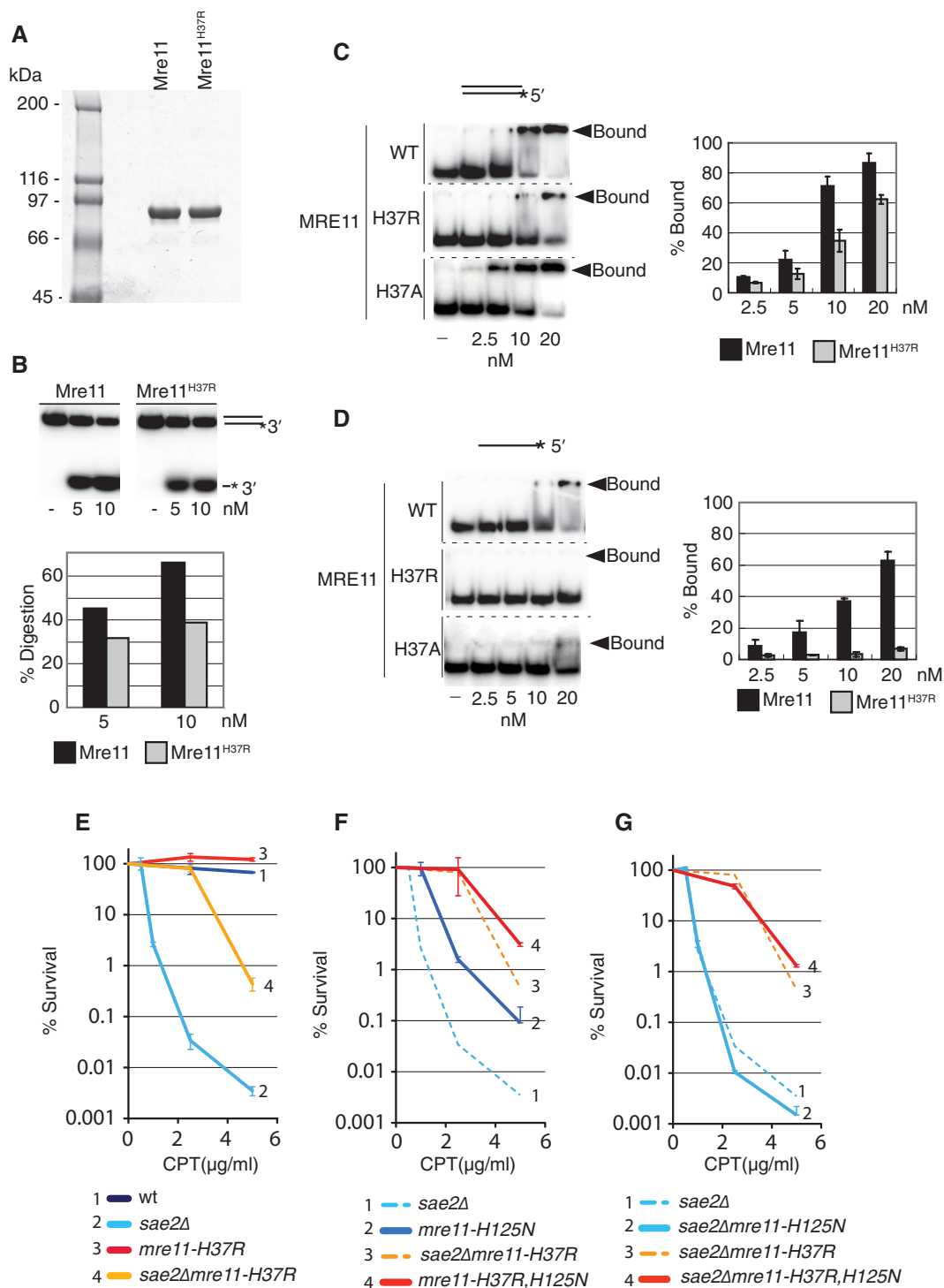


**Figure 4. Mre11<sup>H37R</sup> is impaired biochemically, particularly at the level of ssDNA binding.**

**A** Mre11 and Mre11<sup>H37R</sup> were purified to homogeneity from yeast cultures.  
**B** 3' exonuclease activity assay on Mre11 and Mre11<sup>H37R</sup> leading to release of a labelled single nucleotide, as indicated.  
**C, D** Electrophoretic mobility shift assays on Mre11, Mre11<sup>H37R</sup> and Mre11<sup>H37A</sup> with dsDNA (C) or ssDNA (D).  
**E** Quantification of *mre11-H37R* suppression of *sae2Δ* cell DNA damage hypersensitivity. Overnight grown cultures of the indicated strains were diluted and plated on medium containing the indicated doses of CPT. Colony growth was scored 3–6 days later. Averages and standard deviations are shown for each point.  
**F** Intragenic suppression of CPT hypersensitivity of *mre11-nd* (*mre11-H125N*) by *mre11-H37R*. Overnight grown cultures of the indicated strains were treated as in (E). Dotted lines represent data from (E). Averages and standard deviations are shown for each point.  
**G** Mre11 nuclease activity is not required for *mre11-H37R*-mediated suppression of *sae2Δ* CPT hypersensitivity. Overnight grown cultures of the indicated strains were treated as in (E). The dotted lines represent data from (E). Averages and standard deviations are shown for each point.

were not linked to effects on resection or Mre11 nuclease activity. In line with this idea, by combining mutations in the same Mre11 polypeptide, we established that *mre11-H37R* substantially rescued camptothecin hypersensitivity caused by mutating the Mre11 active site residue His125 to Asn (Moreau *et al*, 2001; *mre11-H125N*; Fig 4E and Supplementary Fig S2F and G), which abrogates all Mre11 nuclease activities and prevents processing of DSBs when their 5' ends are blocked (Moreau *et al*, 1999). Even *sae2Δ mre11-H37R,H125N* cells were resistant to camptothecin and MMS, indicating that Mre11-nuclease-mediated processing of DNA ends is not required for H37R-dependent suppression, nor for DNA repair in this Sae2-deficient setting (Fig 4G and Supplementary Fig S2G). Furthermore, while *sae2Δ* strains were more sensitive to camptothecin than *mre11-H125N* strains, the sensitivities of the corresponding strains carrying the *mre11-H37R* allele were comparable (compare curves 1 and 2 with 3 and 4 in Fig 4F) indicating that *mre11-H37R* suppresses not only the *sae2Δ*-induced lack of Mre11 nuclease activity, but also other nuclease-independent functions of Sae2. Nevertheless, *mre11-H37R* did not rescue the camptothecin hypersensitivity of *sae2Δ* cells to wild-type levels, suggesting that not all functions of Sae2 are suppressed by this *MRE11* allele (Fig 4E and F).

### Identifying an Mre11 interface mediating *sae2Δ* suppression

To gain further insights into how *mre11<sup>SUPsae2Δ</sup>* alleles operate and relate this to the above functional and biochemical data, we screened for additional *MRE11* mutations that could suppress camptothecin hypersensitivity caused by Sae2 loss. Thus, we propagated a plasmid carrying wild-type *MRE11* in a mutagenic *E. coli* strain, thereby generating libraries of plasmids carrying *mre11* mutations. We then introduced these libraries into a *sae2Δmre11Δ* strain and screened for transformants capable of growth in the presence of camptothecin (Fig 5A). Through plasmid retrieval, sequencing and functional verification, we identified 12 *sae2Δ* suppressors, nine carrying single *mre11* point mutations and three being double mutants (Supplementary Fig S3A). One single mutant was *mre11-H37R*, equivalent to an initial spontaneously arising suppressor that we had identified. Among the other single mutations were *mre11-P110L* and *mre11-L89V*, both of which are located between Mre11 nuclease domains II and III, in a region with no strong secondary structure predictions (Fig 5B). Two of the three double mutants contained *mre11-P110L* combined with another mutation that was presumably not responsible for the resistance phenotype (because *mre11-P110L* acts as a suppressor on its own), whereas the third

contained both *mre11-Q70R* and *mre11-G193S*. Subsequent studies, involving site-directed mutagenesis, demonstrated that effective *sae2Δ* suppression was mediated by *mre11-Q70R*, which alters a residue located in a highly conserved  $\alpha$ -helical region (Fig 5C). Ensuing comparisons revealed that the mutations identified did not alter Mre11 protein levels (Supplementary Fig S3B) and that *mre11-Q70R* suppressed *sae2Δ* camptothecin hypersensitivity to similar extents as *mre11-H37R* and *mre11-H37Y*, whereas *mre11-L89V* and *mre11-P110L* were marginally weaker suppressors (Fig 5D).

To map the locations of the various *mre11<sup>SUPsae2Δ</sup>* mutations within the Mre11 structure, we used the dimeric tertiary structure (Schiller *et al*, 2012) of the *Schizosaccharomyces pombe* Mre11 counterpart, Rad32, as a template to generate a molecular model of *S. cerevisiae* Mre11. The resulting structure had a near-native QMEAN score (0.705 vs 0.778; Benkert *et al*, 2008), indicating a reliable molecular model. Strikingly, ensuing analyses indicated that the *mre11<sup>SUPsae2Δ</sup>* mutations clustered in a region of the protein structure distal from the nuclease catalytic site and adjacent to, but distinct from, the interface defined as mediating contacts with dsDNA in the *Pyrococcus furiosus* Mre11 crystal structure (Williams *et al*, 2008; Fig 5E; the predicted path of dsDNA is shown in black, while the *mre11<sup>SUPsae2Δ</sup>* mutations and residues involved in nuclease catalysis are indicated in red and orange, respectively). Furthermore, this analysis indicated that H37 and Q70 are located close together, on two parallel  $\alpha$ -helices and are both likely to be solvent exposed (Fig 5F). By contrast, the L89 side chain is predicted to be in the Mre11 hydrophobic core, although modelling suggested that the *mre11-L89V* mutation might alter the stability of the  $\alpha$ -helix containing Q70. We noted that, in the context of the Mre11 dimer, H37 and Q70 are located in a hemi-cylindrical concave area directly below the position where dsDNA is likely to bind (Fig 5E right, shown by pink hemispheres). Furthermore, by specifically mutating other nearby residues to arginine, we found that the *mre11-L77R* mutation also strongly suppressed *sae2Δ* camptothecin hypersensitivity (Fig 5G). As discussed further below, while it is possible that certain *mre11<sup>SUPsae2Δ</sup>* alleles somehow influence the established dsDNA-binding interface of Mre11, we speculate that *mre11-H37R/Y* and *mre11-Q70R*, and at least some of the other suppressors, act by perturbing interactions normally mediated between the Mre11 hemi-cylindrical concave region and ssDNA (modelled in Fig 5G and discussed further below). Consistent with this idea, we found that the Mre11<sup>Q70R</sup> protein was markedly impaired in binding to ssDNA but not to dsDNA (Supplementary Figs S2E and S3C). However, because P110 lies in the 'latching loop' region of eukaryotic Mre11

### Figure 5. Identifying additional mutations in *MRE11* that mediate *sae2Δ* suppression.

- Outline of the plasmid mutagenesis approach to identify new *mre11<sup>SUPsae2Δ</sup>* alleles. *LOF*: loss-of-function alleles. *SUP*: suppressor alleles.
- Mre11 with shaded boxes and blue shapes indicating phosphoesterase motifs and secondary structures, respectively; additional *mre11<sup>SUPsae2Δ</sup>* mutations recovered from the screening are indicated.
- Fungal alignment and secondary structure prediction of the region of Mre11 containing Q70.
- mre11-Q70R*, *mre11-L89V* and *mre11-P110L* alleles recovered from plasmid mutagenesis screening suppress *sae2Δ* hypersensitivity to camptothecin.
- Structural prediction of *S. cerevisiae* Mre11 residues 1–414, obtained by homology modelling using the corresponding *S. pombe* and human structures. The water-accessible surface of the two monomers is shown in different shades of blue. Red: residues whose mutation suppresses *sae2Δ* DNA damage hypersensitivity. Orange: residues whose mutation abrogates Mre11 nuclease activity.
- Model of Mre11 tertiary structure (residues 1–100). Residues are colour-coded as in (E).
- Top: *mre11-L77R* suppresses the DNA damage hypersensitivity of *sae2Δ* cells. Bottom: localisation of *mre11<sup>SUPsae2Δ</sup>* suppressors on the molecular model of the Mre11 dimer. The two Mre11 monomers are shown in different shades of blue, and the proposed path of bound ssDNA is indicated by the orange filament.
- Model in which the two DNA filaments of the two DSB ends melt when binding to Mre11; the 5' ends being channelled towards the active site and the 3' end being channelled towards the Mre11<sup>SUPsae2Δ</sup> region.

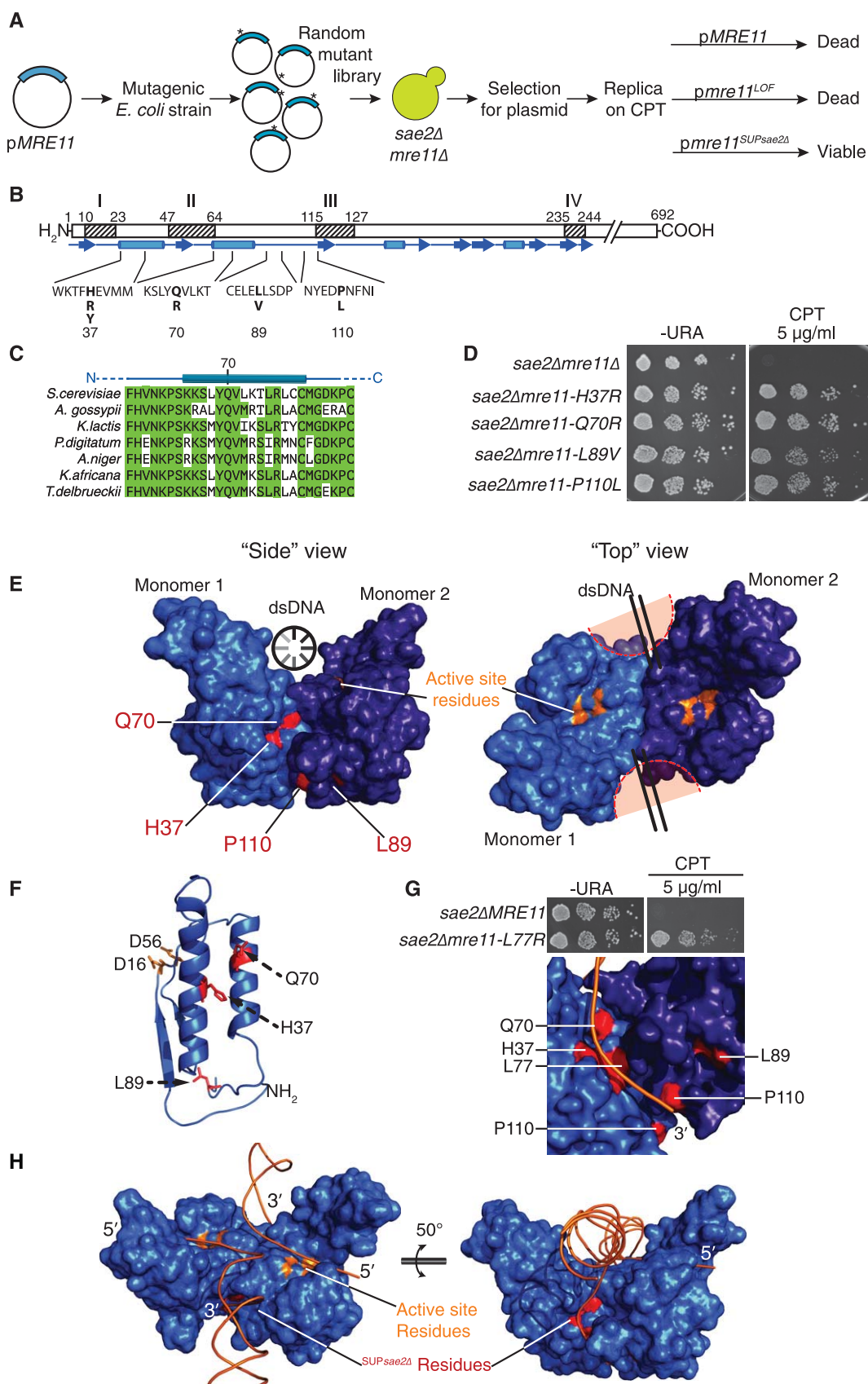
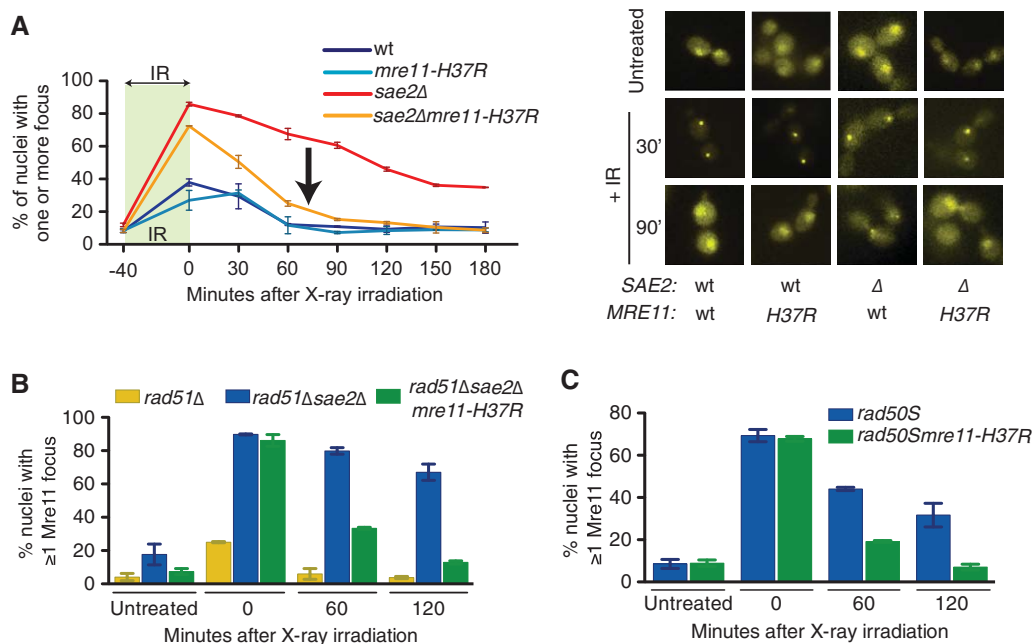


Figure 5.



**Figure 6.** *mre11<sup>SUPsae2Δ</sup>* alleles bypass the need for Sae2 to remove Mre11 from DSB ends.

- A IR-induced Mre11<sup>H37R</sup> foci (IRIF) persist for shorter times than Mre11-wt IRIF in exponentially growing *sae2Δ* cells (average and standard deviations from two or more independent experiments).
- B Effects of *sae2Δ* and *mre11-H37R* on Mre11 IRIF persistence still occur when Rad51 is absent, revealing that Mre11 IRIF persistence causes defective HR (average and standard deviation from two independent experiments).
- C *mre11-H37R* suppresses Mre11 IRIF persistence in exponentially growing *rad50S* cells (average and standard deviation from two independent experiments).

that is likely to mediate contacts with Xrs2 (Schiller *et al.*, 2012), *sae2Δ* suppression by this mutation might arise through altering such contacts. A recent report by L. Symington and colleagues reached similar conclusions (Chen *et al.*, 2015).

Taken together, our findings suggested that, in addition to its established dsDNA-binding mode, Mre11 mediates distinct, additional functional contacts with DNA that, when disrupted, lead to suppression of *sae2Δ* phenotypes. Thus, we suggest that, during DSB processing, duplex DNA entering the Mre11 structure may become partially unwound, with the 5' end being channelled towards the nuclease catalytic site and the resulting ssDNA—bearing the 3' terminal OH—interacting with an adjacent Mre11 region that contains residues mutated in *mre11<sup>SUPsae2Δ</sup>* alleles (Fig 5G and H). In this regard, we note that Mre11 was recently shown in biochemical studies to promote local DNA unwinding (Cannon *et al.*, 2013). Such a model would explain our biochemical findings, and would also explain our biological data if persistent Mre11 binding to the nascent 3' terminal DNA impairs HR unless counteracted by the actions of Sae2 or weakened by *mre11<sup>SUPsae2Δ</sup>* alleles.

#### *sae2Δ* phenotypes reflect Mre11-bound DNA repair intermediates

A prediction arising from the above model is that Mre11 persistence and associated Tel1 hyperactivation in *sae2Δ* cells would be counteracted by *mre11<sup>SUPsae2Δ</sup>* mutations. To test this, we constructed yeast strains expressing wild-type Mre11 or Mre11<sup>H37R</sup> fused to yellow-fluorescent protein (YFP) and then used fluorescence microscopy to examine their recruitment and retention at sites of DNA damage induced by ionising radiation. In line with published work (Lisby

*et al.*, 2004), recruitment of wild-type Mre11 to DNA damage foci was more robust and persisted longer when Sae2 was absent (Fig 6A). Moreover, such Mre11 DNA damage persistence in *sae2Δ* cells was largely attenuated by *mre11-H37R* (Fig 6A; compare red and orange curves). By contrast, *mre11-H37R* had little or no effect on Mre11 recruitment and dissociation kinetics when Sae2 was present (compare dark and light blue curves). Importantly, we found that HR-mediated DSB repair was not required for H37R-induced suppression of Mre11-focus persistence in *sae2Δ* cells, as persistence and suppression still occurred in the absence of the key HR factor, Rad51 (Fig 6B). Also, in accord with our other observations, we found that the *rad50S* allele caused Mre11 DNA damage-focus persistence in a manner that was suppressed by the *mre11-H37R* mutation (Fig 6C).

Previous work has established that Mre11 persistence on DSB ends, induced by lack of Sae2, leads to enhanced and prolonged DNA damage-induced Tel1 activation, associated with Rad53 hyperphosphorylation (Usui *et al.*, 2001; Lisby *et al.*, 2004; Clerici *et al.*, 2006; Fukunaga *et al.*, 2011). Supporting our data indicating that, unlike wild-type Mre11, Mre11<sup>H37R</sup> is functionally released from DNA ends even in the absence of Sae2, we found that in a *mec1Δ* background (in which Tel1 is the only kinase activating Rad53; Sanchez *et al.*, 1996), DNA damage-induced Rad53 hyperphosphorylation was suppressed by *mre11-H37R* (Fig 7A).

While we initially considered the possibility that persistent Tel1 hyperactivation might cause the DNA damage hypersensitivity of *sae2Δ* cells, we concluded that this was unlikely to be the case because *TEL1* inactivation did not suppress *sae2Δ* DNA damage hypersensitivity phenotypes (Supplementary Fig S3D). Furthermore, Tel1 loss actually reduced the ability of *mre11-H37R* to suppress the

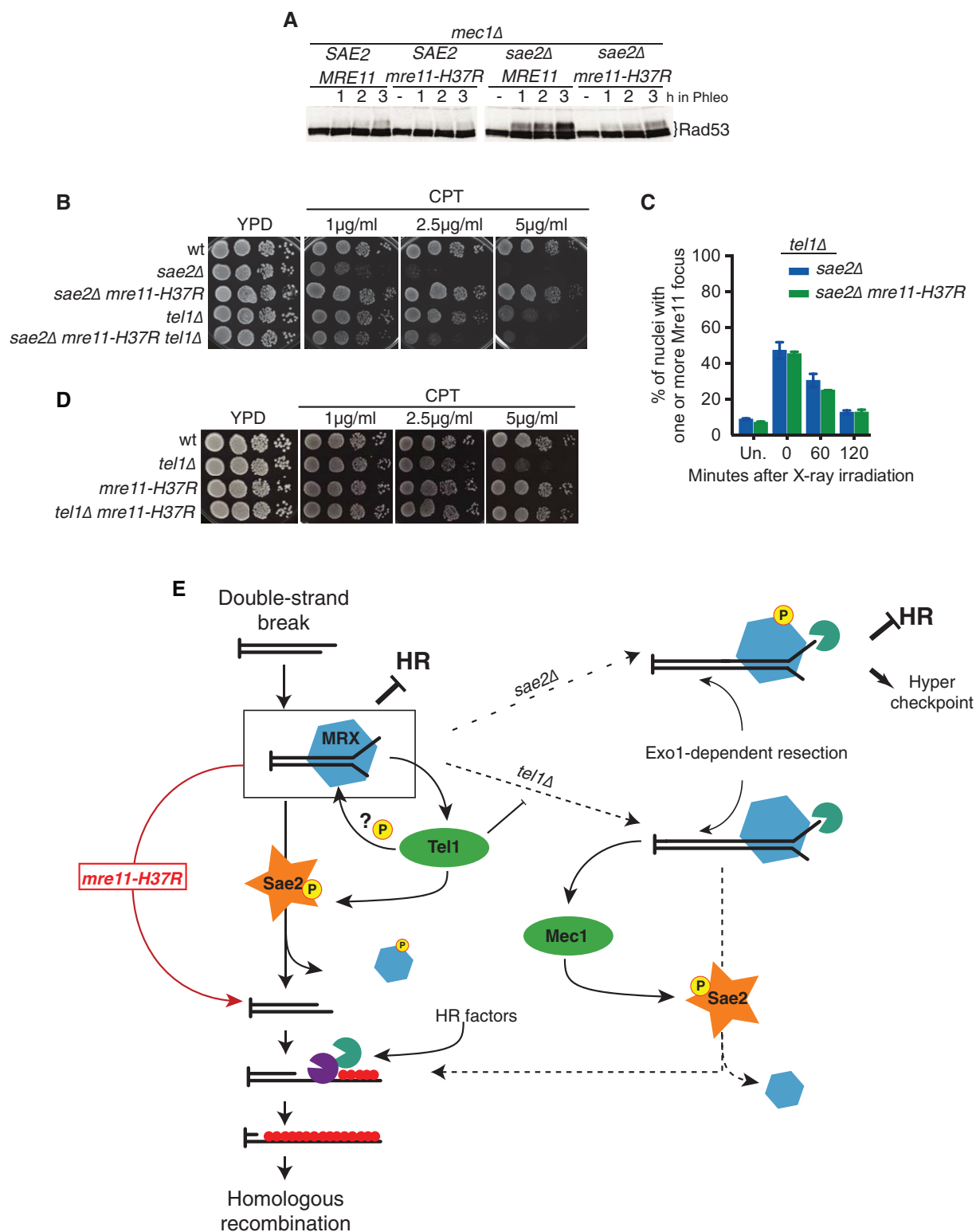


**Figure 7. Tel1 participates in regulating Mre11 dynamics after DNA damage.**

- A *mre11-H37R* suppresses Tel1 hyperactivation induced by Mre11 IRIF persistence in *sae2Δ* cells.
- B Deletion of *TEL1* weakens the suppression of the sensitivity of a *sae2Δ* strain mediated by *mre11-H37R*.
- C Deletion of *TEL1* reduces the hyperaccumulation of Mre11 to IRIF and impairs the suppression of their persistence mediated by *mre11-H37R* (average and standard deviation from two independent experiments).
- D *mre11-H37R* suppresses the sensitivity to CPT of a *tel1Δ* strain.
- E Model for the role of MRX, Sae2 and Tel1 in response to DSBs.

camptothecin hypersensitivity of *sae2Δ* cells (Fig 7B). In accord with this, in the absence of Tel1, *mre11-H37R* no longer affected the dissociation kinetics of IR-induced Mre11 foci in *sae2Δ* cells (Fig 7C). Collectively, these data suggested that Tel1 functionally cooperates with Sae2 to promote the removal of Mre11 from DNA ends. In this regard, we noted that *mre11-H37R* suppressed the moderate camptothecin hypersensitivity of a *tel1Δ* strain (Fig 7D). We therefore propose that, while persistent DNA damage-induced Tel1 activation is certainly a key feature of *sae2Δ* cells, it is persistent binding of the MRX complex to nascent 3' terminal DNA that causes toxicity in *sae2Δ* cells, likely through it delaying downstream HR events. Accordingly, mutations that reduce Mre11 ssDNA binding enhance the release of the Mre11 complex from DSB ends in the absence of Sae2, through events promoted by Tel1 (Fig 7E). In this model, Mre11 persistence at DNA damage sites is a cause, and not just a consequence, of impaired HR-mediated repair in *sae2Δ* cells.

## Discussion

Our data help resolve apparent paradoxes regarding Sae2 and MRX function by suggesting a revised model for how these and associated factors function in HR (Fig 7E). In this model, after being recruited to DSB sites and promoting Tel1 activation, resection and ensuing Mec1 activation, the MRX complex disengages from processed DNA termini in a manner promoted by Sae2 and facilitated by Tel1 and Mre11 nuclease activity. Sae2 is required to stimulate Mre11 nuclease activity (Cannavo & Cejka, 2014) and subsequently to promote MRX eviction from the DSB end. However, our data suggest that Sae2 can also promote MRX eviction in the absence of DNA-end processing, as *mre11-H37R* suppresses the phenotypes caused by *sae2Δ* and *mre11-nd* to essentially the same extent. Thus, according to our model, when Sae2 is absent, both the nuclease activities of Mre11 and MRX eviction are impaired. Under these circumstances, despite resection taking place—albeit with somewhat slower kinetics than in wild-type cells—MRX persists on ssDNA bearing the 3' terminal OH, thereby delaying repair by HR. In cells containing the *mre11-H37R* mutation, however, weakened DNA binding together with Tel1 activity promotes MRX dissociation from DNA even in the absence of Sae2, thus allowing the nascent ssDNA terminus to effectively engage in the key HR events of strand invasion and DNA synthesis (Fig 7E). Nevertheless, it is conceivable that abrogation of pathological Tel1-mediated checkpoint hyperactivation contributes to the resistance of *sae2Δmre11-H37R* cells to DNA-damaging agents. In this regard, we note that the site of one of the *sae2Δ* suppressors, P110, lies in the 'latching loop' region of eukaryotic Mre11 that is likely to mediate contacts with Xrs2 (Schiller *et al*, 2012), suggesting that, in this case, *sae2Δ* suppression might arise through weakening this interaction and dampening Tel1 activity.

Our results also highlight how the camptothecin hypersensitivity of strains carrying a nuclease-defective version of Mre11 does not reflect defective Mre11-dependent DNA-end processing *per se*, but rather stems from stalling of MRX on DNA ends. We propose that this event delays or prevents HR, possibly by impairing the removal of 3'-bound Top1 as is suggested by the fact that in *S. pombe*, *rad50S* or *mre11-nd* alleles are partially defective in Top1 removal from damaged DNA (Hartsuiker *et al*, 2009). This interpretation also offers an explanation for the higher DNA damage hypersensitivity of

*sae2Δ* cells compared to cells carrying *mre11-H125N* alleles: while *sae2Δ* cells are impaired in both Mre11 nuclease activity and Mre11 eviction—leading to MRX persistence at DNA damage sites and Tel1 hyperactivation—*mre11-H125N* cells are only impaired in Mre11 nuclease activity. Indeed, despite having no nuclease activity, the *mre11-H125N* mutation does not impair NHEJ, telomere maintenance, mating type switching or Mre11 interaction with Rad50/Xrs2 or interfere with the recruitment of the Mre11–Rad50–Xrs2 complex to foci at sites of DNA damage (Moreau *et al*, 1999; Lisby *et al*, 2004; Krogh *et al*, 2005). In addition, our model explains why the *mre11-H37R* mutation does not suppress meiotic defects of *sae2Δ* cells, because Sae2-stimulated Mre11 nuclease activity is crucial for removing Spo11 from meiotic DBS 5' termini. Finally, this model explains why *mre11-H37R* does not suppress the *sae2Δ* deficiency in DSB repair by SSA because the *sae2Δ* defect in SSA is suggested to stem from impaired bridging between the two ends of a DSB rather than from the persistence of MRX on DNA ends (Clerici *et al*, 2005; Andres *et al*, 2015; Davies *et al*, 2015). In this regard, we note that SSA does not require an extendable 3'-OH DNA terminus to proceed and so could ensue even in the presence of blocked 3'-OH DNA ends.

We have also found that the *mre11-H37R* mutation suppresses the DNA damage hypersensitivities of cells impaired in CDK- or Mec1/Tel1-mediated Sae2 phosphorylation. This suggests that such kinase-dependent control mechanisms—which may have evolved to ensure that HR only occurs after the DNA damage checkpoint has been triggered—also operate, at least in part, at the level of promoting MRX removal from partly processed DSBs. Accordingly, we found that *TEL1* deletion causes moderate hypersensitivity to camptothecin that can be rescued by the *mre11-H37R* allele, implying that the same type of toxic repair intermediate is formed in *sae2Δ* and *tel1Δ* cells and that in each case, this can be rescued by MRX dissociation caused by *mre11-H37R* (Fig 7E). Supporting this idea, it has been previously shown that resection relies mainly on Exo1 in both *tel1Δ* and *sae2Δ* cells (Clerici *et al*, 2006; Mantiero *et al*, 2007). We suggest that the comparatively mild hypersensitivity of *tel1Δ* strains to camptothecin is due to Tel1 loss allowing DSB repair intermediates to be channelled into a different pathway, in which Exo1-dependent resection (Mantiero *et al*, 2007) leads to the activation of Mec1, which can then promote Sae2 phosphorylation and subsequent MRX removal (Fig 7E). The precise role of Tel1 in these events is not yet clear, although during the course of our analyses, we found that the deletion of *TEL1* reduced the suppressive effects of *mre11-H37R* on *sae2Δ* DNA damage sensitivity and Mre11-focus persistence. This suggests that, in the absence of Sae2, Tel1 facilitates MRX eviction by *mre11-H37R*, possibly by phosphorylating the MRX complex itself.

Given the apparent strong evolutionary conservation of Sae2, the Mre11–Rad50–Xrs2 complex and their associated control mechanisms, it seems likely that the model we have proposed will also apply to other systems, including human cells. Indeed, we speculate the profound impacts of proteins such as mammalian CtIP and BRCA1 on HR may not only relate to their effects on resection but may also reflect them promoting access to ssDNA bearing 3' termini so that HR can take place effectively. Finally, our data highlight the power of SVGS to identify genetic interactions—including those such that we have defined that rely on separation-of-function mutations rather than null ones—and also to inform on underlying biological and biochemical mechanisms. In addition to

being of academic interest, such mechanisms are likely to operate in medical contexts, such as the evolution of therapy resistance in cancer.

## Materials and Methods

### Strain and plasmid construction

Yeast strains used in this work are derivatives of SK1 (meiotic phenotypes), YMV80 (SSA phenotypes) and haploid derivatives of W303 (all other phenotypes). All deletions were introduced by one-step gene disruption. pRS303-derived plasmids, carrying a wt or mutant *MRE11* version, were integrated at the *MRE11* locus in an *mre11Δ::KanMX6* strain. Alternatively, the same strain was transformed with pRS416-derived plasmids containing wild-type or mutant *MRE11* under the control of its natural promoter. Strains expressing mutated *mre11-YFP* were obtained in two steps: integration of a pRS306-based plasmid (pFP118.1) carrying a mutated version of Mre11 in a *MRE11-YFP sae2Δ* strain, followed by selection of those ‘pop-out’ events that suppressed camptothecin hypersensitivity of the starting strain. The presence of mutations was confirmed by sequencing. Full genotypes of the strains used in this study are described in Supplementary Table S1; plasmids are described in Supplementary Table S2.

### Whole-genome paired-end DNA sequencing and data analysis

DNA (1–3 μg) was sheared to 100–1,000 bp by using a Covaris E210 or LE220 (Covaris, Woburn, MA, USA) and size-selected (350–450 bp) with magnetic beads (Ampure XP; Beckman Coulter). Sheared DNA was subjected to Illumina paired-end DNA library preparation and PCR-amplified for six cycles. Amplified libraries were sequenced with the HiSeq platform (Illumina) as paired-end 100 base reads according to the manufacturer’s protocol. A single sequencing library was created for each sample, and the sequencing coverage per sample is given in Supplementary Table S3. Sequencing reads from each lane were aligned to the *S. cerevisiae* S288c assembly (RG4-1-1) from *Saccharomyces* Genome Database (obtained from the Ensembl genome browser) by using BWA (v0.5.9-r16) with the parameter ‘-q 15’. All lanes from the same library were then merged into a single BAM file with Picard tools, and PCR duplicates were marked by using Picard ‘MarkDuplicates’ (Li et al, 2009). All of the raw sequencing data are available from the ENA under accession ERP001366. SNPs and indels were identified by using the SAMtools (v0.1.19) mpileup function, which finds putative variants and indels from alignments and assigns likelihoods, and BCFtools that performs the variant calling (Li et al, 2009). The following parameters were used: for SAMtools (v0.1.19) mpileup -EDS -C50 -m2 -F0.0005 -d 10,000’ and for BCFtools (v0.1.19) view ‘-p 0.99 -vcgN’. Functional consequences of the variants were produced by using the Ensembl VEP (McLaren et al, 2010).

### *MRE11* random mutagenesis

Plasmid pRS316 carrying *MRE11* coding sequence under the control of its natural promoter was transformed into mutagenic XL1-Red competent *E. coli* cells (Agilent Technologies) and propagated

following the manufacturer’s instructions. A plasmid library of ~3,000 independent random mutant clones was transformed into *mre11Δsae2Δ* cells, and transformants were screened for their ability to survive in the presence of camptothecin. Plasmids extracted from survivors losing their camptothecin resistance after a passage on 5-fluoro-orotic acid (FOA) were sequenced and independently reintroduced in a *mre11Δsae2Δ* strain.

### Molecular modelling

A monomeric molecular model of *S. cerevisiae* Mre11 was generated with the homology modelling program MODELLER (Sali & Blundell, 1993) v9.11, using multiple structures of Mre11 from *S. pombe* (PDB codes: 4FBW and 4FBK) and human (PDB code: 3T1I) as templates. A structural alignment of them was made with the program BATON (Sali & Blundell, 1990) and manually edited to remove unmatched regions. The quality of the model was found to be native-like as evaluated by MODELLER’s NDOPE (–1.2) and GA341 (1.0) metrics and the QMEAN server (Benkert et al, 2009) (<http://swissmodel.expasy.org/qmean/>) (0.705). The monomeric model was subsequently aligned on the dimeric assembly of the 4FBW template to generate a dimer, and the approximate position of DNA binding was determined by aligning the *P. furiosus* structure containing dsDNA (PDB code: 3DSC) with the dimeric model. All images were obtained using the PyMOL Molecular Graphics System.

### Microscopy

Exponentially growing yeast strains carrying wild-type or mutant Mre11-YFP were treated with 40 Gy of ionising radiations with a Faxitron irradiator (CellRad). At regular intervals, samples were taken and fixed with 500 μl of Fixing Solution (4% paraformaldehyde, 3.4% sucrose). Cells were subsequently washed with wash solution (100 mM potassium phosphate pH 7.5, 1.2 M sorbitol) and mounted on glass slides. Images were taken at a DeltaVision microscope. All these experiments were carried out at 30°C.

### In vitro assays

For the electrophoretic mobility shift assay (EMSA), a radiolabelled DNA substrate (5 nM) was incubated with the indicated amount of Mre11 or Mre11<sup>H37R</sup> in 10 μl buffer (25 mM Tris-HCl, pH 7.5, 1 mM DTT, 100 μg/ml BSA, 150 mM KCl) at 30°C for 10 min. The reaction mixtures were resolved in a 10% polyacrylamide gel in TBE buffer (89 mM Tris-borate, pH 8.0, 2 mM EDTA). The gel was dried onto Whatman DE81 paper and then subjected to phosphorimaging analysis. For nuclease assay, 1 mM MnCl<sub>2</sub> was added to the reactions and the reaction mixtures were incubated at 30°C for 20 min and deproteinised by treatment with 0.5% SDS and 0.5 mg/ml proteinase K for 5 min at 37°C before analysis in a 10% polyacrylamide gel electrophoresis in TBE buffer.

Additional Materials and Methods can be found in the Supplementary Methods.

Supplementary information for this article is available online: <http://emboj.embopress.org>

## Acknowledgements

We thank M.P. Longhese, R. Rothstein and J. Haber for providing strains and plasmids; Sir T. Blundell and T. Ochi for advice on structural biology and for providing comments to the manuscript. Research in the Jackson laboratory is funded by Cancer Research UK Programme Grant C6/A11224, the European Research Council and the European Community Seventh Framework Programme Grant Agreement No. HEALTH-F2-2010-259893 (DDResponse). Core funding is provided by CRUK (C6946/A14492) and the Wellcome Trust (WT092096). SPJ receives his salary from the University of Cambridge, UK, supplemented by CRUK. TO, IG and FP were funded by Framework Programme Grant Agreement No. HEALTH-F2-2010-259893 (DDResponse). FP also received funding from EMBO (Fellowship ALTF 1287-2011); NG and IS are funded by the Wellcome Trust (101126/Z/13/Z). DJA and TMK were supported by Cancer Research UK and the Wellcome Trust (WT098051). PS and HN were supported by NIH grants RO1ES007061 and K99ES021441, respectively.

## Author contributions

The initial screening was conceived and designed by TO, EV, DJA and SPJ. Alignment of whole-genome sequencing data, variant calling and subsequent analysis was carried out by MH and TMK. Experiments for the *in vivo* characterisation of the *mre11-H37R* mutant were conceived by TO, IG, FP and SPJ, and were carried out by TO, FP, IG, NJG, EV and IS. Biochemical assays were designed by SPJ, PS and HN and carried out by HN. The identification of further *mre11<sup>SupSae2Δ</sup>* mutants was designed by FP and SPJ and carried out by NJG. Modelling of *S. cerevisiae* Mre11 was performed by BO-M, and subsequent analyses were carried out by BO-M and FP. The manuscript was largely written by SPJ and FP, and was edited by all other authors.

## Conflict of interest

The authors declare that they have no conflict of interest.

## References

- Andres SN, Appel CD, Westmoreland JW, Williams JS, Nguyen Y, Robertson PD, Resnick MA, Williams RS (2015) Tetrameric Ctp1 coordinates DNA binding and DNA bridging in DNA double-strand-break repair. *Nat Struct Mol Biol* 22: 158–166
- Baroni E, Viscardi V, Cartagena-Lirola H, Lucchini G, Longhese MP (2004) The functions of budding yeast Sae2 in the DNA damage response require Mec1- and Tel1-dependent phosphorylation. *Mol Cell Biol* 24: 4151–4165
- Barton O, Naumann SC, Diemer-Biehs R, Künzel J, Steinlage M, Conrad S, Makharashvili N, Wang J, Feng L, Lopez BS, Paull TT, Chen J, Jeggo PA, Löbrich M (2014) Polo-like kinase 3 regulates CtIP during DNA double-strand break repair in G1. *J Cell Biol* 206: 877–894
- Benkert P, Tosatto SCE, Schomburg D (2008) QMEAN: a comprehensive scoring function for model quality assessment. *Proteins* 71: 261–277
- Benkert P, Künzli M, Schwede T (2009) QMEAN server for protein model quality estimation. *Nucleic Acids Res* 37: W510–W514
- Cannavo E, Cejka P (2014) Sae2 promotes dsDNA endonuclease activity within Mre11–Rad50–Xrs2 to resect DNA breaks. *Nature* 514, 122–125
- Cannon B, Kuhnlein J, Yang S-H, Cheng A, Schindler D, Stark JM, Russell R, Paull TT (2013) Visualization of local DNA unwinding by Mre11/Rad50/Nbs1 using single-molecule FRET. *Proc Natl Acad Sci USA* 110: 18868–18873
- Chen H, Donnianni RA, Handa N, Deng SK, Oh J, Timashev LA, Kowalczykowski SC, Symington LS (2015) Sae2 promotes DNA damage resistance by removing the Mre11–Rad50–Xrs2 complex from DNA and attenuating Rad53 signaling. *Proc Natl Acad Sci USA* 112: E1880–E1887
- Clerici M, Mantiero D, Lucchini G, Longhese MP (2005) The *Saccharomyces cerevisiae* Sae2 protein promotes resection and bridging of double strand break ends. *J Biol Chem* 280: 38631–38638
- Clerici M, Mantiero D, Lucchini G, Longhese MP (2006) The *Saccharomyces cerevisiae* Sae2 protein negatively regulates DNA damage checkpoint signalling. *EMBO Rep* 7: 212–218
- Daley JM, Palmbos PL, Wu D, Wilson TE (2005) Nonhomologous end joining in yeast. *Annu Rev Genet* 39: 431–451
- Davies OR, Forment JV, Sun M, Belotserkovskaya R, Coates J, Galanty Y, Demir M, Morton CR, Rzechorzek NJ, Jackson SP, Pellegrini L (2015) CtIP tetramer assembly is required for DNA-end resection and repair. *Nat Struct Mol Biol* 22: 150–157
- Deng C, Brown JA, You D, Brown JM (2005) Multiple endonucleases function to repair covalent topoisomerase I complexes in *Saccharomyces cerevisiae*. *Genetics* 170: 591–600
- Fishman-Lobell J, Rudin N, Haber JE (1992) Two alternative pathways of double-strand break repair that are kinetically separable and independently modulated. *Mol Cell Biol* 12: 1292–1303
- Foster SS, Balestrini A, Petrini JHJ (2011) Functional interplay of the Mre11 nuclease and Ku in the response to replication-associated DNA damage. *Mol Cell Biol* 31: 4379–4389
- Fukunaga K, Kwon Y, Sung P, Sugimoto K (2011) Activation of protein kinase Tel1 through recognition of protein-bound DNA ends. *Mol Cell Biol* 31: 1959–1971
- Furuse M, Nagase Y, Tsubouchi H, Murakami-Murofushi K, Shibata T, Ohta K (1998) Distinct roles of two separable *in vitro* activities of yeast Mre11 in mitotic and meiotic recombination. *EMBO J* 17: 6412–6425
- Goldway M, Sherman A, Zenvirth D, Arbel T, Simchen G (1993) A short chromosomal region with major roles in yeast chromosome III meiotic disjunction, recombination and double strand breaks. *Genetics* 133: 159–169
- Hardy J, Churikov D, Géli V, Simon M-N (2014) Sgs1 and Sae2 promote telomere replication by limiting accumulation of ssDNA. *Nat Commun* 5: 5004
- Hartsuiker E, Neale MJ, Carr AM (2009) Distinct requirements for the Rad32Mre11 nuclease and Ctp1CtIP in the removal of covalently bound topoisomerase I and II from DNA. *Mol Cell* 33: 117–123
- Hopfner KP, Karcher A, Shin DS, Craig L, Arthur LM, Carney JP, Tainer JA (2000) Structural biology of Rad50 ATPase: ATP-driven conformational control in DNA double-strand break repair and the ABC-ATPase superfamily. *Cell* 101: 789–800
- Huertas P, Cortés-Ledesma F, Sartori AA, Aguilera A, Jackson SP (2008) CDK targets Sae2 to control DNA-end resection and homologous recombination. *Nature* 455: 689–692
- Huertas P, Jackson SP (2009) Human CtIP mediates cell cycle control of DNA end resection and double strand break repair. *J Biol Chem* 284: 9558–9565
- Ivanov EL, Sugawara N, White CI, Fabre F, Haber JE (1994) Mutations in XRS2 and RAD50 delay but do not prevent mating-type switching in *Saccharomyces cerevisiae*. *Mol Cell Biol* 14: 3414–3425
- Jackson SP, Bartek J (2009) The DNA-damage response in human biology and disease. *Nature* 461: 1071–1078
- Keeney S, Kleckner N (1995) Covalent protein-DNA complexes at the 5' strand termini of meiosis-specific double-strand breaks in yeast. *Proc Natl Acad Sci USA* 92: 11274–11278

- Keeney S, Giroux CN, Kleckner N (1997) Meiosis-specific DNA double-strand breaks are catalyzed by Spo11, a member of a widely conserved protein family. *Cell* 88: 375–384
- Krogh BO, Llorente B, Lam A, Symington LS (2005) Mutations in Mre11 phosphoesterase motif I that impair *Saccharomyces cerevisiae* Mre11-Rad50-Xrs2 complex stability in addition to nuclease activity. *Genetics* 171: 1561–1570
- Lengsfeld BM, Rattray AJ, Bhaskara V, Ghirlando R, Paull TT (2007) Sae2 is an endonuclease that processes hairpin DNA cooperatively with the Mre11/Rad50/Xrs2 complex. *Mol Cell* 28: 638–651
- Li H, Handsaker B, Wysoker A, Fennell T, Ruan J, Homer N, Marth G, Abecasis G, Durbin R (2009) The sequence alignment/Map format and SAMtools. *Bioinformatics* 25: 2078–2079
- Lisby M, Barlow JH, Burgess RC, Rothstein R (2004) Choreography of the DNA damage response: spatiotemporal relationships among checkpoint and repair proteins. *Cell* 118: 699–713
- Makharashvili N, Tubbs AT, Yang S-H, Wang H, Barton O, Zhou Y, Deshpande RA, Lee J-H, Lobrich M, Sleckman BP, Wu X, Paull TT (2014) Catalytic and noncatalytic roles of the CtIP endonuclease in double-strand break end resection. *Mol Cell* 54: 1022–1033
- Mantiero D, Clerici M, Lucchini G, Longhese MP (2007) Dual role for *Saccharomyces cerevisiae* Tel1 in the checkpoint response to double-strand breaks. *EMBO Rep* 8: 380–387
- McLaren W, Pritchard B, Rios D, Chen Y, Flicek P, Cunningham F (2010) Deriving the consequences of genomic variants with the Ensembl API and SNP effect predictor. *Bioinformatics* 26: 2069–2070
- Mimitou EP, Symington LS (2008) Sae2, Exo1 and Sgs1 collaborate in DNA double-strand break processing. *Nature* 455: 770–774
- Mimitou EP, Symington LS (2010) Ku prevents Exo1 and Sgs1-dependent resection of DNA ends in the absence of a functional MRX complex or Sae2. *EMBO J* 29: 3358–3369
- Moreau S, Ferguson JR, Symington LS (1999) The nuclease activity of Mre11 is required for meiosis but not for mating type switching, end joining, or telomere maintenance. *Mol Cell Biol* 19: 556–566
- Moreau S, Morgan EAA, Symington LSS (2001) Overlapping functions of the *Saccharomyces cerevisiae* mre11, exo1 and rad27 nucleases in DNA metabolism. *Genetics* 159: 1423
- Nairz K, Klein F (1997) mre11S—a yeast mutation that blocks double-strand-break processing and permits nonhomologous synapsis in meiosis. *Genes Dev* 11: 2272–2290
- Prinz S, Amon A, Klein F (1997) Isolation of COM1, a new gene required to complete meiotic double-strand break-induced recombination in *Saccharomyces cerevisiae*. *Genetics* 146: 781–795
- Sali A, Blundell TL (1990) Definition of general topological equivalence in protein structures. A procedure involving comparison of properties and relationships through simulated annealing and dynamic programming. *J Mol Biol* 212: 403–428
- Sali A, Blundell TL (1993) Comparative protein modelling by satisfaction of spatial restraints. *J Mol Biol* 234: 779–815
- Sanchez Y, Desany BA, Jones WJ, Liu Q, Wang B, Elledge SJ (1996) Regulation of RAD53 by the ATM-like kinases MEC1 and TEL1 in yeast cell cycle checkpoint pathways. *Science* 271: 357–360
- Sartori AA, Lukas C, Coates J, Mistrik M, Fu S, Bartek J, Baer R, Lukas J, Jackson SP (2007) Human CtIP promotes DNA end resection. *Nature* 450: 509–514
- Schiller CB, Lammens K, Guerini I, Coords B, Feldmann H, Schlauderer F, Möckel C, Schele A, Strässer K, Jackson SP, Hopfner K-P (2012) Structure of Mre11-Nbs1 complex yields insights into ataxia-telangiectasia-like disease mutations and DNA damage signaling. *Nat Struct Mol Biol* 19: 693–700
- Stracker TH, Petrini JHJ (2011) The MRE11 complex: starting from the ends. *Nat Rev Mol Cell Biol* 12: 90–103
- Symington LS, Gautier J (2011) Double-strand break end resection and repair pathway choice. *Annu Rev Genet* 45: 247–271
- Usui T, Ogawa H, Petrini JH (2001) A DNA damage response pathway controlled by Tel1 and the Mre11 complex. *Mol Cell* 7: 1255–1266
- Vaze MB, Pelliccioli A, Lee SE, Ira G, Liberi G, Arbel-Eden A, Foiani M, Haber JE (2002) Recovery from checkpoint-mediated arrest after repair of a double-strand break requires Srs2 helicase. *Mol Cell* 10: 373–385
- Wang H, Li Y, Truong LN, Shi LZ, Hwang PY-H, He J, Do J, Cho MJ, Li H, Negrete A, Shiloach J, Berns MW, Shen B, Chen L, Wu X (2014) CtIP maintains stability at common fragile sites and inverted repeats by end resection-independent endonuclease activity. *Mol Cell* 54: 1012–1021
- Williams RS, Moncalian G, Williams JS, Yamada Y, Limbo O, Shin DS, Grocock LM, Cahill D, Hitomi C, Guenther G, Moiani D, Carney JP, Russell P, Tainer JA (2008) Mre11 dimers coordinate DNA end bridging and nuclease processing in double-strand-break repair. *Cell* 135: 97–109
- You Z, Shi LZ, Zhu Q, Wu P, Zhang Y-W, Basilio A, Tonnu N, Verma IM, Berns MW, Hunter T (2009) CtIP links DNA double-strand break sensing to resection. *Mol Cell* 36: 954–969
- Zhu Z, Chung W-H, Shim EY, Lee SE, Ira G (2008) Sgs1 helicase and two nucleases Dna2 and Exo1 resect DNA double-strand break ends. *Cell* 134: 981–994



**License:** This is an open access article under the terms of the Creative Commons Attribution 4.0 License, which permits use, distribution and reproduction in any medium, provided the original work is properly cited.

1 **Genome-wide genetic screening with chemically-mutagenized haploid**  
2 **embryonic stem cells**

3

4 Josep V. Forment<sup>1,2</sup>, Mareike Herzog<sup>1,2</sup>, Julia Coates<sup>1</sup>, Tomasz Konopka<sup>3</sup>, Bianca V.  
5 Gapp<sup>3</sup>, Sebastian M. Nijman<sup>3,4</sup>, David J. Adams<sup>2</sup>, Thomas M. Keane<sup>2</sup> and Stephen  
6 P. Jackson<sup>1,2</sup>

7

8 <sup>1</sup>The Wellcome Trust CRUK Gurdon Institute and Department of Biochemistry,  
9 University of Cambridge, Cambridge, UK

10

11 <sup>2</sup>The Wellcome Trust Sanger Institute, Hinxton, Cambridge, UK

12

13 <sup>3</sup>Ludwig Institute for Cancer Research Ltd. and Target Discovery Institute, Nuffield  
14 Department of Medicine, University of Oxford, Oxford, UK

15

16 <sup>4</sup>Research Center for Molecular Medicine of the Austrian Academy of Sciences  
17 (CeMM), Vienna, Austria

18

19 **Authors for correspondence:**

20 Josep V. Forment [j.forment@gurdon.cam.ac.uk](mailto:j.forment@gurdon.cam.ac.uk)

21 Stephen P. Jackson [s.jackson@gurdon.cam.ac.uk](mailto:s.jackson@gurdon.cam.ac.uk)

22

23 **Abstract**

24 In model organisms, classical genetic screening via random mutagenesis has  
25 provided key insights into the molecular bases of genetic interactions, helping  
26 defining synthetic-lethality, -viability and drug-resistance mechanisms. The limited  
27 genetic tractability of diploid mammalian cells, however, has precluded this  
28 approach. Here, we demonstrate the feasibility of classical genetic screening in  
29 mammalian systems by using haploid cells, chemical mutagenesis and next-  
30 generation sequencing, providing a new tool to explore mammalian genetic  
31 interactions.

32

33 Classical genetic screens with mutagens have been extremely valuable in assigning  
34 functionality to genes in many model organisms<sup>1-3</sup>. Since most mutagenic agents  
35 yield random single-nucleotide variants (SNVs), clustering of mutations can provide  
36 valuable information on the functionality of protein domains and also define key  
37 amino acid residues<sup>4</sup>. The discovery of RNA interference (RNAi) allowed forward  
38 genetic screening in human cell cultures<sup>4</sup> and, more recently, insertional  
39 mutagenesis in near-haploid human cancer cells<sup>5</sup> and whole-genome CRISPR/Cas9  
40 small-guide RNA (sgRNA) libraries have been used for this purpose<sup>6-8</sup>. Although  
41 powerful, such loss-of-function (LOF) approaches miss phenotypes caused by  
42 separation-of-function or gain-of-function SNV mutations<sup>9,10</sup>, are less informative on  
43 protein function, and are not well suited to studying functions of essential genes.  
44 Here, we describe the generation of SNV-mutagenized mammalian cell libraries, and  
45 establish their suitability to identify recessive suppressor mutations using resistance  
46 to the antimetabolite 6-thioguanine (6-TG) as a proof-of-principle.

47

48 Comprehensive libraries of homozygous SNV-containing mutant clones are not  
49 feasible to obtain in cells with diploid genomes. To circumvent this issue, we used  
50 H129-3 haploid mouse embryonic stem cells (mESCs)<sup>11</sup> treated with varying doses  
51 of the DNA-alkylating agent ethylmethanesulfonate (EMS), a chemical inducer of  
52 SNVs<sup>12</sup> (**Fig. 1a, Supp. Fig. 1a**). For comparison purposes, the same procedure was  
53 performed on diploid H129-3 mESCs (**Supp. Fig. 1b**). Haploid and diploid mutant  
54 libraries were then screened for suppressors of cellular sensitivity to the toxic  
55 nucleotide precursor 6-TG (**Fig. 1b**). Libraries of the EMS dose that produced more  
56 6-TG resistant clones showed a near 6-fold difference between haploid and diploid  
57 cells (**Supp. Fig. 1c**), highlighting the increased accumulation of suppressor  
58 mutations in the haploid genetic background.

59 196 resistant clones were isolated from haploid libraries treated with 6-TG. To test  
60 the feasibility of identifying causative suppressor mutations, DNA from seven of  
61 these resistant clones and from control mESCs not treated with EMS was subjected  
62 to whole-exome sequencing. Homozygous SNVs and base insertions/deletions  
63 (INDELs) were identified (**Fig. 1c**), and only a small proportion of them affected  
64 coding sequences and were non-synonymous (**Fig. 1d, Supp. Table 1**). When

65 analyzing this subset, suppressor gene candidates were defined as those appearing  
66 mutated in multiple independent clones and harboring potential deleterious mutations  
67 **(Supp. Table 1)**. Importantly, *Hprt*, the gene encoding hypoxanthine-guanine  
68 phosphoribosyltransferase, the sole 6-TG target<sup>13</sup> **(Fig. 1b)**, appeared mutated in  
69 five of the sequenced clones. Moreover, it was the only candidate suppressor gene  
70 carrying potentially deleterious mutations in all clones where mutational  
71 consequences could be assigned **(Fig. 1e, Supp. Table 1)**. These results  
72 established that, without using any previous knowledge regarding the identity of  
73 suppressor loci, we identified *Hprt* as a top gene candidate after sequencing of very  
74 few clones.

75

76 In addition to mutations in the *Hprt* gene, inactivation of DNA mismatch repair (MMR)  
77 protein components Msh2, Msh6, Mlh1 and Pms2 has also been shown to confer  
78 resistance to 6-TG<sup>14</sup>, as does mutations in DNA methyltransferase Dnmt1<sup>15</sup>. In fact,  
79 the two whole-exome sequenced clones that did not carry mutations in *Hprt*  
80 presented nonsense mutations in *Msh6* and *Pms2* **(Supp. Table 1, Supp. Fig. 1d)**.  
81 To analyze coverage of the mutant libraries, we subjected the 189 additional  
82 suppressor clones to targeted sequencing of the known suppressor genes **(Fig. 1b)**.  
83 Importantly, deleterious mutations in most of these genes were identified in several  
84 independent resistant clones **(Fig. 2a, Supp. Table 2)**. Thus, if the same non-  
85 targeted whole-exome sequence approach carried out in the initial analysis of seven  
86 suppressor clones would have been applied to all of them, *Hprt*, *Msh2*, *Msh6*, *Mlh1*  
87 and *Pms2* (as genes carrying independent homozygous deleterious mutations in  
88 different resistant clones) would have been identified as strong suppressor gene  
89 candidates, confirming the feasibility of the approach.

90 Interestingly, a subset of clones presented heterozygous deleterious mutations in  
91 known suppressor genes **(Supp. Table 2)**. These could have arisen after  
92 diploidization of the original EMS-treated haploid population, or could have occurred  
93 in the small proportion of diploid H129-3 cells present during EMS treatment of the  
94 enriched haploid population **(Fig. 1a)**. Regardless of their origin, deleterious  
95 heterozygous mutations could only generate 6-TG resistance if each would affect  
96 one allele of the gene, effectively inactivating both copies. Heterozygous mutations in

97 the *Dnmt1* gene occurred in such close proximity that they could be analyzed from  
98 the same sequencing reads. No co-occurrence of heterozygous mutations in the  
99 same reads indicated that *Dnmt1* mutant clones were compound heterozygotes (**Fig.**  
100 **2b**). As these mutations all scored as potentially deleterious for Dnmt1 protein  
101 function (**Supp. Table 2**), it is likely that they are causative of the suppression to 6-  
102 TG sensitivity in these clones (see below). When deleterious heterozygous mutations  
103 were taken into account, *Dnmt1* could also be included in the list of suppressor gene  
104 candidates (**Fig. 2c**).

105

106 Highlighting the applicability of the methodology to identify functionally important  
107 protein regions, missense and nonsense variants linked to clinically-relevant  
108 mutations in *Hprt* (causative of the inherited neurological disorder Lesch-Nyhan  
109 syndrome and its variants<sup>16</sup>) and in genes involved in DNA MMR (linked to the  
110 inherited colon cancer predisposition Lynch syndrome<sup>17</sup>) were effectively retrieved  
111 (**Fig. 3a**). Furthermore, and due to the mutational preferences of EMS (see below),  
112 mRNA splicing variant mutations potentially affecting total protein levels of Dnmt1,  
113 *Hprt*, *Mlh1*, *Msh2* and *Msh6* were also found (**Supp. Table 2**). These were  
114 particularly prevalent in *Hprt* (**Fig. 3a**), and a detailed analysis of them confirmed  
115 their deleterious consequence at the protein level (**Supp. Figure 2**). Production of  
116 aberrant mRNA splicing forms, with the subsequent reduction or absence of protein  
117 product, is thus an important consequence of the mutagenic action of EMS.

118 Non-described mutations in *Dnmt1*, *Hprt*, *Mlh1*, *Msh6* and *Pms2* were also identified,  
119 most of which with predicted deleterious effects on the protein product (**Fig. 3b**,  
120 **Supp. Table 2**). Newly identified A612T and G1157E mutations in *Mlh1* and *Dnmt1*,  
121 respectively, were introduced *de novo* into wild-type mESCs by CRISPR/Cas9 gene  
122 editing (**Supp. Fig. 3**). We chose these mutations as they are missense mutations  
123 only identified in heterozygotes, and we wanted to test their ability to generate  
124 suppression when occurring in homozygosis. Importantly, H129-3 mESCs carrying  
125 engineered A612T *Mlh1* or G1157E *Dnmt1* mutations were resistant to 6-TG  
126 treatment to differing extents when compared to their wild type counterparts (**Fig.**  
127 **3c**), showing their potential as causative mutations of the suppressor phenotype.

128

129 A small group of resistant clones (23) did not present mutations in any of the known  
130 suppressor genes (**Fig. 2a,c**). These “orphan” clones were subjected to whole-  
131 exome DNA sequencing and RNA sequencing. DNA sequencing of the unassigned  
132 suppressor clones and several control samples allowed an unprecedented  
133 description of EMS mutagenic action at the whole-exome level, confirming its  
134 preference in producing SNVs, and transitions rather than transversions (**Supp. Fig.**  
135 **4**). Although whole-exome sequencing effectively retrieved causative mutations in all  
136 control samples resistant to 6-TG, no other obvious gene candidate could be  
137 identified from the remaining orphan suppressors (**Supp. Table 3**). RNA sequencing,  
138 however, revealed significantly reduced expression levels of *Hprt*, *Mlh1* or *Msh6* as  
139 potential causes of suppression in several such clones (**Fig. 3d,e; Supp. Table 4**).  
140 Further studies will be required to define whether epigenetic alterations or mutations  
141 in transcriptional regulatory sequences outside of exon regions, and hence not  
142 covered during DNA sequencing, could explain the nature of these orphan  
143 suppressor clones.

144

145 Collectively, our findings establish that classical genetic screening can be effectively  
146 performed in mammalian systems by combining the use of haploid cells, a chemical  
147 inducer of SNVs, and next-generation DNA and RNA sequencing techniques. Use of  
148 haploid cells when creating libraries of SNV mutants allowed identification of  
149 recessive suppressor point mutations, in contrast to diploid cell screening where only  
150 dominant mutations are effectively retrieved<sup>18</sup>. Furthermore, EMS induction of SNVs  
151 allowed generation of complex mutant libraries, thus increasing the probability of  
152 identification of suppressor loci compared to isolation of rare, spontaneous  
153 suppressor events<sup>19</sup>. Importantly, through screening for cellular resistance to 6-TG  
154 we identified point mutations in all described suppressor genes, showing high  
155 coverage capability. Moreover, as we have established for 6-TG suppressor loci,  
156 SNVs have value in delineating key residues required for protein function, thus  
157 helping to explain molecular mechanisms of suppression. SNV-based mutagenesis  
158 will also be a useful technique to investigate genetic interactions of essential genes,  
159 and we envisage the applicability of this approach into haploid cells of human  
160 origin<sup>20-22</sup>. Chemical mutagenesis of haploid cells, either alone or in combination with

161 LOF screens, thus has the potential to bring functional genomics in mammalian  
162 systems to a hitherto unachieved comprehensive level.

163

164 **Methods**

165 Methods and any associated references are available in the online version of the  
166 paper.

167

168 **Figure legends**

169

170 **Figure 1. Generation of mutagenized libraries. (a)** Experimental workflow. **(b)**  
171 Schematic of 6-TG metabolism and genotoxicity. Inactivating mutations in the genes  
172 highlighted in red have been shown to confer resistance to 6-TG. **(c)** Mutation types  
173 identified by whole-exome sequencing of 7 suppressor clones. **(d)** Consequences of  
174 identified mutations. **(e)** Genes harboring independent mutations in different clones.  
175 Mutations were assigned as deleterious or neutral according to PROVEAN and SIFT  
176 software (see Methods).

177

178 **Figure 2. Identification of suppressor mutations. (a)** Distribution of homozygous  
179 mutations identified in suppressor gene candidates; numbers of independent clones  
180 are in brackets and types of *Hprt* mutations are shown in detail. **(b)** Examples of  
181 sequencing reads obtained for heterozygous mutations affecting the *Dnmt1* gene.  
182 SNVs causing missense mutations G1157E or G1157R (top panel) and G1477R or  
183 affecting the splicing donor sequence on intron 36 (bottom panel; see also Supp. Fig.  
184 2), were never detected in the same sequencing read, indicating that they locate to  
185 different alleles. **(c)** Distribution of suppressor gene candidate mutations identified,  
186 including heterozygous deleterious mutations.

187

188 **Figure 3. Clinically-relevant and newly-identified suppressor mutations. (a)**  
189 Distribution of point mutations on Dnmt1, Hprt and MMR proteins; each square  
190 represents an independent clone. Asterisks (\*) denote STOP-codon gains. **(b)**  
191 Predicted consequences of potential new suppressor mutations. Consequences  
192 were predicted as in Fig. 1e. **(c)** *De novo* introduction of new mutations Dnmt1  
193 G1157E and Mlh1 A612T confers cellular resistance to 6-TG. **(d)** *Hprt*, *Mlh1* and  
194 *Msh6* mRNA expression levels (fragments per kilobase per million reads). Black dots  
195 indicate wild-type (WT) samples, red dots represent clones with already identified  
196 mutations (controls), and white dots represent samples for which no causative  
197 mutations were identified (see Supp. Table 2 for identifiers). Error bars represent  
198 uncertainties on expression estimates. **(e)** Reduced *Hprt* mRNA levels correspond to  
199 reduced protein production as detected by western blot.



201 **References**

- 202 1. Forsburg, S. L. The art and design of genetic screens: yeast. *Nat Rev Genet* **2**,  
203 659–668 (2001).
- 204 2. St Johnston, D. The art and design of genetic screens: *Drosophila*  
205 *melanogaster*. *Nat Rev Genet* **3**, 176–188 (2002).
- 206 3. Jorgensen, E. M. & Mango, S. E. The art and design of genetic screens:  
207 *Caenorhabditis elegans*. *Nat Rev Genet* **3**, 356–369 (2002).
- 208 4. Boutros, M. & Ahringer, J. The art and design of genetic screens: RNA  
209 interference. *Nat Rev Genet* **9**, 554–566 (2008).
- 210 5. Carette, J. E. *et al.* Haploid genetic screens in human cells identify host factors  
211 used by pathogens. *Science* **326**, 1231–1235 (2009).
- 212 6. Koike-Yusa, H., Li, Y., Tan, E.-P., Velasco-Herrera, M. D. C. & Yusa, K.  
213 Genome-wide recessive genetic screening in mammalian cells with a lentiviral  
214 CRISPR-guide RNA library. *Nat Biotechnol* **32**, 267–273 (2014).
- 215 7. Shalem, O. *et al.* Genome-scale CRISPR-Cas9 knockout screening in human  
216 cells. *Science* **343**, 84–87 (2014).
- 217 8. Wang, T., Wei, J. J., Sabatini, D. M. & Lander, E. S. Genetic screens in human  
218 cells using the CRISPR-Cas9 system. *Science* **343**, 80–84 (2014).
- 219 9. Rolef Ben-Shahar, T. *et al.* Eco1-dependent cohesin acetylation during  
220 establishment of sister chromatid cohesion. *Science* **321**, 563–566 (2008).
- 221 10. Puddu, F. *et al.* Synthetic viability genomic screening defines Sae2 function in  
222 DNA repair. *Embo J* **34**, 1509–1522 (2015).
- 223 11. Leeb, M. & Wutz, A. Derivation of haploid embryonic stem cells from mouse  
224 embryos. *Nature* **479**, 131–134 (2011).
- 225 12. Munroe, R. R. & Schimenti, J. J. Mutagenesis of mouse embryonic stem cells  
226 with ethylmethanesulfonate. *Methods Mol. Biol.* **530**, 131–138 (2009).
- 227 13. LePage, G. A. & Jones, M. Purinethiols as feedback inhibitors of purine  
228 synthesis in ascites tumor cells. *Cancer Res* **21**, 642–649 (1961).
- 229 14. Swann, P. F. *et al.* Role of postreplicative DNA mismatch repair in the cytotoxic  
230 action of thioguanine. *Science* **273**, 1109–1111 (1996).
- 231 15. Guo, G., Wang, W. & Bradley, A. Mismatch repair genes identified using  
232 genetic screens in Blm-deficient embryonic stem cells. *Nature* **429**, 891–895

- 233 (2004).
- 234 16. Jinnah, H. A., De Gregorio, L., Harris, J. C., Nyhan, W. L. & O'Neill, J. P. The  
235 spectrum of inherited mutations causing HPRT deficiency: 75 new cases and a  
236 review of 196 previously reported cases. *Mutat Res* **463**, 309–326 (2000).
- 237 17. Jiricny, J. Postreplicative mismatch repair. *Cold Spring Harb Perspect Biol* **5**,  
238 a012633 (2013).
- 239 18. Kasap, C., Elemento, O. & Kapoor, T. M. DrugTargetSeqR: a genomics- and  
240 CRISPR-Cas9-based method to analyze drug targets. *Nat Chem Biol* **10**, 626–  
241 628 (2014).
- 242 19. Smurnyy, Y. *et al.* DNA sequencing and CRISPR-Cas9 gene editing for target  
243 validation in mammalian cells. *Nat Chem Biol* **10**, 623–625 (2014).
- 244 20. Blomen, V. A. *et al.* Gene essentiality and synthetic lethality in haploid human  
245 cells. *Science* **350**, 1092–1096 (2015).
- 246 21. Wang, T. *et al.* Identification and characterization of essential genes in the  
247 human genome. *Science* **350**, 1096–1101 (2015).
- 248 22. Sagi, I. *et al.* Derivation and differentiation of haploid human embryonic stem  
249 cells. *Nature* (2016). doi:10.1038/nature17408
- 250

251 **Acknowledgements**

252 We thank all S.P.J. lab members for discussion, and especially A. Blackford, F.  
253 Puddu and C. Schmidt for critical reading of the manuscript. We thank M. Leeb for  
254 H129-3 cells and advice on haploid ES cell culture conditions. We thank C.D.  
255 Robles-Espinoza for helping designing the array of baits for the exon-capture  
256 experiment, and J. Hewinson for technical support. Research in the S.P.J. laboratory  
257 is funded by Cancer Research UK (CRUK; programme grant C6/A11224), the  
258 European Research Council and the European Community Seventh Framework  
259 Programme (grant agreement no. HEALTH-F2-2010-259893; DDResponse). Core  
260 funding is provided by Cancer Research UK (C6946/A14492) and the  
261 WellcomeTrust (WT092096). S.P.J. receives salary from the University of  
262 Cambridge, supplemented by CRUK. J.V.F. is funded by Cancer Research UK  
263 programme grant C6/A11224 and the Ataxia Telangiectasia Society. J.C. is funded  
264 by Cancer Research UK programme grant C6/A11224. D.J.A. is supported by  
265 CRUK. The research leading to these results has received funding from the  
266 European Research Council under the European Union's Seventh Framework  
267 Programme (FP7/2007-2013)/ERC grant agreement no. [311166]. B.V.G. is  
268 supported by a Boehringer Ingelheim Fonds PhD fellowship.

269

270 **Supplementary Figure legends**

271

272 **Supplementary Figure 1. Mutant library production controls and top candidate**  
273 **suppressor mutations identified. (a)** Cellular toxicity to various EMS doses used  
274 to generate mutant libraries. **(b)** Cell cycle profile of haploid and diploid H129-3  
275 mESCs. **(c)** EMS-mutagenized haploid and diploid mESC libraries were treated with  
276 2  $\mu$ M 6-TG for 6 days, and surviving cells were stained with crystal violet (left panel).  
277 Suppressor frequencies to 6-TG treatment of the different EMS-mutagenized  
278 libraries, represented as number of suppressor clones isolated per 10,000 plated  
279 cells (right panel). **(d)** Top candidate mutations conferring 6-TG resistance in the 7  
280 suppressor clones sequenced (left panel). Asterisks (\*) denote STOP-codon gains.  
281 SDV, splicing donor variant (see Supp. Fig. 2). Protein depletion in some clones was  
282 confirmed by western blotting (right panel).

283

284 **Supplementary Figure 2. Splicing mutants in the *Hprt* gene. (a)** Types of splicing  
285 variant mutations identified in *Hprt*. Mutated positions are highlighted in bold, and  
286 followed by the changed base in brackets. Exonic sequences are in capital letters,  
287 intronic sequences in lower case. SDV, splicing donor variant. SAV, splicing acceptor  
288 variant. SRV, splicing region variant. **(b)** Position of splicing variant mutations in *Hprt*  
289 exon-intron junctions. **(c)** *Hprt* splicing variant mutations result in reduced Hprt  
290 protein levels as judged by western blot analysis.

291

292 **Supplementary Figure 3. Knock-in generation of Dnmt1 G1157E and Mlh1**  
293 **A612T mutant cell lines. (a) Upper panel.** Position of small-guide RNAs (sgRNAs)  
294 designed to introduce the *Dnmt1* G3662A mutation (nucleotide number based on  
295 cDNA sequence; amino acid G1157E mutation). Protospacer adjacent motif (PAM)  
296 sequences for each sgRNA are also depicted, and Cas9 nickase cutting sites  
297 marked with arrows. *Lower panel.* *Dnmt1* sequence after gene editing. Mutations to  
298 abolish sgRNA binding, introduce the G1157E mutation and an *EcoRI* restriction site  
299 to allow screening, are in lower case and highlighted in pink. *Right panel.* *EcoRI*  
300 digestion of the PCR amplification of the region surrounding G3662 in wild-type (WT)  
301 and gene-edited cells. **(b) Upper panel.** Position of sgRNAs designed to introduce

302 the *Mlh1* G2101A mutation (nucleotide number of cDNA sequence; amino acid  
303 A612T mutation). PAM sequences are also depicted and Cas9 nickase cutting sites  
304 marked with arrows. *Lower panel.* *Mlh1* sequence after gene editing (annotations as  
305 in *a*). *Right panel.* *EcoRI* digestion of the PCR amplification of the region surrounding  
306 G2101 in WT and gene-edited cells.

307

308 **Supplementary Figure 4. EMS mutagenic action.** **(a)** Distribution of mutation  
309 types identified by whole-exome sequencing of 66 suppressor clones (23 orphan  
310 clones plus 43 clones with identified mutations). SNV, single-nucleotide variant.  
311 INDEL, insertion or deletion. Only homozygous mutations were considered. **(b)**  
312 Distribution of identified SNVs. **(c)** EMS mutational pattern. **(d)** Number of mutations  
313 per chromosome in sequenced clones. Mutation numbers (both homozygous and  
314 heterozygous) were normalized to exon bait coverage. **(e)** Heat map showing  
315 homogenous distribution of EMS-induced mutations in all chromosomes. Differences  
316 observed in the X chromosome could be accounted by its frequent loss in ES cells in  
317 culture (Robertson et al, *J Embryol Exp Morphol*, 74, 1983). *P* values were  
318 calculated by the Kruskal-Wallis test for multiple comparisons.

319

320 **Supplementary Table legends**

321

322 **Supplementary Table 1.** Homozygous mutations identified through whole-exome  
323 sequencing of 7 suppressor clones.

324

325 **Supplementary Table 2.** Homozygous mutations identified on the targeted exon-  
326 capture experiment performed on 189 suppressor clones. Heterozygous mutations  
327 affecting *Dnmt1*, *Hprt*, *Mlh1*, *Msh2*, *Msh6* and *Pms2* are also shown.

328

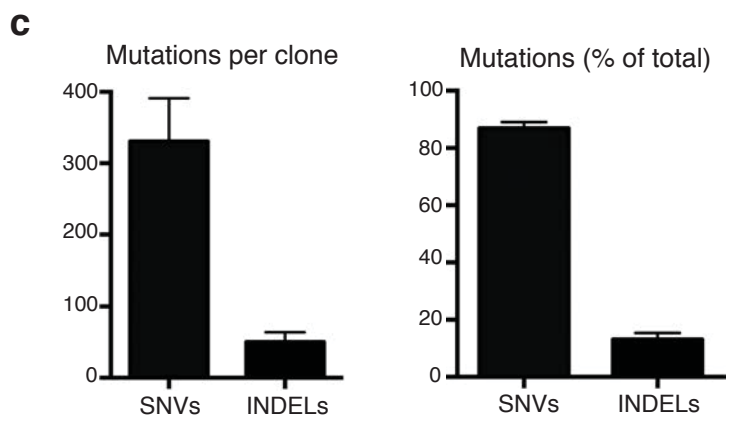
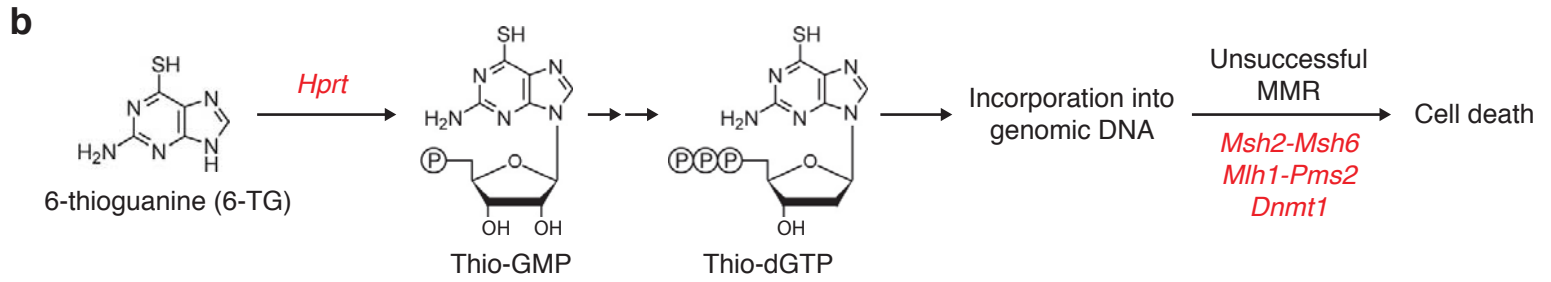
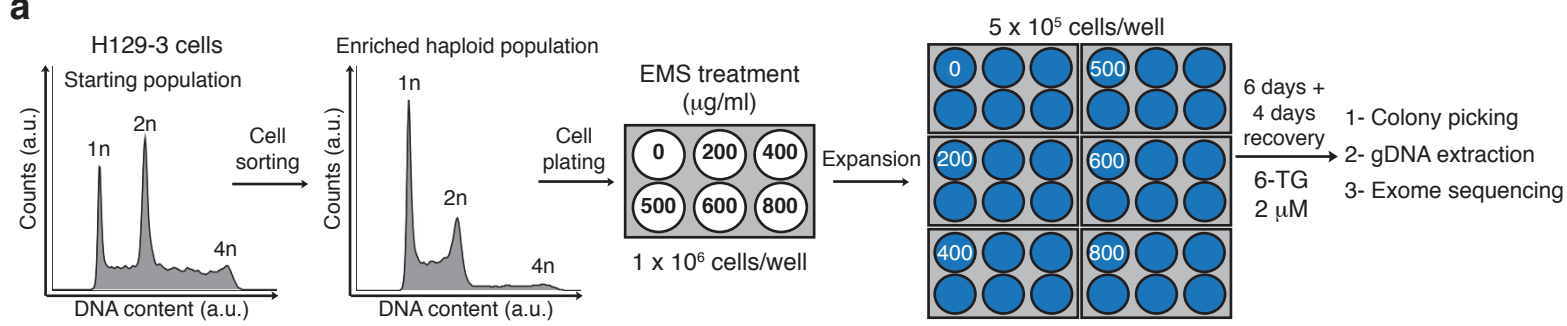
329 **Supplementary Table 3.** Homozygous mutations identified through whole-exome  
330 sequencing of 66 suppressor clones (23 orphan clones plus 43 clones with identified  
331 mutations). Heterozygous mutations affecting *Dnmt1*, *Hprt*, *Mlh1*, *Msh2*, *Msh6* and  
332 *Pms2* are also shown.

333

334 **Supplementary Table 4.** RNA sequencing data from 5 wild-type samples, 5  
335 identified suppressor clones and 21 unidentified suppressor clones. Values  
336 represent fragments per kilobase per million reads.

337

338 **Supplementary Table 5.** DNA sequencing coverage for the whole-exome and  
339 targeted exon-capture experiments.

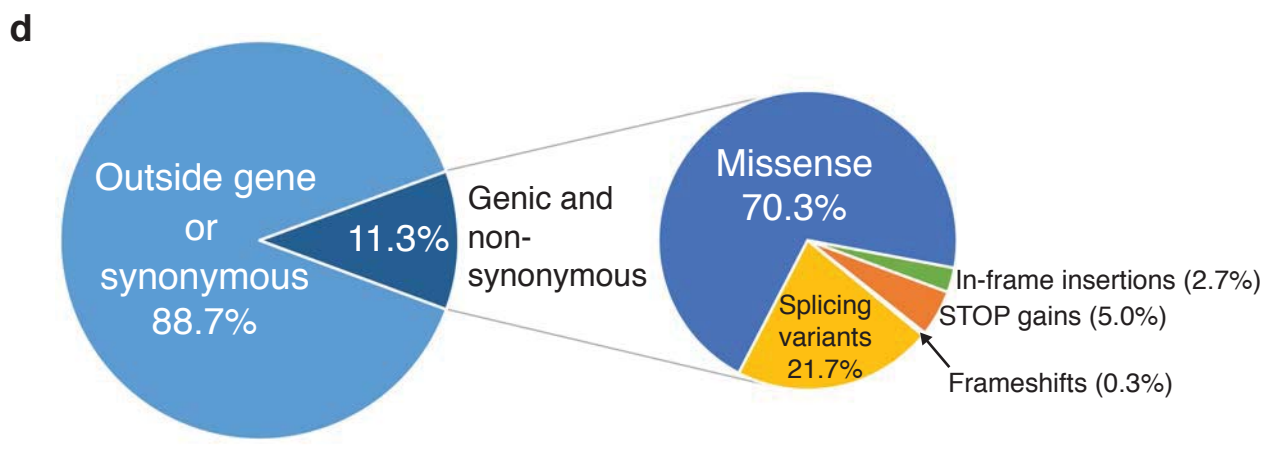


**e**

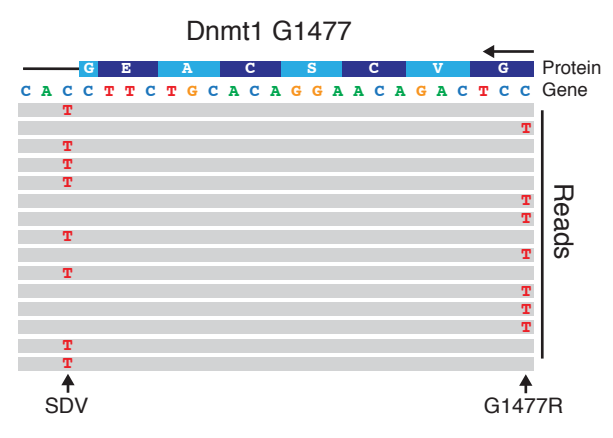
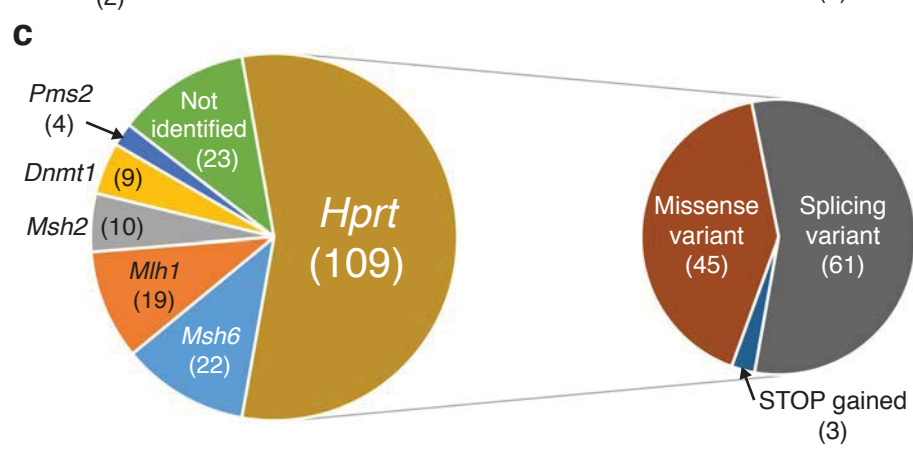
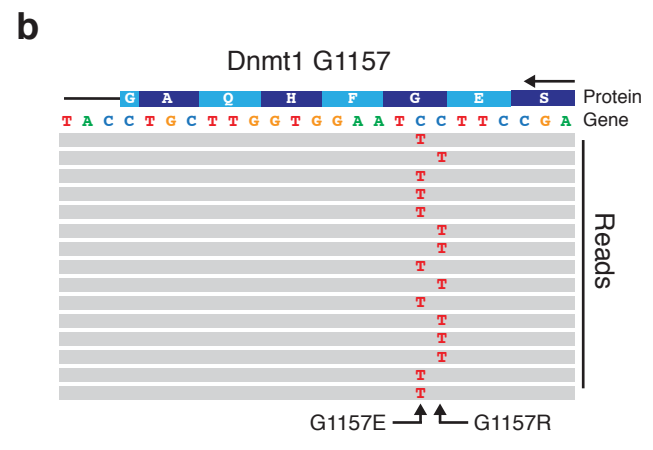
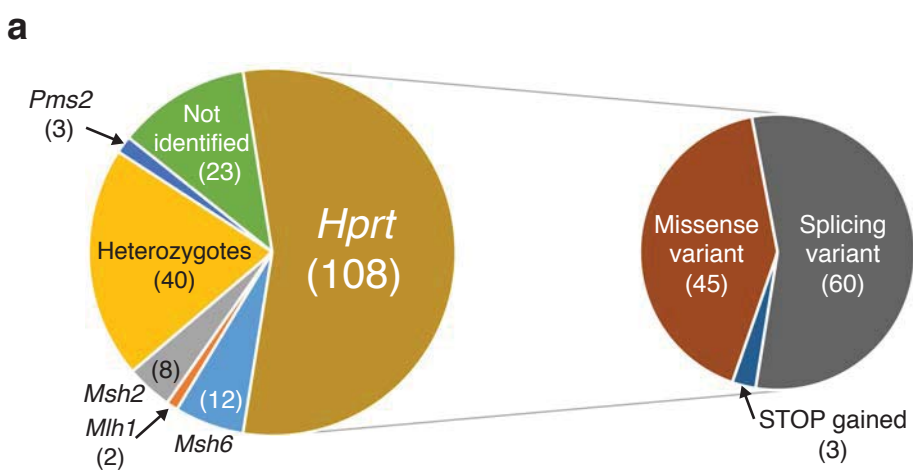
Gene	<i>Amer1</i>	<i>Armcx2</i>	<i>Dmd</i>	<i>Hprt</i>	<i>Prp2</i>	<i>Spast</i>	<i>Zfp142</i>
Sample A4							
A11							
B3							
D3							
D11							
E11							
F4							

Identified mutation with predicted deleterious consequence

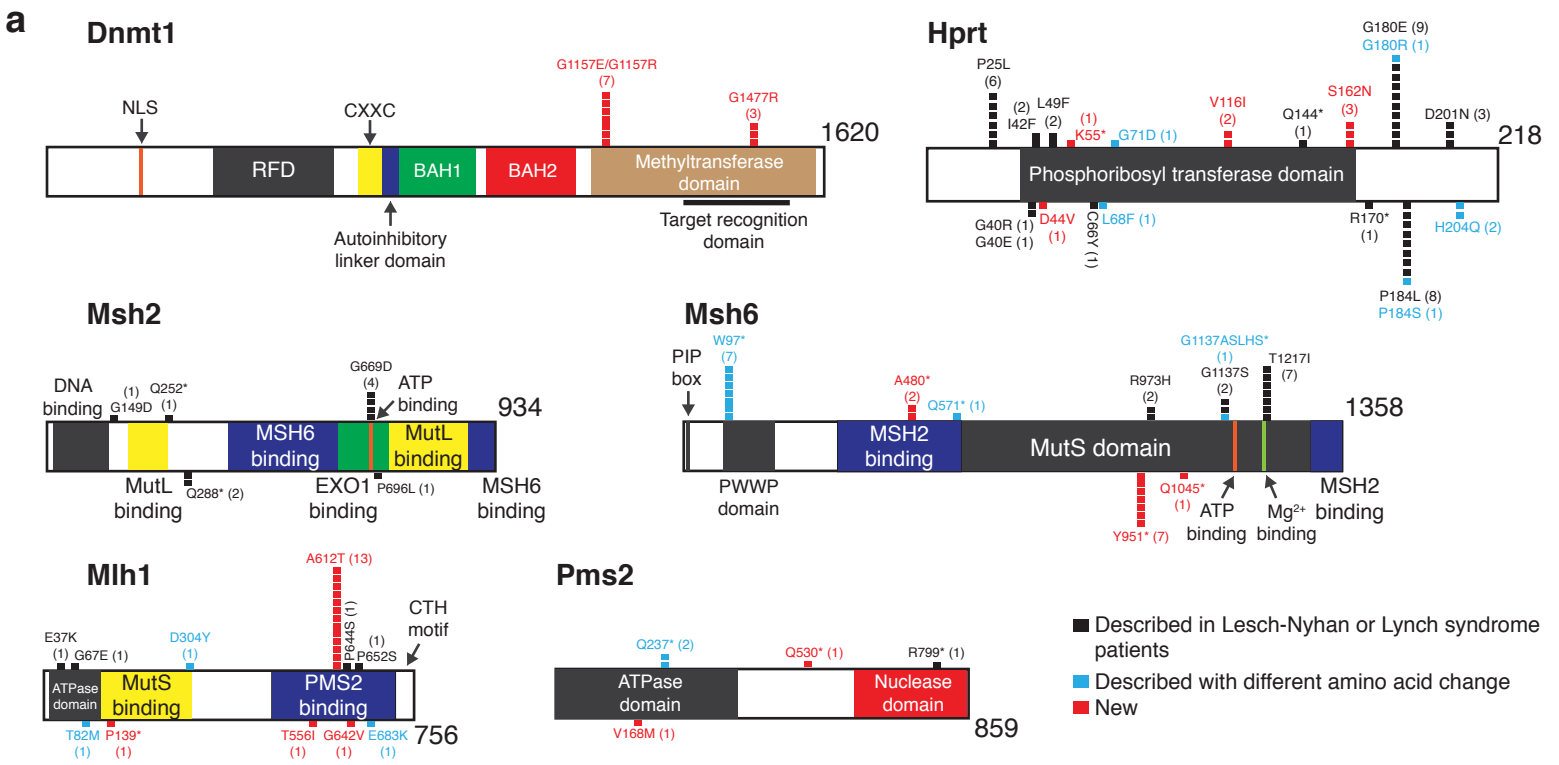
Identified mutation with predicted neutral consequence



Forment et al, Figure 1

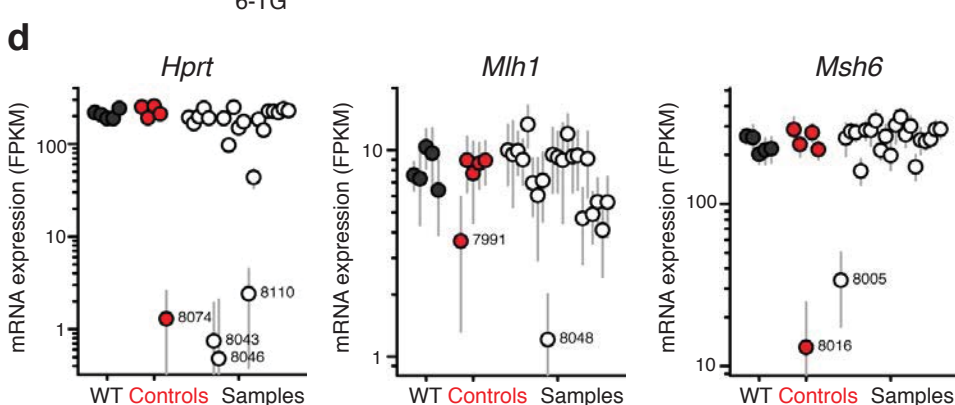
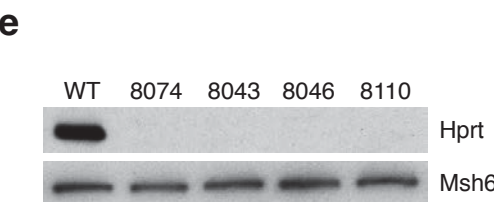
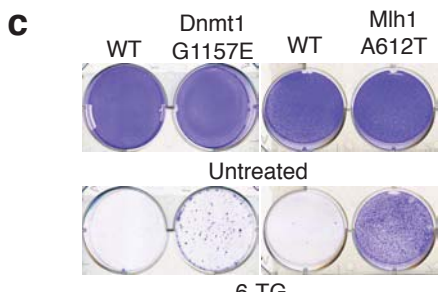


Forment et al, Figure 2

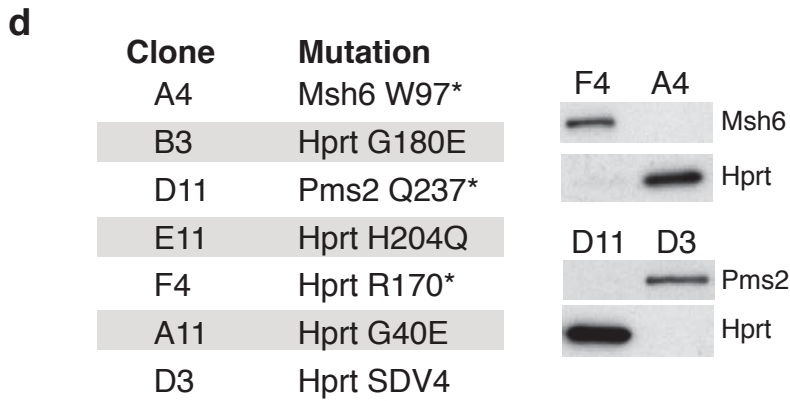
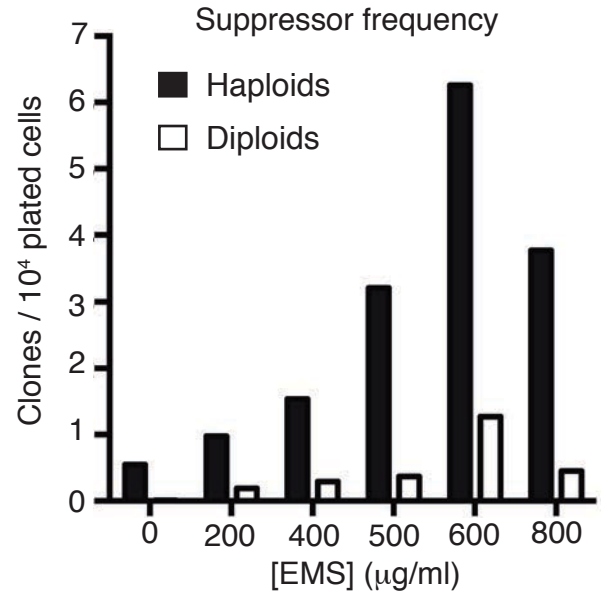
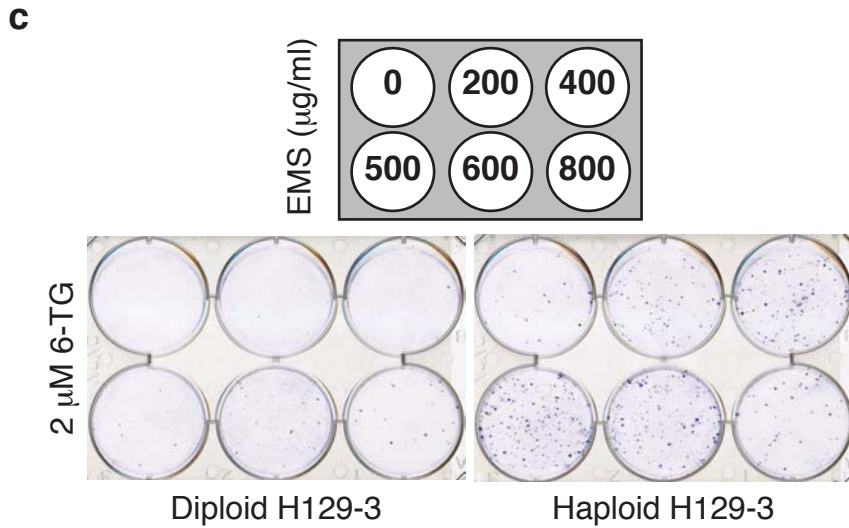
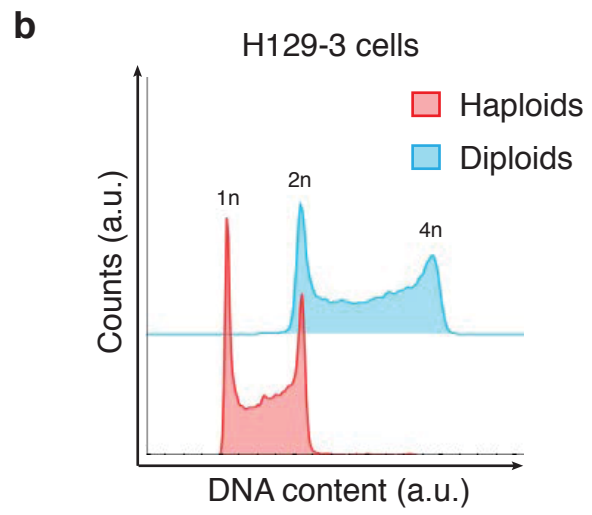
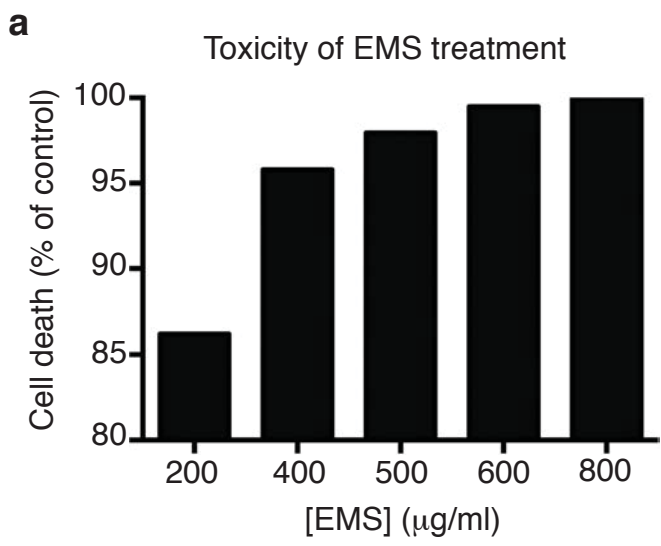


**b**

Protein	Mutation	Consequence		
		PROVEAN	SIFT	Summary
Dnmt1	G1157E	-7.67	0	Deleterious
	G1477E	-7.67	0	Deleterious
	G1477R	-7.17	0	Deleterious
Hprt	D44V	-7.45	0	Deleterious
	V116I	-0.03	0.841	Neutral
	S162N	-2.18	0.004	Deleterious
Mlh1	T556I	-2.5	0.05	Deleterious
	A612T	-3.06	0.002	Deleterious
	G642V	-3.77	0.017	Deleterious
Pms2	V168M	-2.73	0	Deleterious



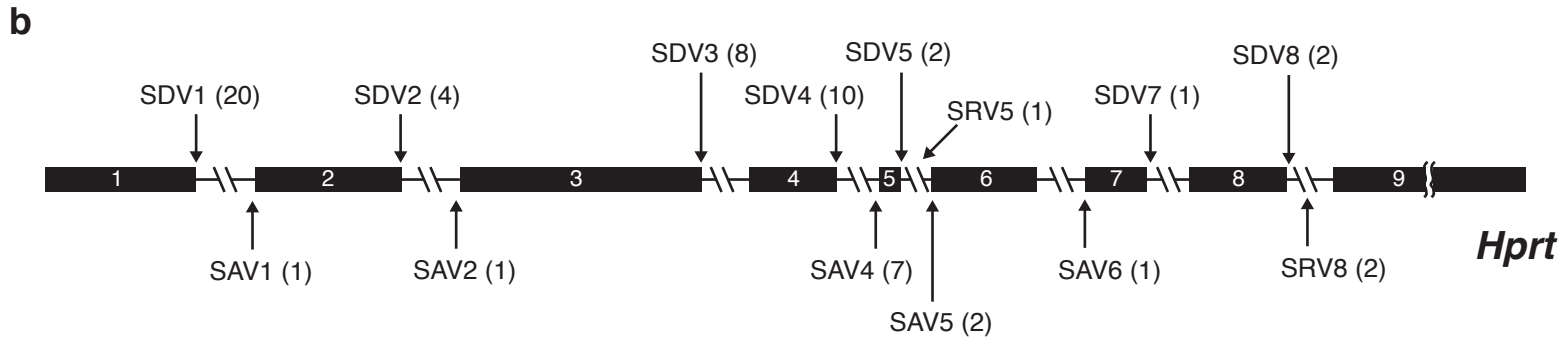
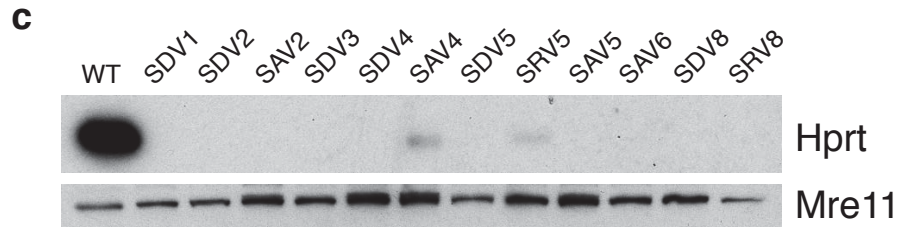
Forment et al, Figure 3



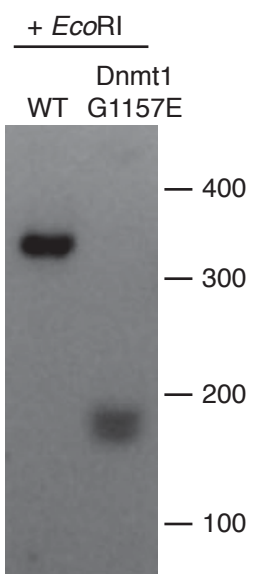
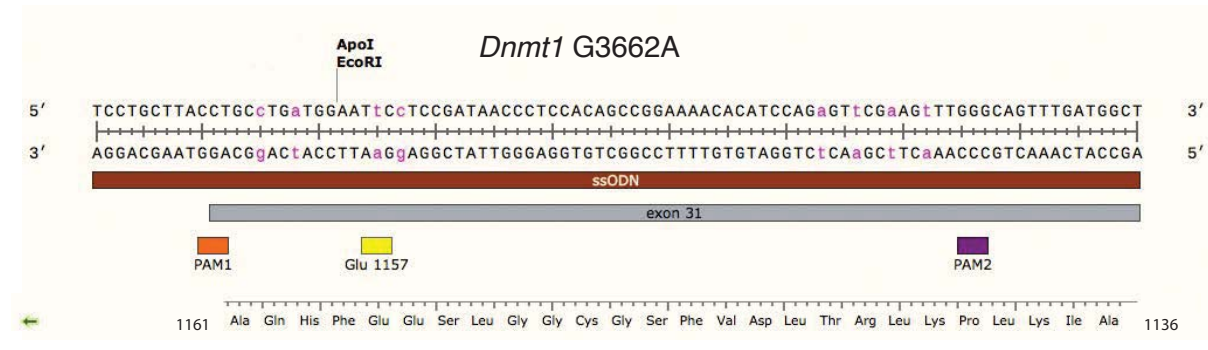
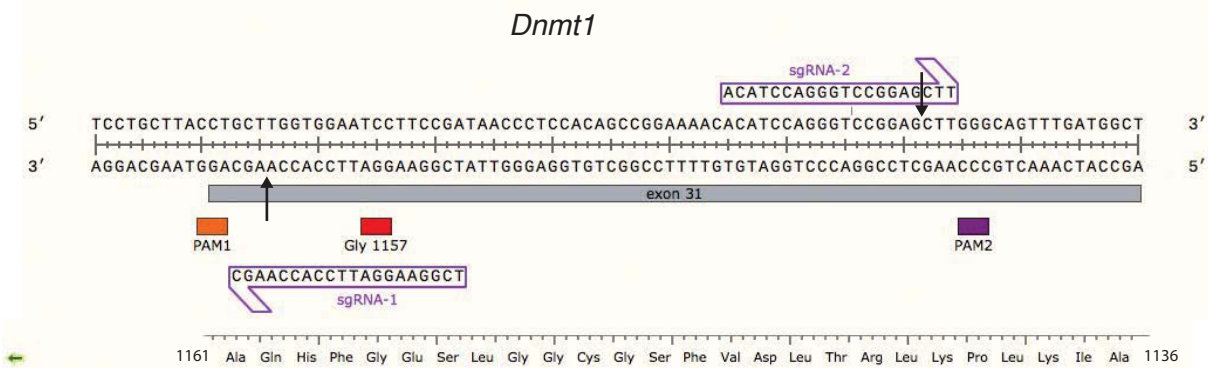
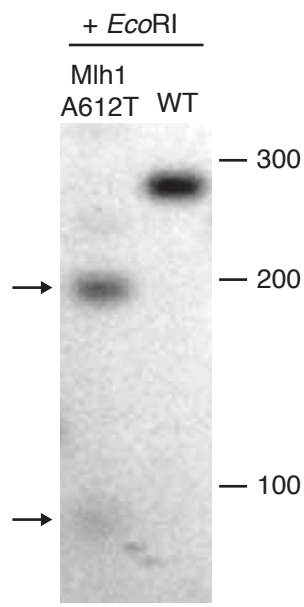
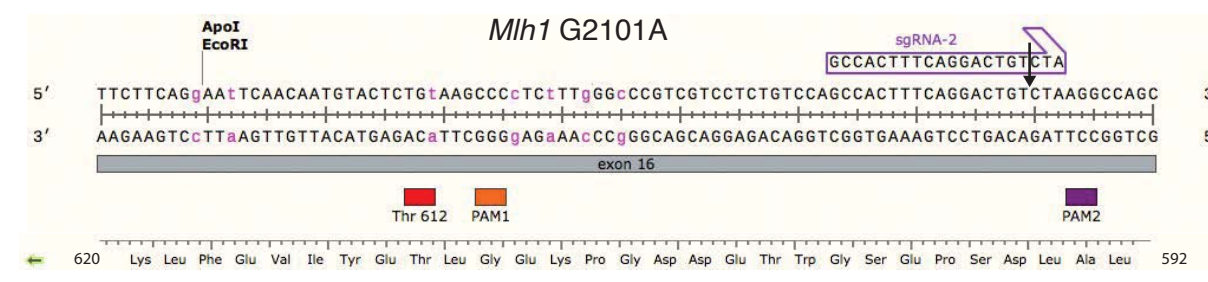
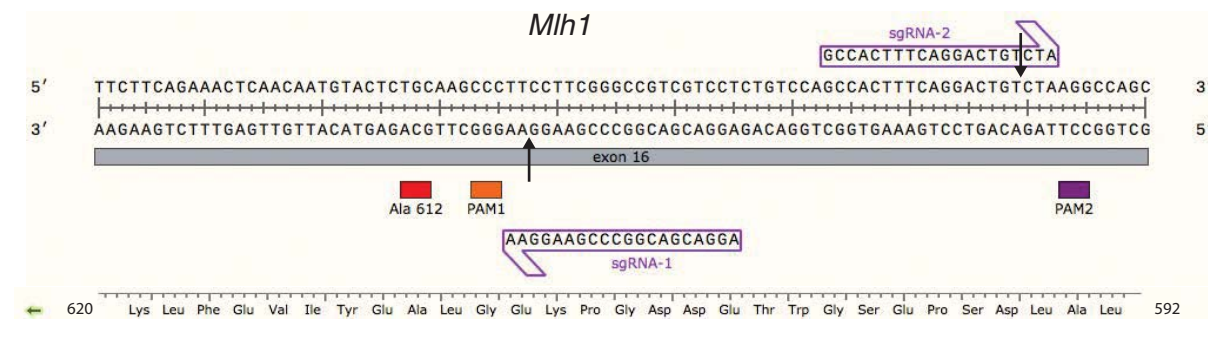
Forment et al, Supplementary Figure 1

**a**

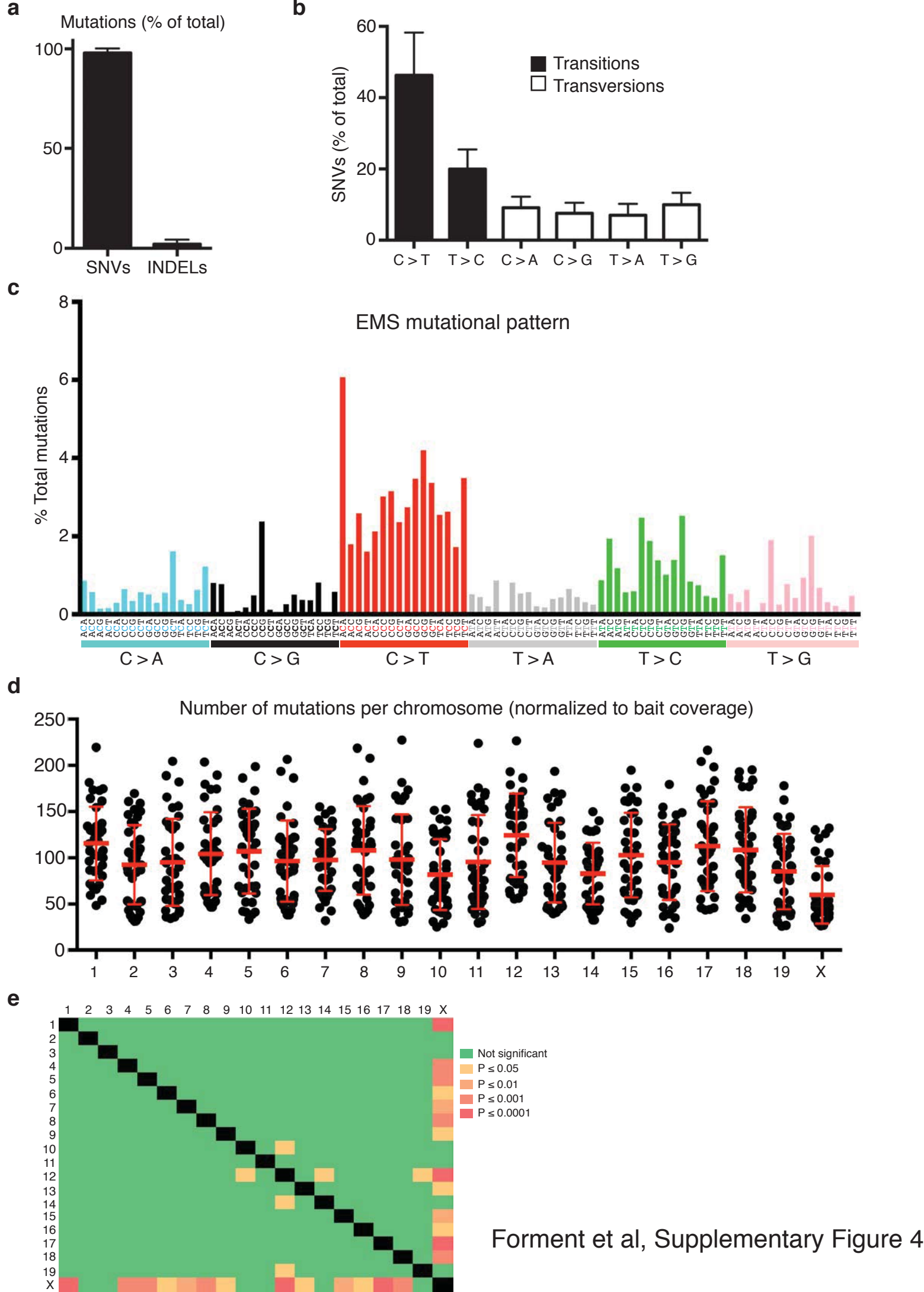
Splicing variant	Mutation
SDV1	...GTG- <b>g</b> (a)tg...
SAV1	...cag(a)-ATT...
SDV2	...CAG- <b>g</b> (a)tt...
SAV2	...tag(a)-GAC...
SDV3	...TGT- <b>g</b> (a)ta...
SDV4	...AAG- <b>g</b> (a)ta...
SAV4	...tag(a)-AAT...
SDV5	...AAG- <b>g</b> (a)ta...
SRV5	...GAA-gtaag( <b>t</b> )...
SAV5	...aag(a)-GAT...
SAV6	...cag(a)-CTT...
SDV7	...ACT- <b>g</b> (a)ta...
SDV8	...AAT- <b>g</b> (a)ta...
SRV8	...AAT-gtaag(a)...



Forment et al, Supplementary Figure 2

**a****b**

Forment et al, Supplementary Figure 3



Forment et al, Supplementary Figure 4

**Some supplementary files may need to be viewed online via your Referee Centre at <http://mc.manuscriptcentral.com/nar>.**

**Chromatin determinants impart camptothecin hypersensitivity in the absence of the Tof1/Csm3 replication pausing complex**

Journal:	<i>Nucleic Acids Research</i>
Manuscript ID	NAR-01713-M-2016
Manuscript Type:	1 Standard Manuscript
Key Words:	Synthetic viability, Tof1, Fork Protection Complex, Camptothecin, SIR complex

SCHOLARONE™  
Manuscripts

1  
2  
3  
4  
5  
6  
7  
8  
9  
10  
11  
12  
13  
14  
15  
16  
17  
18  
19  
20  
21  
22  
23

## Chromatin determinants impart camptothecin hypersensitivity in the absence of the Tof1/Csm3 replication pausing complex

24 Fabio Puddu<sup>1,†</sup>, Mareike Herzog<sup>1,2</sup>, Nicola J. Geisler<sup>1</sup>, Vincenzo Costanzo<sup>3</sup> and Stephen P.  
25 Jackson<sup>1,2,†</sup>  
26  
27  
28  
29  
30  
31  
32

33 <sup>1</sup>The Gurdon Institute and Department of Biochemistry, University of Cambridge, Tennis  
34 Court Road, Cambridge CB2 1QN, UK  
35  
36

37 <sup>2</sup>The Wellcome Trust Sanger Institute, Hinxton, Cambridge CB10 1SA, UK.

38  
39 <sup>3</sup>IFOM (Fondazione Istituto FIRC di Oncologia Molecolare) via Adamello 16, 20139 Milan,  
40 Italy.  
41  
42  
43

44 † to whom correspondence should be addressed:

45  
46 Stephen P. Jackson, s.jackson@gurdon.cam.ac.uk  
47

48  
49 Correspondence may also be addressed to:

50  
51 Fabio Puddu, f.puddu@gurdon.cam.ac.uk  
52  
53  
54  
55  
56  
57  
58  
59  
60

## Abstract

Camptothecin-induced Top1 locking on DNA generates a physical barrier to replication fork progression and creates topological stress. In *Saccharomyces cerevisiae*, absence of the Tof1/Csm3 complex causes camptothecin hypersensitivity by allowing replisome rotation, which converts impending topological stress to DNA catenation. By using a synthetic viability screening approach, we have discovered that inactivation of histone H4-K16 deacetylation suppresses much of the sensitivity of wild-type cells to camptothecin and the hypersensitivity of *tof1Δ* strains towards this agent. We show that disruption of Sir1-dependent heterochromatin that is established at silent mating-type loci and likely in other regions of the genome is sufficient to suppress camptothecin sensitivity in wild-type and *tof1Δ* cells. We have also found that the Tof1/Csm3 complex prevents loss of epigenetic silencing when this cannot be re-established by Sir1, and suggest a model in which DNA hypercatenation generated in the absence of the Tof1/Csm3 complex perturbs histone deposition.

## Introduction

Separation of the two parental DNA strands during DNA replication creates positive supercoiling ahead of the replication fork. Such over-winding hinders replisome progression and must be removed for DNA replication to be completed. In *Saccharomyces cerevisiae*, the main DNA topoisomerase that relaxes positive supercoiling during DNA replication is Top1, a type IB topoisomerase (1, 2). Despite the importance of DNA uncoiling for replication, cells lacking Top1 can fully replicate their genome because replisomes, by rotating along their axes, can convert impending positive supercoiling into intertwinings/catenation between the two daughter DNA strands (3). The catenation generated in this way is an obstacle to chromosome segregation and must be resolved by Top2, a type II topoisomerase, before the onset of mitosis (4). In contrast to Top1, Top2 is essential in yeast cells because a certain amount of catenation is generated even in wild-type cells, possibly because Top1 cannot relieve topological stress between replisomes converging towards replication termination zones (5). Consistent with this model, increased fork rotation has been observed when replication forks approach stable fork-pausing structures, such as centromeres, tRNA genes, inactive replication origins (6) and potentially retrotransposon long terminal repeats (LTRs) and transcriptionally repressed chromatin (7, 8).

To reduce the requirement for decatenation, replisome rotation is normally restricted by the Tof1/Csm3 complex (6), the yeast homolog of the mammalian Timeless/Tipin complex. Tof1 and Csm3 are also crucial for proper pausing of replication forks at the replication fork

1  
2 barriers present in the tandem arrays that form the large ribosomal DNA locus (9).  
3  
4 Independently of these functions, the Tof1/Csm3 complex also interacts with Mrc1 (10),  
5  
6 which functions as an adaptor to transmit signals from the apical replication-checkpoint  
7  
8 kinase Mec1 to the transducer kinase Rad53 during replication stress induced by nucleotide  
9  
10 depletion (11). The fact that *tof1Δ* strains, similarly to *mrc1Δ* strains, show synergistic  
11  
12 phenotypes in combination with loss of Rad9 – the other major checkpoint adaptor protein in  
13  
14 *S. cerevisiae* – suggests that the Tof1/Csm3 complex recruits Mrc1 for the purpose of Rad53  
15  
16 activation (9, 12). In this regard, it is noteworthy that Mrc1 also has checkpoint-independent  
17  
18 functions and can be recruited to replication forks independently of Tof1/Csm3 (11, 13, 14).  
19  
20  
21

22  
23 Despite the above findings, certain results have remained unexplained, and the exact role of  
24  
25 the Tof1/Csm3 complex has remained elusive. For instance, *tof1Δ* and *csm3Δ* yeast strains  
26  
27 were shown to be hypersensitive to high doses of camptothecin (15), a drug that induces DNA  
28  
29 double-strand DNA breaks (DSBs) during S phase by trapping Top1 in a covalent complex  
30  
31 with DNA. These strains, however, are not hypersensitive to other agents that induce DSBs,  
32  
33 such as ionising radiation, or to drugs such as hydroxyurea that affect S phase progression  
34  
35 (15), suggesting that the camptothecin hypersensitivity of *tof1Δ* and *csm3Δ* strains might arise  
36  
37 through topologically stressed DNA structures generated by Top1 inhibition rather than from  
38  
39 DNA damage per se (16, 17).  
40  
41  
42  
43

## 44 **Materials and Methods**

45  
46  
47  
48 **Yeast Strains and Plasmids.** Yeast strains used for this work are haploid derivatives of W303  
49  
50 unless otherwise indicated, and are listed in Supplementary Table 1. All deletions were  
51  
52 introduced by one-step gene disruption/tagging (18). Strains carrying histone H4 mutations  
53  
54 were obtained by plasmid shuffling, transforming the strain JHY6 (*hht1-hhf1Δ::KanMX6 hht2-*  
55  
56 *hhf2Δ::HPH*) with plasmids obtained by site-directed mutagenesis of plasmid pMR206 (*HHT2-*  
57  
58  
59  
60

1  
2 *HHF2; TRP1*). Strains to detect transient loss of silencing events were prepared by introducing  
3  
4 *TOF1* deletion in the diploid strain JRY9730 (*sir1Δ::LEU2/SIR1 HMRα/HMRα-α2Δ::cre*  
5  
6 *ura3Δ::PGPD-loxP-yEmRFP-TCYC1-kanMX-loxP-yEGFP-TADH1/ura3*) (19) and by recovering  
7  
8 the appropriate spores after sporulation.  
9

10  
11 **Whole-genome paired-end DNA sequencing and data analysis** was performed as  
12  
13 previously described (20). All raw sequencing data are available from the European  
14  
15 Nucleotide Archive (ENA) under the accession codes detailed in Supplementary Table 2. SNPs  
16  
17 and indels were identified by using the SAMtools (v0.1.19) mpileup function, which finds  
18  
19 putative variants and indels from alignments and assigns likelihoods, and BCFtools that  
20  
21 performs the variant calling (21). The following parameters were used: for SAMtools (v0.1.19)  
22  
23 mpileup -EDS -C50 -m2 -F0.0005 -d 10000' and for BCFtools (v0.1.19) view '-p 0.99 -vcgN'.  
24  
25 Functional consequences of the variants were produced by using the Ensembl VEP (22).  
26  
27  
28

29  
30 **Drug sensitivity assays.** Overnight-grown saturated cultures of the indicated strains were  
31  
32 serially diluted (10 fold) in water. 10 µl drops of each dilution were the deposited on each  
33  
34 plate. Images were scanned two to three days after plating and growth at 30°C.  
35  
36

37  
38 **Analysis of cell cycle progression.** Exponentially growing cultures (30°C) were  
39  
40 synchronised in G1 by addition of 5 µg/ml alpha factor for 2 hours. G1 synchronised cultures  
41  
42 were then transferred to fresh YPD and released into S phase in the presence or in the  
43  
44 absence of camptothecin and/or sirtinol. 45 minutes after the release, 20 µg/ml alpha factor  
45  
46 was added to allow quantification of G1 cells by preventing re-entry into the cell cycle.  
47  
48

49  
50 **Mating and silencing assays.** Mating assays were performed by using saturated cultures of  
51  
52 the indicated strains. 10 fold serial dilutions of each culture were prepared and deposited on  
53  
54 plates lacking amino acids previously seeded with tester strains 6122a and 6122alpha (*HIS3*  
55  
56 *TRP1 LEU2 URA3 lys2*). Growth ensued only after mating of the deposited strain with the  
57  
58  
59  
60

1  
2 tester strain by mutual complementation of auxotrophies. Assays to detect transient loss of  
3  
4 silencing events were performed as previously described (19).  
5  
6

### 7 **Analysis of ChIP-seq data**

8  
9  
10 ChIP-seq data were downloaded from the Sequence Read Archive (NCBI) using accession  
11  
12 numbers specified in Supplementary Table 3. Reads were aligned using BWA-MEM. For each  
13  
14 genomic position, coverage was calculated using bedtools genomecov and normalised using  
15  
16 the genome-wide median of each sample. For each genomic position, the enrichment (E) was  
17  
18 calculated as the ratio of the normalised coverages of IP and input samples. Every genomic  
19  
20 position showing  $E_{\text{Sir2}} > 0.9$  and  $E_{\text{Sir3}} > 1.1$  and  $E_{\text{Sir2}} > 0.9$  and  $E_{\text{GFP}} < 1.1$  and  $E_{\text{H4-K16ac}} < 0.75$  and  
21  
22  $E_{\text{H3}} > 0.75$  was exported to a bed file. These values were determined empirically and small  
23  
24 adjustments did not substantially alter the final results. The bed file was queried with the  
25  
26 coordinates of every annotated ORF to calculate the total number of positions in each ORF for  
27  
28 which the above conditions are true. The final SIR score was obtained by dividing this number  
29  
30  
31  
32  
33 by the length of the ORF.  
34

## 35 **Results**

36  
37  
38 To understand the roles of the Tof1/Csm3 complex during DNA replication, we investigated  
39  
40 the basis for the camptothecin hypersensitivity of *TOF1*- or *CSM3*-deleted cells. This  
41  
42 hypersensitivity arises from the well-established trapping of Top1 in a covalent complex with  
43  
44 DNA, as shown by the fact that it was rescued by *TOP1* deletion (**Figure 1A**). Notably, *mrc1Δ*  
45  
46 strains were not hypersensitive to camptothecin (**Figure 1A and (15)**), indicating that a  
47  
48 defect in replication checkpoint activation does not explain the camptothecin hypersensitivity  
49  
50 of *tof1Δ* or *csm3Δ* strains. Moreover, *tof1Δ/csm3Δ* sensitivity does not arise from issues  
51  
52 connected to fork pausing at the replication fork barrier on ribosomal DNA, as pausing-  
53  
54  
55  
56  
57  
58  
59  
60

1  
2 deficient *fob1Δ* strains were not hypersensitive to camptothecin and *FOB1* deletion did not  
3  
4 alleviate the camptothecin hypersensitivity of a *csm3Δ* strain (**Figure 1B**).

### 7 ***SIR* gene mutations suppress camptothecin hypersensitivity of** 8 ***tof1Δ/csm3Δ* cells**

11  
12 To understand the origin of the hypersensitivity of *tof1Δ* and *csm3Δ* strains to camptothecin,  
13  
14 we carried out a synthetic viability genomic screening (20) to identify mutations capable of  
15  
16 suppressing such hypersensitivity (**Figure 1C**). We isolated sixteen resistant colonies and  
17  
18 verified that they indeed displayed both resistance to camptothecin and absence of *TOF1*  
19  
20 (**Figure 1D and Supplementary Figure 1A**). We then sequenced their genomic DNAs to  
21  
22 identify candidate mutations responsible for the suppression phenotype (Supplementary  
23  
24 Table 1). Two of the sixteen strains – the most resistant ones – carried mutations that  
25  
26 inactivated *TOP1*, which encodes the drug target. Three strains carried either of two nonsense  
27  
28 mutations that inactivated *SIR3*, while eight of the remaining strains carried a nonsense  
29  
30 mutation inactivating *SIR4* (**Figure 1D**; premature stop codons are designated by a Δ  
31  
32 following the position of the last amino acid residue encoded by the truncated gene).  
33  
34 Importantly, by directly introducing deletions of *SIR3* and *SIR4* in *tof1Δ* and *csm3Δ* strains, we  
35  
36 verified that *SIR3* or *SIR4* inactivation mediated suppression of camptothecin hypersensitivity  
37  
38 (**Figure 2A**). In the three remaining suppressor strains – the weakest suppressors – we could  
39  
40 not identify any mutation responsible for the suppression. In one of these, no mutations were  
41  
42 detected, while the other two carried point mutations in *IME2* (Inducer of MEiosis, which is  
43  
44 not expressed in exponentially growing cells) or *IRC15*. However, ensuing studies established  
45  
46 that neither *IME2* nor *IRC15* deletion suppressed the camptothecin hypersensitivity of *tof1Δ*  
47  
48 cells (**Supplementary Figure 1B and 1C**).

51  
52  
53  
54  
55  
56 Sir3 and Sir4 form a ternary protein complex with the histone deacetylase catalytic subunit  
57  
58 Sir2 (reviewed in (23)), with removal of any of the three subunits inactivating the  
59  
60

1 transcriptional silencing functions of the complex (24). Significantly, we established that, as  
2  
3 for cells lacking Sir3 or Sir4, loss of Sir2 also alleviated the camptothecin hypersensitivity of  
4  
5 *tof1Δ* cells (**Figure 2B**). Furthermore, by increasing the concentration of camptothecin, we  
6  
7 found that deletion of *SIR2*, *SIR3* and *SIR4* also promoted camptothecin resistance in a wild-  
8  
9 type yeast background (**Figure 2B and supplementary Figure 1D**). By contrast, *SIR2*  
10  
11 deletion did not alleviate the strong camptothecin hypersensitivity of a *rad51Δ* strain, which is  
12  
13 defective in DSB repair (**Figure 2C**). These data thus indicated that the SIR complex affects  
14  
15 camptothecin sensitivity only under specific genetic contexts, and that inactivating the SIR  
16  
17 complex does not act as a general mediator of camptothecin sensitivity, for example by  
18  
19 reducing Top1 activity, increasing cell permeability, or enhancing DNA DSB induction by  
20  
21 camptothecin.  
22  
23  
24  
25

### 26 27 **Sir2 mediated deacetylation of H4-K16 imparts camptothecin sensitivity.**

28  
29 To assess whether loss of the deacetylase activity of the Sir complex was responsible for the  
30  
31 suppression of *tof1Δ* hypersensitivity to camptothecin, we used the small-molecule Sir2  
32  
33 inhibitor, sirtinol (25). This established that addition of 20μM sirtinol suppressed the  
34  
35 camptothecin sensitivity of a *tof1Δ* strain and enhanced the resistance of a wild-type strain  
36  
37 (**Figure 2D and data not shown**). While Sir2 homologs in higher eukaryotes have been  
38  
39 implicated in the deacetylation of proteins involved in DNA repair, such as PARP1, Ku70 and  
40  
41 CtIP (26-28), the prime target for *S. cerevisiae* Sir2 is histone H4 lysine 16 (H4-K16), which is  
42  
43 found in an acetylated state through much of the transcriptionally active yeast genome. In *S.*  
44  
45 *cerevisiae*, deacetylation of this residue by Sir2 allows binding of Sir3, thus recruiting further  
46  
47 Sir2 that removes acetylation marks from flanking H4-K16 residues, a process that is then  
48  
49 propagated to produce a transcriptionally silent heterochromatic state (23). To explore  
50  
51 whether the relevant target for Sir2 in relation to its effects on the camptothecin sensitivity of  
52  
53 *tof1Δ* cells was H4-K16, we mutated this residue to glutamine (Q), a residue that mimics a  
54  
55  
56  
57  
58  
59  
60

1  
2  
3  
4  
5  
6  
7  
8  
9  
10  
11  
12  
13  
14  
15  
16  
17  
18  
19  
20  
21  
22  
23  
24  
constitutively acetylated lysine and abrogates Sir3 binding (29). Strikingly, this *hhf-K16Q* mutation suppressed the camptothecin hypersensitivity of a *tof1Δ* strain, and at higher doses also reduced the camptothecin sensitivity of a wild-type strain (**Figure 2E**). Similarly, mutation of H4-K16 to glycine (G), which prevents binding by Sir3(29), strongly counteracted the camptothecin sensitivity of both *tof1Δ* and wild-type cells. By contrast, mutating histone H4-K16 to non-acetylatable arginine (R) produced much weaker suppression (**Figure 2E**). This finding was in agreement with published data showing that, despite encoding for a non-acetylatable residue and allowing increased Sir3 binding (29), the *hhf-K16R* mutation actually reduces transcriptional silencing (30). Taken together, these results highlighted a correlation between loss of silencing and camptothecin resistance.

### 25 26 27 28 29 30 **An “acetylated H4-K16” template is responsible for camptothecin induced mitotic arrest.**

31  
32  
33  
34  
35  
36  
37  
38  
39  
40  
41  
42  
43  
44  
45  
46  
47  
48  
49  
50  
51  
52  
53  
54  
55  
56  
57  
58  
59  
60  
The above data supported a model in which the mechanism by which the SIR complex yields camptothecin sensitivity is via effects on H4-K16 deacetylation. In this regard, we reasoned that the SIR complex might impart camptothecin sensitivity by deacetylating newly incorporated histone H4 during DNA replication, or by it promoting a condensed chromatin template that impairs DNA replication. To discriminate between these two possibilities, we took advantage of the fact that camptothecin treatment of synchronised wild-type cells released from G1 into S-phase leads to a prolonged G2/M arrest (31). We first assessed the effect of *TOF1* and *CSM3* deletion on this particular phenotype by releasing synchronised wild-type, *tof1Δ* and *csm3Δ* cultures either in the presence or in the absence of camptothecin. As expected, wild-type cells treated with camptothecin did not delay bulk DNA replication compared to strains released in the absence of camptothecin but they did delay exit from the subsequent mitosis (**Figure 3A**). Significantly, compared to wild-type controls, cells deleted for *TOF1* or *CSM3* arrested for longer periods of time in G2/M following camptothecin

1  
2 treatment (**Figure 3B**), a phenotype that correlated with persistence of the mitotic cyclin Clb2  
3  
4 (**Figure 3C**). Nevertheless, these cells eventually re-entered the cell cycle and continued  
5  
6 proliferating, consistent with the fact that *tof1Δ* and *csm3Δ* strains were not killed by acute  
7  
8 camptothecin treatment (**Figure 3D**; note that a repair defective *rad51Δ* strain was  
9  
10 hypersensitive even to acute camptothecin treatment).

11  
12  
13  
14 If Sir2 deacetylation activity during S phase promoted camptothecin sensitivity, one would  
15  
16 expect that addition of sirtinol after the release from G1 would rescue the mitotic delay  
17  
18 induced by camptothecin in *tof1Δ* cells. Conversely, if broad acetylation of the chromatin  
19  
20 template was required to rescue the *tof1Δ* phenotype, sirtinol should lead to suppression only  
21  
22 if *tof1Δ* cells were pre-grown in the presence of sirtinol. To discriminate between these two  
23  
24 hypothesis, we grew *hml* and *hmltof1Δ* cells either in the presence or in the absence of sirtinol,  
25  
26 and we then synchronised them in G1 by addition of alpha-factor (**Figure 3E**). We used a  
27  
28 mutant *hml* background because sirtinol makes wild-type cells insensitive to alpha-factor by  
29  
30 derepressing the *HML/R (HM)* loci (25, importantly, as shown in **Supplementary Figure 2A**,  
31  
32 *HML* mutation did not affect camptothecin sensitivity). We then released the G1 synchronised  
33  
34 cells into S phase in the presence of camptothecin alone, or in the presence of camptothecin  
35  
36 plus sirtinol. Crucially, addition of sirtinol after the G1 release was not sufficient to rescue the  
37  
38 mitotic delay of *tof1Δ* cells (**Figure 3E and Supplementary Figure 2B**). By contrast, pre-  
39  
40 growing *tof1Δ* cells in the presence of sirtinol fully suppressed their mitotic delay, whether or  
41  
42 not sirtinol was present during the subsequent camptothecin treatment (**Figure 3E and**  
43  
44 **Supplementary Figure 2B**). Collectively, these findings supported a model in which much of  
45  
46 the toxicity caused by camptothecin reflects replication-associated problems arising within  
47  
48 chromatin regions containing de-acetylated H4-K16, with cells lacking Tof1 or Csm3 being  
49  
50 particularly sensitive to this.  
51  
52  
53  
54  
55  
56  
57  
58  
59  
60

## HM-like chromatin is responsible for *tof1Δ* strain hypersensitivity to camptothecin.

The yeast genome contains three well-studied heterochromatic regions transcriptionally silenced by SIR proteins: the ribosomal DNA (rDNA) array, sub-telomeric regions and the cryptic mating-type loci (**Figure 4A, 4B, and 4C**). To establish whether loss of rDNA silencing mediated suppression of *tof1Δ* camptothecin hypersensitivity, we used a strain carrying a deletion of the entire rDNA locus complemented by a multi-copy plasmid containing the rDNA repeat unit (32). We found that deletion of the rDNA locus did not reduce *tof1Δ* hypersensitivity to camptothecin (**Figure 4A**), suggesting that this genomic region is not the prime target of SIR-mediated silencing that is lethal to *tof1Δ* cells exposed to camptothecin. This notion was also supported by the fact that, while we observed suppression of camptothecin sensitivity with *sir2Δ*, *sir3Δ* or *sir4Δ*, silencing of the rDNA locus only requires Sir2, with *SIR4* deletion actually increasing rDNA silencing by delocalising Sir2 from telomeres (33).

To determine if loss of sub-telomeric silencing could rescue *tof1Δ* hypersensitivity to camptothecin, we employed a strain carrying a C-terminal truncation of Rap1 (*rap1Δ663*), the so-called *rap1-17* allele. This mutation completely disrupts transcriptional silencing at telomeres (telomere position effect) and partially affects silencing of the cryptic mating-type locus *HML* but not of that of *HMR* (34). While strains carrying the *rap1Δ663* allele grew slower than wild-type strains, presumably due to the role of Rap1 in regulating transcription of genes involved in ribosome formation and glycolysis (35, 36), they did not display altered sensitivity to camptothecin (**Figure 4B**). Notably, the *rap1Δ663* mutation also failed to suppress the camptothecin hypersensitivity of *tof1Δ* cells (**Figure 4B**), indicating that loss of telomere position effect does not promote survival in the presence of this drug.

1  
2 At the cryptic mating type loci *HML* and *HMR*, silencing is established by replication origin  
3 recognition complex (ORC)-mediated recruitment of Sir1, which then attracts the SIR complex  
4 via an interaction with Sir4 (37, 38). Sir4 binding is also stabilised by an interaction with  
5 Rap1, which binds to its DNA consensus sequence located next to the ORC binding site (ACS,  
6 ARS consensus sequence, **Figure 4C**). For these reasons, deletion of *SIR1* results in partial loss  
7 of silencing at the cryptic mating-type loci, but does not affect telomeric or rDNA silencing  
8 (39). Strikingly, we found that *SIR1* deletion strongly alleviated the camptothecin  
9 hypersensitivity of a *tof1Δ* strain (**Figure 4C**). Similarly to what we had observed for *SIR2*  
10 deletion, disruption of *SIR1* also decreased the sensitivity of a wild-type strain to high levels of  
11 camptothecin but did not rescue the camptothecin hypersensitivity of a *rad51Δ* strain  
12 (**Figure 4C and Supplementary Figure 2C**). These data indicated that the de-acetylated H4-  
13 K16 bearing chromatin template that is toxic to *tof1Δ* and wild-type cells in the presence of  
14 camptothecin is generated in a Sir1-dependent manner, and were also consistent with our  
15 conclusions that camptothecin sensitivity is not mainly generated via the rDNA or telomeric  
16 loci.

### 36 **Tof1/Csm3 prevents loss of epigenetic information during DNA** 37 **replication.**

38  
39 Rather than being required to maintain epigenetic silencing, Sir1 re-establishes silent  
40 chromatin when it happens to be lost; and thus, within a population of *sir1Δ* cells, only a  
41 fraction has lost silencing (19, 24, 40). In spite of this, we noted that *SIR1* deletion suppressed  
42 *tof1Δ* hypersensitivity to essentially the same extent as *SIR2* deletion. To explain this apparent  
43 paradox, we hypothesised that *tof1Δ* cells might lose silencing more frequently than wild-type  
44 cells, and may thus require Sir1 to re-establish it. To test this hypothesis, we took advantage  
45 of the fact that co-expression of the two *HM* loci results in sterility (41) and used mating  
46 assays to measure the extent of silencing loss in wild-type, *sir1Δ*, *tof1Δ* and *sir1Δtof1Δ* strains.  
47  
48  
49  
50  
51  
52  
53  
54  
55  
56  
57  
58  
59  
60

1  
2 This revealed that, under our experimental conditions, *sir1Δ* strains did not show a detectable  
3 mating defect, but deletion of *TOF1* reduced the ability of *sir1Δ* cells to mate. (**Figure 4D**).  
4  
5 Additionally, like *sir2Δ* cells, *sir1Δtof1Δ* cells failed to arrest in G1 in the presence of alpha-  
6  
7 factor, despite the *sir1Δ* or *tof1Δ* single mutants being proficient in this assay (**Figure 4E**).  
8  
9

10  
11 To directly assess loss of silencing at the *HMR* locus, we employed an experimental system  
12 designed to trap transient loss-of silencing events (19). Briefly, we used a strain in which loss  
13 of silencing induces expression of the Cre recombinase integrated at the *HMR* locus. Cre then  
14 excises a fragment of DNA carrying genes encoding for red-fluorescent protein (RFP),  
15 expressed from the constitutive GPD promoter, and resistance to the antibiotic G418. This  
16 excision juxtaposes the GPD promoter to the gene coding for green-fluorescent protein (GFP),  
17 resulting in cells switching from red to green fluorescence (as well as from G418 sensitivity to  
18 resistance, **Figure 4F**). We grew cultures of wild-type, *tof1Δ*, *sir1Δ*, and *tof1Δsir1Δ* strains in  
19 the presence of G418 to prevent expansion of green clones and then plated them to obtain  
20 single colonies, which were scored for the presence of red/green sectors. The majority of  
21 colonies formed by wild-type and *tof1Δ* cells were either completely red or had very small  
22 sectors/dots of GFP signal, with *tof1Δ* colonies showing a larger proportion of the latter  
23 (**Figure 4G**). In agreement with previous results, most *sir1Δ* colonies had large green sectors  
24 and many of them were mainly or completely green, indicating prevalent loss of *HMR*  
25 silencing (19). Strikingly, all colonies of the double mutant *sir1Δtof1Δ* were completely green,  
26 highlighting extensive loss of *HMR* silencing (**Figure 4G**; we noticed that, while most colonies  
27 were fully green, small patches of red fluorescence could be detected in some of them,  
28 indicating that the cell that started the colony was originally red). Collectively, these findings  
29 supported a model in which replication in the absence of the Tof1/Csm3 complex strictly  
30 requires Sir1 for silencing maintenance, possibly because chromosome hyper-catenation  
31 created in the absence of Tof1 alters the dynamics of histone deposition and favours loss of  
32 HMR-like silencing.  
33  
34  
35  
36  
37  
38  
39  
40  
41  
42  
43  
44  
45  
46  
47  
48  
49  
50  
51  
52  
53  
54  
55  
56  
57  
58  
59  
60

## Various SIR-bound genomic regions mediate camptothecin sensitivity.

To establish whether loss of H4-K16Ac or the associated leak of genetic information from *HML* and *HMR* was responsible for the suppression of *tof1Δ* phenotypes by SIR complex loss, we analysed the sensitivity of diploid *tof1Δ/tof1Δ* cells, which express simultaneously, at the *MAT* locus, the genetic information encoded by *HMR* and *HML*. If a leak of *HML* genetic information reduced the camptothecin hypersensitivity of MATa *tof1Δ* strains, one would expect a homozygous *tof1Δ* diploid strain to be less camptothecin sensitive than the corresponding haploid strain; however, this was not the case (**Figure 5A**). Moreover, the hypersensitivity of diploid *tof1Δ/tof1Δ* cells was also rescued by sirtinol, indicating that the loss of heterochromatin structure rather than leaked *HM* genetic information is responsible for suppression of camptothecin hypersensitivity (**Figure 5A**). However, when we then deleted the *HML* and *HMR* loci, we were surprised to observe that this did not rescue the camptothecin hypersensitivity of *tof1Δ* cells (**Figure 5B**), suggesting the existence of other genomic loci targeted by the Sir1/2/3/4 pathway.

To identify such genomic regions, we analysed a dataset of chromatin immunoprecipitation-sequencing (ChIP-seq) data for Sir2, Sir3, Sir4, GFP, acetylated histone H4-K16, and histone H3 (42, 43). In these datasets, we searched for genomic regions displaying increased binding of Sir2, Sir3 and Sir4 compared to neighbouring regions, even below the levels of statistical significance. We then removed any region that showed increased GFP binding to exclude ChIP bias towards highly expressed genes (43). We also removed any region where we could not observe a decrease in H4-K16 acetylation, the functional consequence Sir complex binding, or where such a decrease co-localised with loss of the H3 ChIP signal, suggesting depletion of nucleosomes. Strikingly, genomic regions identified in this manner co-localised with confirmed open reading frames (ORFs; three examples of which are shown in **Figure 5C**). We then defined a “SIR-binding score” for every ORF as the fraction of nucleotides for which the

1  
2 above conditions held. While the majority of all ORFs had a null SIR score (indicative of no  
3 enrichment of SIR complex binding), we found that 111 of them showed an enrichment of  
4 Sir2/3/4 and concomitant loss of H4-K16 acetylation in at least 20% of their sequence  
5 (Supplementary Table 4). Of these 111 ORFs, 29 were localised in sub-telomeric regions or in  
6 regions proximal to the *HM* loci (**Figure 5D**, small grey dots), while the remaining 82 hits  
7 were positioned along chromosome lengths (**Figure 5D**, green dots). While the majority of the  
8 identified ORFs are expressed at high levels during exponential growth, high expression was  
9 not sufficient for a high SIR score (**Supplementary Figure 2D** based on data from (44)).  
10 Collectively, these findings highlighted how, in addition to functioning at its well-defined  
11 target loci, the SIR complex may also act at a variety of loci scattered throughout the genome,  
12 and suggested that these loci might also promote camptothecin toxicity in wild-type and *tof1Δ*  
13 cells.  
14  
15  
16  
17  
18  
19  
20  
21  
22  
23  
24  
25  
26  
27  
28  
29

30 Recruitment of Sir1 at *HM* loci requires its interaction with the bromo-adjacent domain (BAH)  
31 region of Orc1. We therefore asked whether any of the loci we identified above was also  
32 positioned in proximity to a site bound by ORC. To do this, we calculated the distance between  
33 the centre of each ORF and the nearest ORC binding site (45). This analysis revealed that  
34 ~50% of SIR-positive ORFs were located less than 1.7 kbp from a site of ORC binding (**Figure**  
35 **5E**). This distance is smaller than the median value of 7.7 kbp for all yeast ORF. We reasoned  
36 that, if ORC has a functional role in recruiting the SIR complex to these genomic loci, it should  
37 be possible to suppress the camptothecin hypersensitivity of *tof1Δ* by preventing ORC-  
38 mediated recruitment of Sir1. In line with this hypothesis, we found that deleting the BAH  
39 domain of ORC1 suppressed *tof1Δ* camptothecin hypersensitivity (**Figure 5F**; effects of ORC1  
40 deletion could not be studied because it is an essential gene). These findings thus suggested  
41 that the chromatin substrates that become toxic to *tof1Δ* cells exposed to camptothecin is at  
42 least partially formed in an ORC-dependent manner.  
43  
44  
45  
46  
47  
48  
49  
50  
51  
52  
53  
54  
55  
56  
57  
58  
59  
60

## Discussion

We identified the Sir1, 2, 3 and 4 (SIR) genes as major mediators of the sensitivity of both wild-type and *tof1Δ* cells to camptothecin. Furthermore, we established that, rather than merely reducing camptothecin action, deletion of SIR genes removes a factor that hinders cell proliferation in the presence of camptothecin in wild-type cells and that is particularly toxic to cells lacking the Tof1 replication pausing complex. Camptothecin promotes the accumulation of positive supercoiling during DNA replication by locking Topoisomerase 1 on DNA in a non-functional state (16, 17). Since Tof1/Csm3 restricts replisome rotation during DNA replication (6) and since the main force driving fork rotation is positive supercoiling, we hypothesize that an excess of positive supercoiling is the factor that is alleviated by deletion of SIR genes. Lack of Sir2, Sir3, or Sir4 leads to loss of histone H4 lysine 16 (H4-K16) deacetylation and subsequent impairment in heterochromatin formation. We have observed that inhibition of Sir2 deacetylase activity or mutation of H4-K16 to glutamine — a residue that mimics an acetylated lysine — also suppresses *tof1Δ* camptothecin sensitivity. Importantly, this suppression is observed only if Sir2 activity is inhibited prior to camptothecin treatment, suggesting that a heterochromatic template becomes toxic to *tof1Δ* cells when replicated in the presence of camptothecin.

Yeast genomes contain three well-characterized regions of transcriptionally silenced chromatin, namely the ribosomal DNA, sub-telomeric regions and the cryptic mating-type loci *HML* and *HMR*; and of these, only the cryptic mating type loci require Sir1 for their silencing (39). The fact that *SIR1* deletion also suppresses the camptothecin sensitivity of *tof1Δ* cells initially suggested to us that *HML* and *HMR* represent the chromatin templates that are toxic to *tof1Δ* cells. However, we did not observe a reduction in *tof1Δ* sensitivity to camptothecin by deleting *HML* and *HMR*, meaning that these two genomic loci alone are not responsible for the strong camptothecin sensitivity phenotype displayed by *tof1Δ* cells.

1  
2 By analysing publicly available ChIP-seq data, we identified various genomic loci that exhibit  
3 enhanced localisation of Sir2, Sir3 and Sir4 as well as H4-K16 under-acetylation. Notably, we  
4 found that these genomic loci co-localise with confirmed ORFs and are located closer to sites  
5 of ORC binding than the average yeast ORF. Indeed, we found that many of these sites co-  
6 localise with genomic loci that were previously shown to bind ORC despite not having origin  
7 activity (45). Importantly, some of the SIR-enriched loci also co-localise with sites of  
8 replication fork pausing and sites enriched in binding of Rrm3, a DNA helicase that relieves  
9 replication fork pauses (46, 47), suggesting that SIR-enriched loci are inherently difficult to  
10 replicate even in the absence of camptothecin. The fact that these ORFs are amongst the most  
11 highly expressed yeast genes and yet exhibit enhanced recruitment of the SIR silencing  
12 complex and signs of histone de-acetylation is enigmatic. One possibility is that strong  
13 transcription could prevent heterochromatin formation despite presence of the SIR complex.  
14 Indeed it has been shown that promoter strength affects the efficiency of silencing (48). By  
15 affecting transcription, camptothecin, could stimulate a temporary heterochromatinization of  
16 these genes, creating topological barriers to DNA replication. In this regard the  
17 hypersensitivity of *tof1Δ* cells to camptothecin might stem from the hyper-catenation that is  
18 generated when replication forks lacking Tof1/Csm3 approach barriers created by the  
19 Sir2/3/4 complex. In this regard, we note that increased catenation would likely require more  
20 time to be resolved, thereby potentially accounting for the M/G1 delay observed in *tof1Δ* cells  
21 following camptothecin treatment.

22  
23  
24  
25  
26  
27  
28  
29  
30  
31  
32  
33  
34  
35  
36  
37  
38  
39  
40  
41  
42  
43  
44  
45  
46  
47  
48 Lack of Sir1 does not lead automatically to loss of transcriptional silencing, but rather it  
49 removes the pathway required for its re-establishment after it is lost. We were thus initially  
50 surprised that *SIR1* deletion also produced a strong suppression of camptothecin sensitivity,  
51 similar to that we observed with *SIR2* deletion. To explain this unexpected result, we  
52 hypothesised that increased DNA catenation caused by loss of Tof1 might increase the  
53 frequency of silencing loss. Accordingly, we observed that *sir1Δtof1Δ* cells show phenotypes  
54  
55  
56  
57  
58  
59  
60

1  
2 that are consistent with loss of silencing at cryptic mating type loci. It is difficult to imagine  
3  
4 how loss of Tof1 might lead to loss of silencing, but one possibility is that hyper-catenation of  
5  
6 sister chromatids generated in the absence of Tof1 could transiently impair normal histone  
7  
8 deposition/recycling, thereby promoting loss of parental heterochromatic marks. In regard to  
9  
10 this, we note that yeast strains lacking histone chaperones Asf1 or CAF-1 also lose *HML*  
11  
12 silencing in the absence of Sir1 (49, 50). Despite the threat to genome integrity, loss of  
13  
14 nucleosomes on intertwined DNA strands might also represent a signal for stimulating Top2  
15  
16 decatenating activity, as it is suggested by the fact that nucleosome loss increases Top2  
17  
18 occupancy (51).  
19  
20

21  
22  
23 Inhibition of topoisomerase 1 is a widely used therapeutic strategy to selectively kill  
24  
25 proliferating cancer cells, with camptothecin analogues being part of the standard-of-care  
26  
27 provided by many cancer clinics worldwide. Various mechanisms of camptothecin resistance  
28  
29 have been observed, ranging from overexpression of drug-efflux transporters that actively  
30  
31 reduce intracellular drug concentration (52) to specific Top1 mutations that prevent its  
32  
33 interaction with camptothecin (53, 54). Using yeast as a model system, we have found that  
34  
35 inhibition of H4-K16 deacetylation by inactivation of the Sir2/3/4 complex represents an  
36  
37 additional mechanism of camptothecin resistance. Further studies will be required to  
38  
39 determine if this mechanism is evolutionary conserved and whether it plays a significant role  
40  
41 in the emergence of resistance to camptothecin analogues in human cancers.  
42  
43  
44  
45

## 46 **Supplementary Data**

47  
48  
49  
50 This manuscript contains two supplementary figures and four supplementary tables.  
51  
52

## 53 **Funding**

54  
55  
56 This work was supported by the European Molecular Biology Organization [ALTF1287-2011  
57  
58 to FP]; the Associazione Italiana per la Ricerca sul Cancro [to VC, 10932 to FP]; Cancer  
59  
60

1  
2 Research UK [C6/A11224, C6/A18796, C6946/A14492 (core funding)]; the European  
3  
4 Research Council [DDREAM to SPJ, DNAMEREP to VC]; the European Community Seventh  
5  
6 Framework Programme [HEALTH-F2-2010-259893 (DDResponse)]; the Wellcome Trust  
7  
8 [101126/Z/13/Z, 098051 to M.H. and WT092096 (core funding)]; the Armenise-Harvard  
9  
10 Foundation [to VC]; and the Fondazione Telethon [to VC].  
11  
12

13  
14 *Conflict of interest statement.* None declared  
15

## 16 17 **Acknowledgements**

18  
19 We thank Jasper Rine, Catherine A. Fox, Takehiko Kobayashi, Tony Kouzarides and Shelley  
20  
21 Berger for the gift of strains and plasmids, all the members of the SPJ laboratory for helpful  
22  
23 discussions, and Helena Santos-Rosa for advice with designing histone point mutations. The  
24  
25 initial project was conceived by FP, VC and SPJ. Screening for suppressors and DNA  
26  
27 extractions were carried out by FP and NJG. Analysis of whole genome sequencing data was  
28  
29 carried out by MH and FP. Subsequent *in vivo* experiments and analyses of ChIP-seq data were  
30  
31 carried out by MH and FP. Subsequent *in vivo* experiments and analyses of ChIP-seq data were  
32  
33 designed and carried out by FP. The manuscript was largely written by FP and SPJ, with  
34  
35 contributions made by all the other authors.  
36  
37

## 38 39 **References**

- 40  
41  
42 1. Schwartzman, J.B. and Stasiak, A. (2004) A topological view of the replicon. *EMBO reports*, **5**,  
43 256–261.  
44  
45 2. Postow, L., Crisona, N.J., Peter, B.J., Hardy, C.D. and Cozzarelli, N.R. (2001) Topological  
46 challenges to DNA replication: conformations at the fork. *Proc Natl Acad Sci U S A*, **98**,  
47 8219–8226.  
48  
49 3. Sundin, O. and Varshavsky, A. (1980) Terminal stages of SV40 DNA replication proceed via  
50 multiply intertwined catenated dimers. *Cell*, **21**, 103–114.  
51  
52 4. Baxter, J., Sen, N., Mart 'i nez, V.L., De Carandini, M.E.M., Schwartzman, J.B., Diffley, J.F.X. and  
53 Aragón, L. (2011) Positive supercoiling of mitotic DNA drives decatenation by  
54 topoisomerase II in eukaryotes. *Science (New York, N.Y.)*, **331**, 1328–1332.  
55  
56 5. Fachinetti, D., Bermejo, R., Cocito, A., Minardi, S., Katou, Y., Kanoh, Y., Shirahige, K.,  
57 Azvolinsky, A., Zakian, V.A. and Foiani, M. (2010) Replication termination at eukaryotic  
58  
59  
60

- 1 chromosomes is mediated by Top2 and occurs at genomic loci containing pausing  
2 elements. *Molecular Cell*, **39**, 595–605.
- 3  
4  
5 6. Schalbetter,S.A., Mansoubi,S., Chambers,A.L., Downs,J.A. and Baxter,J. (2015) Fork rotation  
6 and DNA precatenation are restricted during DNA replication to prevent chromosomal  
7 instability. *Proc Natl Acad Sci U S A*, **112**, E4565–70.
- 8  
9 7. Ivessa,A.S., Lenzmeier,B.A., Bessler,J.B., Goudsouzian,L.K., Schnakenberg,S.L. and Zakian,V.A.  
10 (2003) The *Saccharomyces cerevisiae* helicase Rrm3p facilitates replication past  
11 nonhistone protein-DNA complexes. *Molecular Cell*, **12**, 1525–1536.
- 12  
13 8. Zaratiegui,M., Vaughn,M.W., Irvine,D.V., Goto,D., Watt,S., Bähler,J., Arcangioli,B. and  
14 Martienssen,R.A. (2011) CENP-B preserves genome integrity at replication forks paused  
15 by retrotransposon LTR. *Nature*, **469**, 112–115.
- 16  
17 9. Tourrière,H., Versini,G., Cerdón-Preciado,V., Alabert,C. and Pasero,P. (2005) Mrc1 and Tof1  
18 promote replication fork progression and recovery independently of Rad53. *Molecular*  
19 *Cell*, **19**, 699–706.
- 20  
21 10. Katou,Y., Kanoh,Y., Bando,M., Noguchi,H., Tanaka,H., Ashikari,T., Sugimoto,K. and  
22 Shirahige,K. (2003) S-phase checkpoint proteins Tof1 and Mrc1 form a stable replication-  
23 pausing complex. *Nature*, **424**, 1078–1083.
- 24  
25 11. Alcasabas,A.A., Osborn,A.J., Bachant,J., Hu,F., Werler,P.J., Bousset,K., Furuya,K., Diffley,J.F.X.,  
26 Carr,A.M. and Elledge,S.J. (2001) Mrc1 transduces signals of DNA replication stress to  
27 activate Rad53. *Nature cell biology*, **3**, 958–965.
- 28  
29 12. Foss,E.J. (2001) Tof1p regulates DNA damage responses during S phase in *Saccharomyces*  
30 *cerevisiae*. *Genetics*, **157**, 567–577.
- 31  
32 13. Osborn,A.J. and Elledge,S.J. (2003) Mrc1 is a replication fork component whose  
33 phosphorylation in response to DNA replication stress activates Rad53. *Genes &*  
34 *development*, **17**, 1755–1767.
- 35  
36 14. Bando,M., Katou,Y., Komata,M., Tanaka,H., Itoh,T., Sutani,T. and Shirahige,K. (2009) Csm3,  
37 Tof1, and Mrc1 form a heterotrimeric mediator complex that associates with DNA  
38 replication forks. *The Journal of biological chemistry*, **284**, 34355–34365.
- 39  
40 15. Redon,C., Pilch,D.R. and Bonner,W.M. (2006) Genetic analysis of *Saccharomyces cerevisiae*  
41 H2A serine 129 mutant suggests a functional relationship between H2A and the sister-  
42 chromatid cohesion partners Csm3-Tof1 for the repair of topoisomerase I-induced DNA  
43 damage. *Genetics*, **172**, 67–76.
- 44  
45 16. Ray Chaudhuri,A., Hashimoto,Y., Herrador,R., Neelsen,K.J., Fachinetti,D., Bermejo,R.,  
46 Cocito,A., Costanzo,V. and Lopes,M. (2012) Topoisomerase I poisoning results in PARP-  
47 mediated replication fork reversal. *Nature structural & molecular biology*, **19**, 417–423.
- 48  
49 17. Koster,D.A., Palle,K., Bot,E.S.M., Bjornsti,M.-A. and Dekker,N.H. (2007) Antitumour drugs  
50 impede DNA uncoiling by topoisomerase I. *Nature*, **448**, 213–217.
- 51  
52 18. Longtine,M.S., McKenzie,A., Demarini,D.J., Shah,N.G., Wach,A., Brachat,A., Philippsen,P. and  
53 Pringle,J.R. (1998) Additional modules for versatile and economical PCR-based gene  
54 deletion and modification in *Saccharomyces cerevisiae*. *Yeast (Chichester, England)*, **14**,
- 55  
56  
57  
58  
59  
60

- 1  
2 953–961.  
3  
4 19. Dodson,A.E. and Rine,J. (2015) Heritable capture of heterochromatin dynamics in  
5 *Saccharomyces cerevisiae*. *eLife*, **4**, 1–22.  
6  
7 20. Puddu,F., Oelschlaegel,T., Guerini,I., Geisler,N.J., Niu,H., Herzog,M., Salguero,I., Ochoa-  
8 Montaña,B., Viré,E., Sung,P., *et al.* (2015) Synthetic viability genomic screening defines  
9 Sae2 function in DNA repair. *The EMBO journal*, **34**, 1509–1522.  
10  
11 21. Li,H., Handsaker,B., Wysoker,A., Fennell,T., Ruan,J., Homer,N., Marth,G., Abecasis,G. and  
12 Durbin,R. (2009) The Sequence Alignment/Map format and SAMtools. *Bioinformatics*  
13 (*Oxford, England*), **25**, 2078–2079.  
14  
15 22. McLaren,W., Pritchard,B., Rios,D., Chen,Y., Flicek,P. and Cunningham,F. (2010) Deriving the  
16 consequences of genomic variants with the Ensembl API and SNP Effect Predictor.  
17 *Bioinformatics (Oxford, England)*, **26**, 2069–2070.  
18  
19 23. Kueng,S., Oppikofer,M. and Gasser,S.M. (2013) SIR proteins and the assembly of silent  
20 chromatin in budding yeast. *Annual review of genetics*, **47**, 275–306.  
21  
22 24. Rine,J. and Herskowitz,I. (1987) Four genes responsible for a position effect on expression  
23 from HML and HMR in *Saccharomyces cerevisiae*. *Genetics*, **116**, 9–22.  
24  
25 25. Grozinger,C.M., Chao,E.D., Blackwell,H.E., Moazed,D. and Schreiber,S.L. (2001)  
26 Identification of a class of small molecule inhibitors of the sirtuin family of NAD-  
27 dependent deacetylases by phenotypic screening. *The Journal of biological chemistry*, **276**,  
28 38837–38843.  
29  
30 26. Rajamohan,S.B., Pillai,V.B., Gupta,M., Sundaresan,N.R., Birukov,K.G., Samant,S.,  
31 Hottiger,M.O. and Gupta,M.P. (2009) SIRT1 promotes cell survival under stress by  
32 deacetylation-dependent deactivation of poly(ADP-ribose) polymerase 1. *Molecular and*  
33 *cellular biology*, **29**, 4116–4129.  
34  
35 27. Jeong,J., Juhn,K., Lee,H., Kim,S.-H., Min,B.-H., Lee,K.-M., Cho,M.-H., Park,G.-H. and Lee,K.-H.  
36 (2007) SIRT1 promotes DNA repair activity and deacetylation of Ku70. *Exp. Mol. Med.*, **39**,  
37 8–13.  
38  
39 28. Kaidi,A., Weinert,B.T., Choudhary,C. and Jackson,S.P. (2010) Human SIRT6 promotes DNA  
40 end resection through CtIP deacetylation. *Science (New York, N.Y.)*, **329**, 1348–1353.  
41  
42 29. Onishi,M., Liou,G.-G., Buchberger,J.R., Walz,T. and Moazed,D. (2007) Role of the conserved  
43 Sir3-BAH domain in nucleosome binding and silent chromatin assembly. *Molecular Cell*,  
44 **28**, 1015–1028.  
45  
46 30. Meijsing,S.H. and Ehrenhofer-Murray,A.E. (2001) The silencing complex SAS-I links  
47 histone acetylation to the assembly of repressed chromatin by CAF-I and Asf1 in  
48 *Saccharomyces cerevisiae*. *Genes Dev.*, **15**, 3169–3182.  
49  
50 31. Redon,C., Pilch,D.R., Rogakou,E.P., Orr,A.H., Lowndes,N.F. and Bonner,W.M. (2003) Yeast  
51 histone 2A serine 129 is essential for the efficient repair of checkpoint-blind DNA damage.  
52 *EMBO reports*, **4**, 678–684.  
53  
54 32. Wai,H.H., Vu,L., Oakes,M. and Nomura,M. (2000) Complete deletion of yeast chromosomal  
55  
56  
57  
58  
59  
60

- 1  
2 rDNA repeats and integration of a new rDNA repeat: use of rDNA deletion strains for  
3 functional analysis of rDNA promoter elements in vivo. *Nucleic acids research*, **28**, 3524–  
4 3534.  
5  
6 33. Smith,J.S., Brachmann,C.B., Pillus,L. and Boeke,J.D. (1998) Distribution of a limited Sir2  
7 protein pool regulates the strength of yeast rDNA silencing and is modulated by Sir4p.  
8 *Genetics*, **149**, 1205–1219.  
9  
10 34. Kyrion,G., Liu,K., Liu,C. and Lustig,A.J. (1993) RAP1 and telomere structure regulate  
11 telomere position effects in *Saccharomyces cerevisiae*. *Genes Dev.*, **7**, 1146–1159.  
12  
13 35. Vignais,M.L., Woudt,L.P., Wassenaar,G.M., Mager,W.H., Sentenac,A. and Planta,R.J. (1987)  
14 Specific binding of TUF factor to upstream activation sites of yeast ribosomal protein  
15 genes. *The EMBO journal*, **6**, 1451–1457.  
16  
17 36. Lieb,J.D., Liu,X., Botstein,D. and Brown,P.O. (2001) Promoter-specific binding of Rap1  
18 revealed by genome-wide maps of protein-DNA association. *Nature genetics*, **28**, 327–334.  
19  
20 37. Triolo,T. and Sternglanz,R. (1996) Role of interactions between the origin recognition  
21 complex and SIR1 in transcriptional silencing. *Nature*, **381**, 251–253.  
22  
23 38. Gardner,K.A., Rine,J. and Fox,C.A. (1999) A region of the Sir1 protein dedicated to  
24 recognition of a silencer and required for interaction with the Orc1 protein in  
25 *saccharomyces cerevisiae*. *Genetics*, **151**, 31–44.  
26  
27 39. Smith,J.S. and Boeke,J.D. (1997) An unusual form of transcriptional silencing in yeast  
28 ribosomal DNA. *Genes Dev.*, **11**, 241–254.  
29  
30 40. Sussel,L., Vannier,D. and Shore,D. (1993) Epigenetic switching of transcriptional states:  
31 cis- and trans-acting factors affecting establishment of silencing at the HMR locus in  
32 *Saccharomyces cerevisiae*. *Molecular and cellular biology*, **13**, 3919–3928.  
33  
34 41. Ivy,J.M., Klar,A.J. and Hicks,J.B. (1986) Cloning and characterization of four SIR genes of  
35 *Saccharomyces cerevisiae*. *Molecular and cellular biology*, **6**, 688–702.  
36  
37 42. Thurtle,D.M. and Rine,J. (2014) The molecular topography of silenced chromatin in  
38 *Saccharomyces cerevisiae*. *Genes Dev.*, **28**, 245–258.  
39  
40 43. Teytelman,L., Thurtle,D.M., Rine,J. and van Oudenaarden,A. (2013) Highly expressed loci  
41 are vulnerable to misleading ChIP localization of multiple unrelated proteins. *Proc Natl*  
42 *Acad Sci U S A*, **110**, 18602–18607.  
43  
44 44. Nagalakshmi,U., Wang,Z., Waern,K., Shou,C., Raha,D., Gerstein,M. and Snyder,M. (2008) The  
45 transcriptional landscape of the yeast genome defined by RNA sequencing. *Science (New*  
46 *York, N.Y.)*, **320**, 1344–1349.  
47  
48 45. Shor,E., Warren,C.L., Tietjen,J., Hou,Z., Müller,U., Alborelli,I., Gohard,F.H., Yemm,A.I.,  
49 Borisov,L., Broach,J.R., *et al.* (2009) The origin recognition complex interacts with a subset  
50 of metabolic genes tightly linked to origins of replication. *PLoS genetics*, **5**, e1000755.  
51  
52 46. Azvolinsky,A., Giresi,P.G., Lieb,J.D. and Zakian,V.A. (2009) Highly transcribed RNA  
53 polymerase II genes are impediments to replication fork progression in *Saccharomyces*  
54 *cerevisiae*. *Molecular Cell*, **34**, 722–734.  
55  
56  
57  
58  
59  
60

- 1  
2  
3  
4  
5  
6  
7  
8  
9  
10  
11  
12  
13  
14  
15  
16  
17  
18  
19  
20  
21  
22  
23  
24  
25  
26  
27  
28  
29  
30  
31  
32  
33  
34  
35  
36  
37  
38  
39  
40  
41  
42  
43  
44  
45  
46  
47  
48  
49  
50  
51  
52  
53  
54  
55  
56  
57  
58  
59  
60
47. Mohanty,B.K., Bairwa,N.K. and Bastia,D. (2006) The Tof1p-Csm3p protein complex counteracts the Rrm3p helicase to control replication termination of *Saccharomyces cerevisiae*. *Proc Natl Acad Sci U S A*, **103**, 897–902.
48. Ren,J., Wang,C.-L. and Sternglanz,R. (2010) Promoter strength influences the S phase requirement for establishment of silencing at the *Saccharomyces cerevisiae* silent mating type Loci. *Genetics*, **186**, 551–560.
49. Osada,S., Sutton,A., Muster,N., Brown,C.E., Yates,J.R., Sternglanz,R. and Workman,J.L. (2001) The yeast SAS (something about silencing) protein complex contains a MYST-type putative acetyltransferase and functions with chromatin assembly factor ASF1. *Genes Dev.*, **15**, 3155–3168.
50. Enomoto,S. and Berman,J. (1998) Chromatin assembly factor I contributes to the maintenance, but not the re-establishment, of silencing at the yeast silent mating loci. *Genes Dev.*, **12**, 219–232.
51. Sperling,A.S., Jeong,K.S., Kitada,T. and Grunstein,M. (2011) Topoisomerase II binds nucleosome-free DNA and acts redundantly with topoisomerase I to enhance recruitment of RNA Pol II in budding yeast. *Proc Natl Acad Sci U S A*, **108**, 12693–12698.
52. Maliepaard,M., van Gastelen,M.A., de Jong,L.A., Pluim,D., van Waardenburg,R.C., Ruevekamp-Helmers,M.C., Floom,B.G. and Schellens,J.H. (1999) Overexpression of the BCRP/MXR/ABCP gene in a topotecan-selected ovarian tumor cell line. *Cancer Res.*, **59**, 4559–4563.
53. Jensen,N.F., Agama,K., Roy,A., Smith,D.H., Pfister,T.D., Rømer,M.U., Zhang,H.-L., Doroshov,J.H., Knudsen,B.R., Stenvang,J., *et al.* (2016) Characterization of DNA topoisomerase I in three SN-38 resistant human colon cancer cell lines reveals a new pair of resistance-associated mutations. *J. Exp. Clin. Cancer Res.*, **35**, 56.
54. Chrencik,J.E., Staker,B.L., Burgin,A.B., Pourquier,P., Pommier,Y., Stewart,L. and Redinbo,M.R. (2004) Mechanisms of camptothecin resistance by human topoisomerase I mutations. **339**, 773–784.

## Figure Legends

**Figure 1. A synthetic viability screening to identify the cause for the hypersensitivity of *tof1Δ* cells to camptothecin**

**(A)** Loss of Tof1 and Csm3 but not Mrc1 causes hypersensitivity to camptothecin in a Top1-dependent manner. **(B)** Loss of pausing at the replication fork barrier on rDNA does not cause camptothecin hypersensitivity. **(C)** Outline of the procedure for a synthetic viability screen.

1  
2  
3  
4  
5  
6  
7  
8  
9  
10  
11  
12  
13  
14  
15  
16  
17  
18  
19  
20  
21  
22  
23  
24  
25  
26  
27  
28  
29  
30  
31  
32  
33  
34  
35  
36  
37  
38  
39  
40  
41  
42  
43  
44  
45  
46  
47  
48  
49  
50  
51  
52  
53  
54  
55  
56  
57  
58  
59  
60

(D) Synthetic viability screening identifies *sir3* and *sir4* alleles as suppressors of the camptothecin hypersensitivity of *tof1Δ* strains.

**Figure 2. Loss of the SIR complex suppresses camptothecin hypersensitivity of *tof1Δ* strains.**

(A) Deletion of *SIR3* or *SIR4* suppresses the hypersensitivity of *tof1Δ* cells to camptothecin.

(B) Deletion of *SIR2* also suppresses the hypersensitivity of *tof1Δ* cells to camptothecin and reduces the sensitivity of a wild-type strain. (C) Deletion of *SIR2* cannot suppress the camptothecin hypersensitivity of a *rad51Δ* strain. (D) Inhibition of Sir2 deacetylase activity with sirtinol suppresses the hypersensitivity of *tof1Δ* cells to camptothecin. (E) Mutations that mimic a permanently acetylated H4-K16 (K16Q) or that remove the binding site for Sir3 (K16G) also suppress the sensitivity to camptothecin of wild-type and *tof1Δ* strains. Mutation K16R (non-acetylatable residue) yields a less strong suppression, in line with reports that this mutation partially impairs silencing.

**Figure 3. An “acetylated H4-K16” template mediates sensitivity to camptothecin during DNA replication.**

(A) A wild-type strain released into S phase in the presence of camptothecin does not delay progression through S phase, but delays progression through the subsequent mitosis. (B) In the absence of Tof1 or Csm3, camptothecin treated cells remain arrested in G2/M for longer periods of time than wild-type cells. (C) *tof1Δ* and *csm3Δ* cells released into S phase in the presence of camptothecin delay destruction of the mitotic cyclin Clb2. (D) *tof1Δ* and *csm3Δ* cells are not hypersensitive to a pulse treatment with camptothecin. (E) *tof1Δ* cells and congenic wild-type cells were pre-grown either in the absence or in the presence of sirtinol. They were subsequently synchronised in G1 and released into S phase in the presence of camptothecin, either with or without sirtinol. Cell cycle progression was monitored by FACS

1  
2 analysis. Quantification of G1 cells shows that sirtinol addition during camptothecin treatment  
3  
4 does not suppress the mitotic delay of *tof1Δ* cells, while pre-growth in the presence of sirtinol  
5  
6 is sufficient to suppresses the camptothecin hypersensitivity phenotype of *tof1Δ* cells.  
7  
8

9  
10 **Figure 4. Disruption of *SIR1* suppresses camptothecin sensitivity in wild-type and *tof1Δ***  
11 **cells.**  
12

13  
14  
15 **(A)** Deletion of the rDNA locus is not sufficient to suppress the hypersensitivity of *tof1Δ* cells  
16  
17 to camptothecin. **(B)** A mutation in *RAP1* that disrupts telomeric silencing does not suppress  
18  
19 the hypersensitivity of *tof1Δ* cells to camptothecin. **(C)** Deletion of *SIR1* suppresses  
20  
21 camptothecin sensitivity in wild-type and *tof1Δ* cells. **(D)** *sir1Δ* and *tof1Δ* show a synergistic  
22  
23 defect in the ability to mate. **(E)** *tof1Δsir1Δ* cells are unable to arrest in G1 after exposure to  
24  
25 alpha factor. **(F)** Outline of the genetic system used to detect loss of silencing events at the  
26  
27 *HMR* locus: transient loss of silencing causes expression of the Cre recombinase and a switch  
28  
29 from RFP and KanMX expression to GFP expression. **(G)** Cells carrying the genetic reporter  
30  
31 described in (F) were grown in the presence of G418 to prevent expansion of the green clones,  
32  
33 and were then plated on YPD plates. A selection of representative colonies is shown. A  
34  
35 quantification of red, green and sectored colonies is shown on the right.  
36  
37  
38  
39

40  
41 **Figure 5. Disruption of ORC1-mediated binding of the SIR complex to highly transcribed**  
42 **genes suppresses the hypersensitivity of *tof1Δ* cells to camptothecin.**  
43

44  
45 **(A)** Homozygous *tof1Δ/tof1Δ* diploid cells are as sensitive to camptothecin as *tof1Δ* haploids  
46  
47 and their hypersensitivity can be rescued by sirtinol. **(B)** Deletion of *HML* and *HMR* cannot  
48  
49 suppress the camptothecin hypersensitivity of *tof1Δ* strains. **(C)** Analysis of ChIP-seq data for  
50  
51 the indicated proteins. In green is the protein tested; in grey are the controls. Input samples  
52  
53 are shown in darker green/grey and immunoprecipitated samples are shown in lighter  
54  
55 green/grey. The position of each ORF is indicated by a black bar. **(D)** Identification of regions  
56  
57  
58  
59  
60

1  
2 bound by the SIR complex: for each ORF in the genome, a “SIR score” was calculated as the  
3  
4 fraction of the ORF for which both increased Sir2, Sir3, Sir4, and decreased H4-K16ac was  
5  
6 observable. ORFs were sorted based of their “SIR score”. Sub-telomeric ORFs and ORFs  
7  
8 proximal to *HML* and *HMR* are shown with small grey dots, while remaining ORFs are shown  
9  
10 with large green dots. **(E)** SIR-positive ORFs are on average located closer to sites of ORC  
11  
12 binding than ORFs in general. All yeast ORFs are shown in purple as a function of their  
13  
14 distance from the nearest site of ORC binding. SIR-positive ORFs (SIR score >0.2), are shown  
15  
16 in green. **(F)** Deletion of the BAH domain of ORC1 partially rescues the camptothecin  
17  
18 hypersensitivity of *tof1Δ* cells.  
19  
20  
21  
22  
23  
24  
25  
26  
27  
28  
29  
30  
31  
32  
33  
34  
35  
36  
37  
38  
39  
40  
41  
42  
43  
44  
45  
46  
47  
48  
49  
50  
51  
52  
53  
54  
55  
56  
57  
58  
59  
60

Figure 1

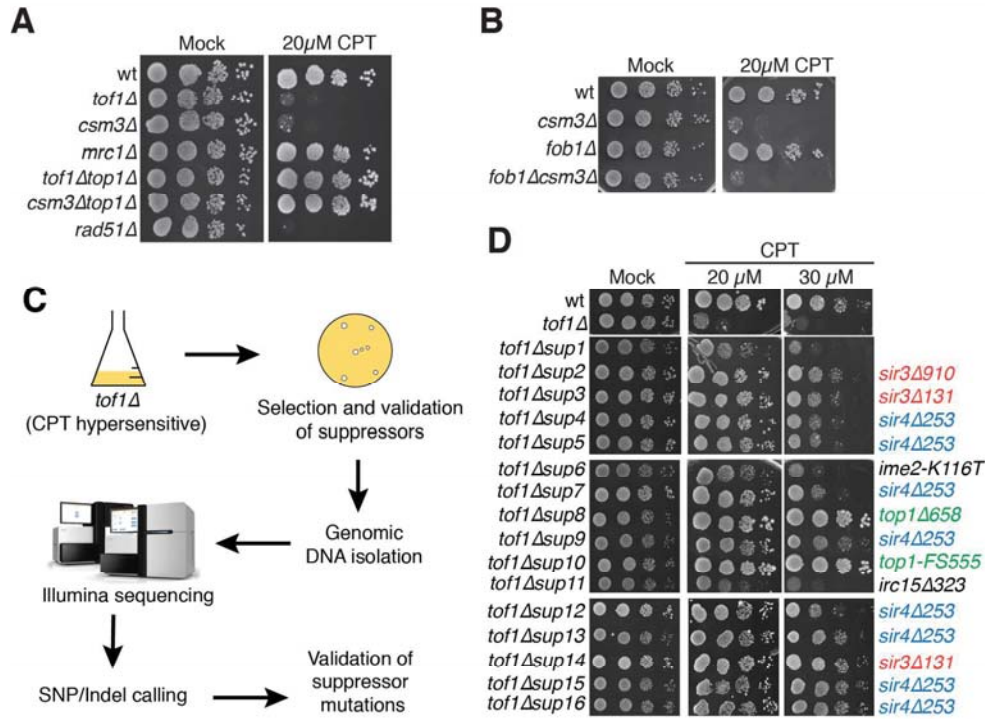


Figure 1

Figure 2

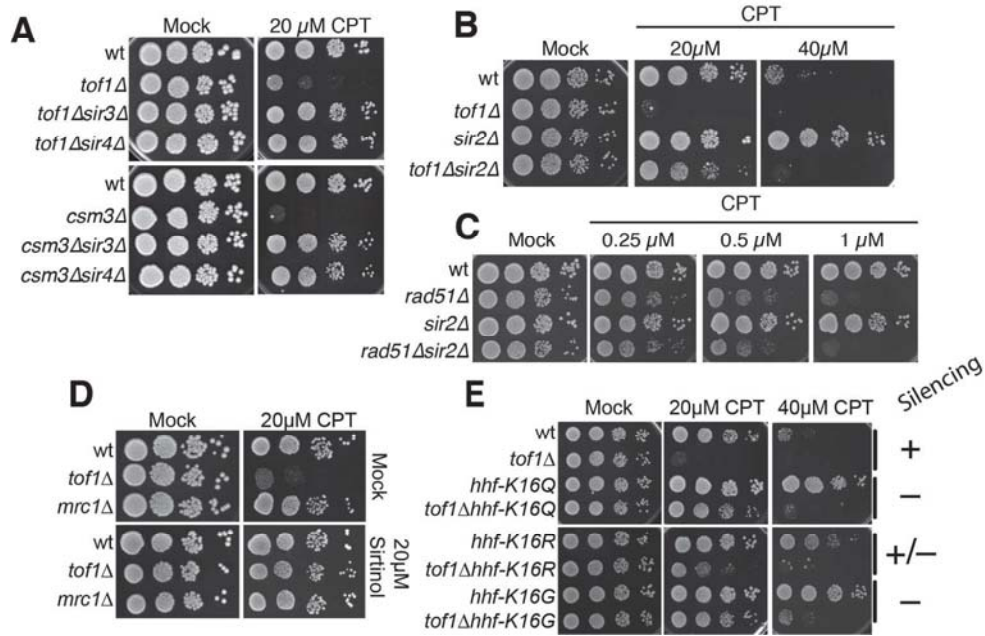


Figure 2

Figure 3

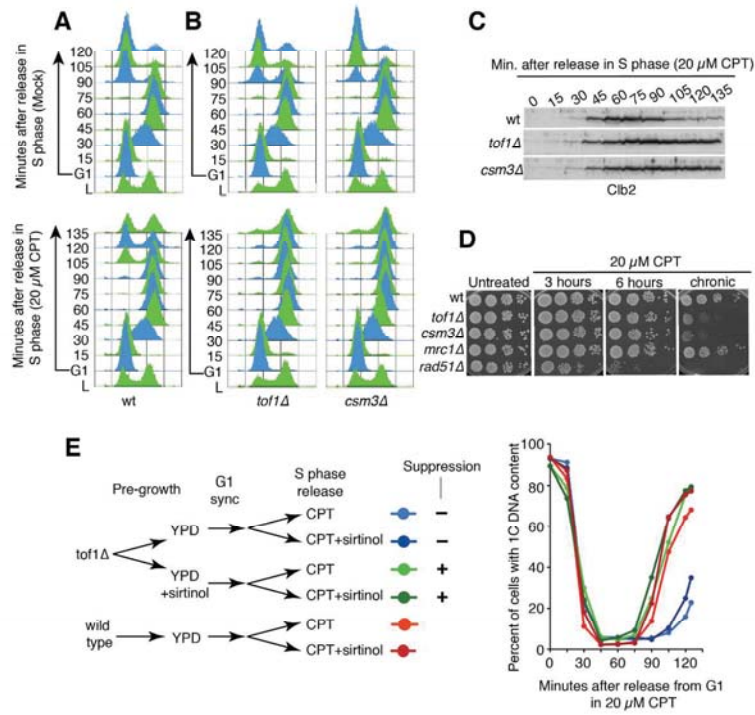


Figure 3

Figure 4

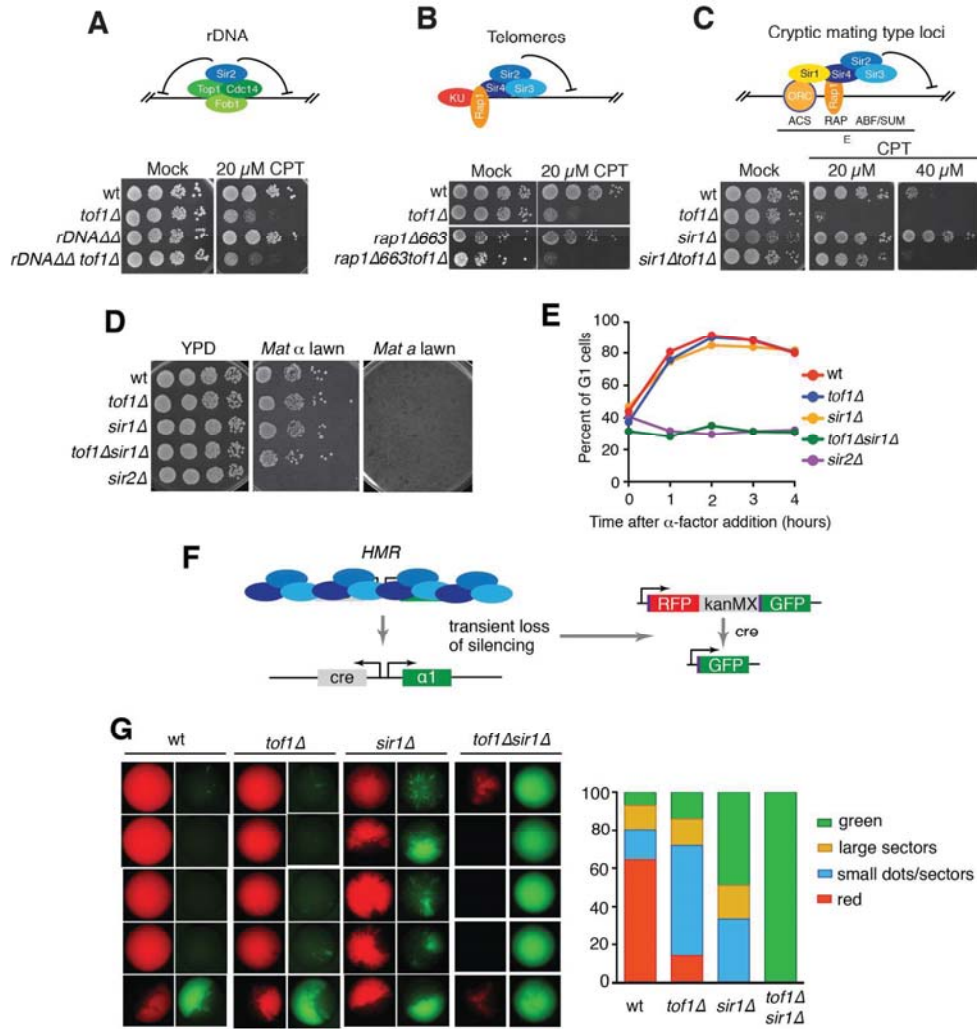


Figure 4

Figure 5

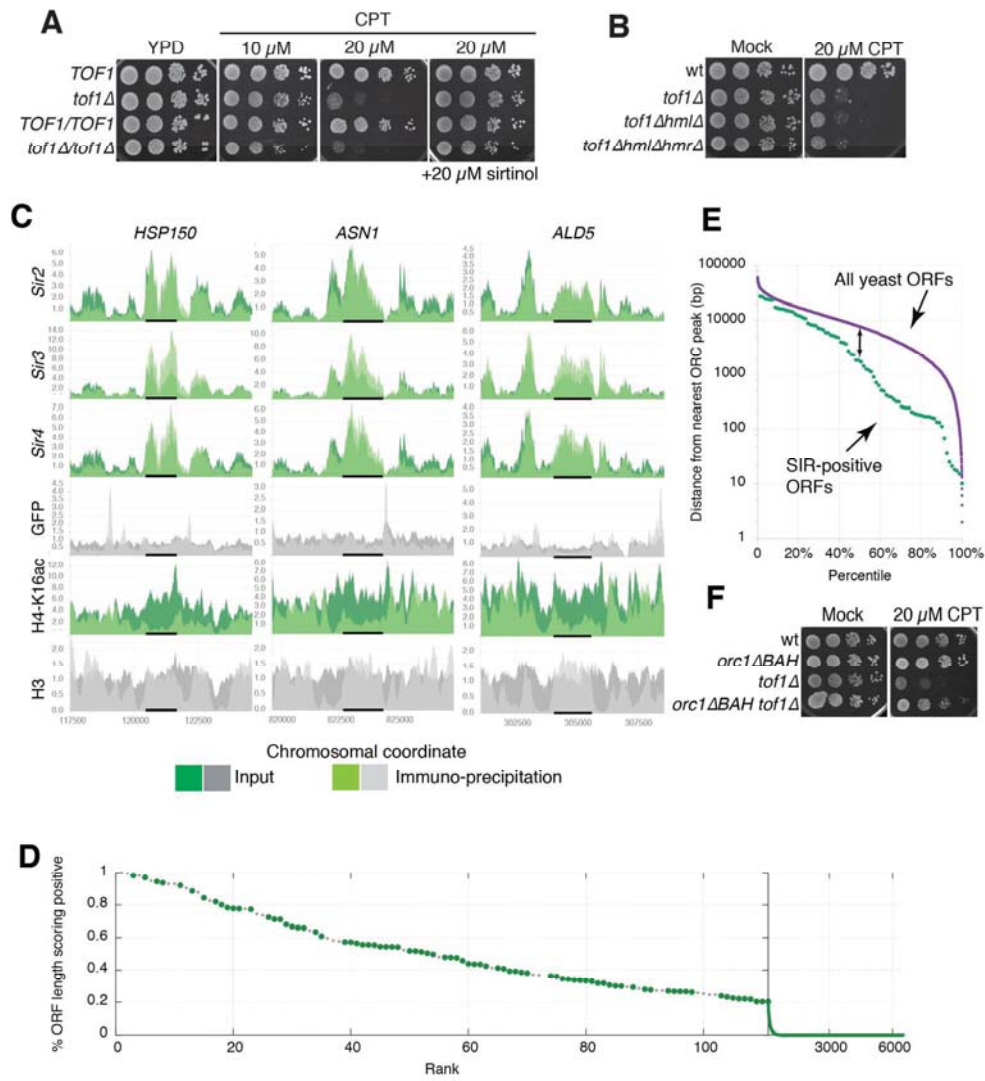


Figure 5

## Supplementary Material

**Supplementary Table 1:** Yeast strains used in this study.

**Supplementary Table 2:** Whole-genome sequencing data.

**Supplementary Table 3:** SRA accession numbers for ChIP-seq data

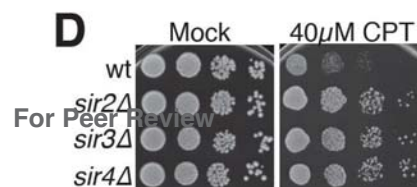
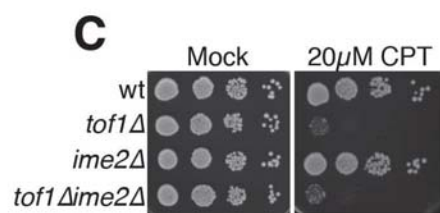
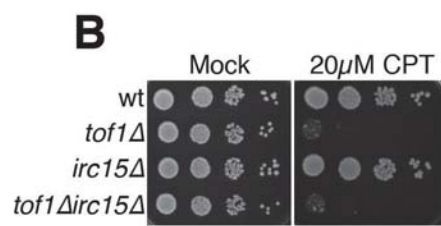
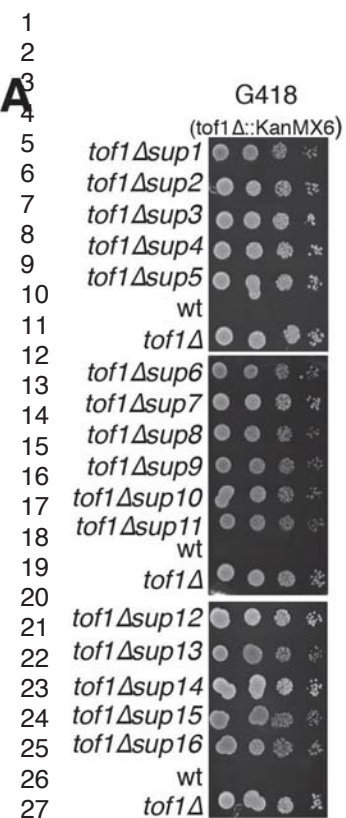
**Supplementary Table 4:** ORFs with SIR score > 0.2

### Supplementary Figure 1

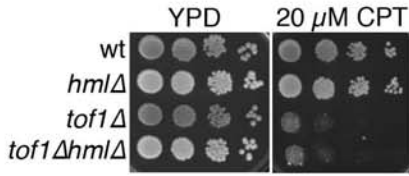
**(A)** Suppressor strains recovered from the *tof1Δ* synthetic-viability screen are G418 resistant, indicating presence of the *TOF1* deletion cassette. **(B)** Deletion of *IRC15* does not suppress *tof1Δ* camptothecin hypersensitivity. **(C)** Deletion of *IME2* does not suppress *tof1Δ* camptothecin hypersensitivity. **(D)** Deletion of *SIR2*, *SIR3* or *SIR4* increases resistance to camptothecin in a wild-type background.

### Supplementary Figure 2

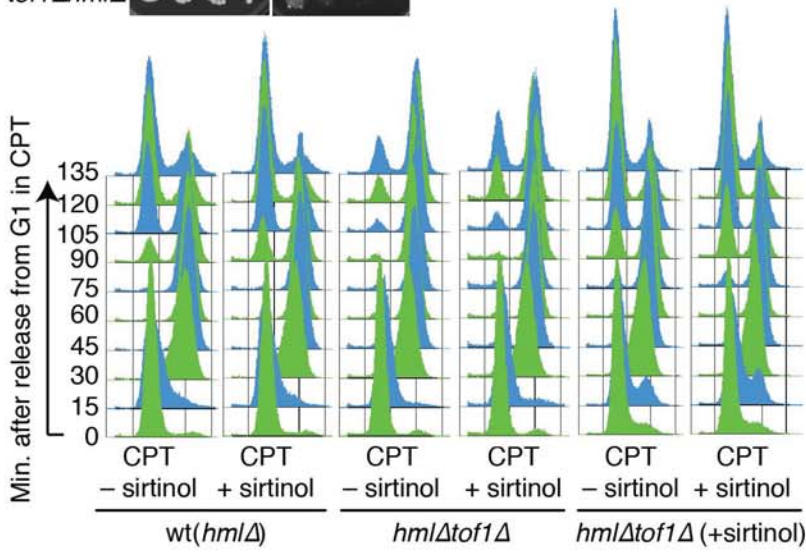
**(A)** Deletion of *HML* does not rescue *tof1Δ* hypersensitivity to camptothecin. **(B)** *tof1Δ* cells and congenic wild-type cells were pre-grown either in the absence or in the presence of sirtinol. They were subsequently synchronised in G1 and released into S phase in the presence of camptothecin, either with or without sirtinol. Cell cycle progression was monitored by FACS analysis. **(C)** Deletion of *SIR1* does not rescue camptothecin hypersensitivity in *rad51Δ* cells. **(D)** The majority of SIR-positive ORFs are highly expressed genes, but high expression does not necessarily correlate with high SIR score.



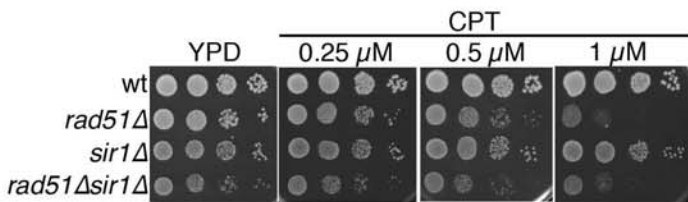
A



B



C



D

